THE UNIVERSITY OF ALBERTA

MECHANISM OF DEHYDRATION OF ISOPROPANOL

by

© Roland Pierre LEAUTE

A THESIS
SUBMITTED TO THE FACULTY OF GRADUATE STUDIES AND RESEARCH
IN PARTIAL FULFILMENT OF THE REQUIREMENTS FOR THE DEGREE
OF Doctor of Philosophy

Chemical Engineering

EDMONTON, ALBERTA
SPRING
1980

THE UNIVERSITY OF ALBERTA

FACULTY OF GRADUATE STUDIES AND RESEARCH

The undersigned certify that they have read, and recommend to the Faculty of Graduate Studies and Research, for acceptance, a thesis entitled, "MECHANISM AND KINETICS OF DEHYDRATION OF 2-PROPANOL" submitted by Roland P. Leaute in partial fulfilment of the requirements for the degree of Doctor of Philosophy in Chemical Engineering.

I G Dalla Lana
Supervisor

Sieghard Wanke

C Kiparissides

John E. B

R. Fiedorow
External Examiner

March 28, 1980

DEDICATION

Pour Karin ,Cecile et Andre qui sont entres dans ma vie pendant ce travail

Abstract

The two novelties in this work are the development of an improved infrared cellreactor and the derivation of a new mechanistic rate equation which was unique in fitting adequately the rates of dehydration of isopropanol on alumina.

The new reactor extends the applicability of simultaneously measuring under dynamic conditions the reaction kinetics as well as infrared spertra of the working catalyst. Although this concept was not new, the use of the technique had remained limited in the past because of the lack of consideration of some design factors. Key improvements consisted of increasing the contacting between the gases and the catalyst wafer, creating a good isothermality in the reaction zon and eliminating accurately the unwanted infrared radiation absorbance by the reacting gases.

In the case of the dehydration of isopropanol on alumina, combined infrared and kinetic results revealed important aspects of the dehydration mechanism. By observing that water had a negligible effect upon the degree of surface coverage by the reactant, it was concluded that water and alcohol occupy different surface sites during rection. On the other hand the pronounced retarding effect of water upon the reaction rate implies that the water adsorption sites are crucial to the dehydration process. The presence of stable carboxylate species formed on the surface was dtected by infrared and these were shown to deactivate the catalyst. Similarly chemisorbed pyridine species could be directly observed and were shown to strongly inhibit the reaction. These species also revealed the heterogeneity of the alumina surface. By combining all the infrared observations Lewis acid-base pairs of sites were proposed as constituting the operative effect for the dehydration process.

A total of 186 experiments at 4 different temperatures between 230 and 280°C and at varying partial pressures of alcohol and water were performed to provide kinetic data. None of many three- or four-parameters Langmuir-Hinshelwood kinetic models could correlate the data adequately. Infrared evidence of a maximum in the rate of reaction at intermediate surface coverages by the reactant indicated the presence of an autoinhibition effect due to some degree of interaction between the adsorbed alcohol molecules. A simple model representing the postulated surface interaction of the adsorbed species was incorporated into the standard Langmuir-Hinshelwood models. A significant improvement in the correlation of the kinetic data was obtained only in the case of a dual-dissimilar sites mechanism. The final 4-parameters rate expression

$r=abP\ .(1+bdP\ )/(1+bP\ )^2.(1+cP\ )$

was selected as the best model after fulfilling various criteria of adequacy.

Acknowledgements

The author wishes to express his sincere gratitude to Dr.I.G.Dalla Lana for his academic guidance and personal encouragement throughout this investigation.

Acknowledgement is also made to the staff of the departemental machine and instrument shops for their friendly cooperation over the years. Mr.John Van Doorn is particularly thanked for his skillful construction of the reactor system. Similarly the author is also indebted to Mr.Peter Lea from Technical Services for the quality of his glass blowing work.

The author is sincerely grateful for the financial support provided by the Department of Chemical Engineering.

Finally, the author wants to acknowledge the fact that it would have been impossible to complete this study without the help and patience of his wife.

Table of Contents

Chapter Page

1. INTRODUCTION 1

2. LITERATURE SURVEY 3

2.1 Properties Of Catalytic Aluminas 3

2.1.1 The crystalline structure of catalytic aluminas 3

2.1.2 Surface models of catalytic aluminas 4

2.1.3 The active sites of catalytic aluminas 13

2.1.4 Acid-base and redox properties of catalytic aluminas 15

2.2 Infrared Studies Of Adsorption Of Alcohols On Alumina 20

2.2.1 Alumina alkoxide structures 21

2.2.2 Carboxylate structures 26

2.2.3 Adsorption of water 29

2.3 Dehydration Reactions Of Alcohols On Alumina 30

2.3.1 Reaction scheme 31

2.3.2 Earlier postulated mechanisms 32

2.3.3 Detailed isotopic effects 35

2.3.4 Stereochemistry of dehydration 38

2.3.5 Kinetics of alcohol dehydration on alumina 40

3. DESIGN CONSIDERATIONS FOR SIMULTANEOUS INFRARED AND KINETIC STUDIES 45

3.1 Infrared Spectroscopy Of Adsorbed Species 45

3.2 Design Factors 47

3.2.1 Infrared design considerations 48

3.2.2 Kinetics design considerations 50

3.3 Tests Of Reactor Performance 57
    3.3.1 Mass transfer characteristics 57
    3.3.2 Mixing characteristics 63
    3.3.3 Compensation for gas phase infrared absorption 64
    3.3.4 Isothermal reaction zone 72
4. CONSTRUCTION AND DESCRIPTION OF APPARATUS 76
4.1 Feed System 76
4.2 Recirculation System 82
4.3 Infrared Cell Compartment 86
4.4 Catalyst Sample Holder 94
5. EXPERIMENTAL PROCEDURES AND DATA EVALUATUION 98
5.1 Reagent And Catalyst 98
5.2 Recording And Monitoring Of Process Temperatures .100
5.3 Infrared Spectrophotometer 106
5.4 Gas Chromatographic Composition Analyses 107
    5.4.1 Gas chromatograph operation 107
    5.4.2 Calibration with gas samples 109
5.5 Data Evaluation 119
    5.5.1 Determination of fractional conversions 121
    5.5.2 Determination of reactant feed flow rate ...125
5.6 Operation Of Equipment And Procedures During A Run 138
    5.6.1 Start-up and catalyst pretreatment 138
    5.6.2 Steady state operation during kinetic runs .142
    5.6.3 Limitations of the technique 144
6. RESULTS AND DISCUSSION 148
6.1 Infrared Spectra Of Alumina Under Reaction Conditions 148

6.1.1 General characteristics of surface spectra .148
6.1.2 Carboxylate adsorbed species 151
6.1.3 Influence of products 155
6.1.4 Poisoning experiments with pyridine 157
6.2 Kinetic Experiments 161
6.2.1 Preliminary kinetic experiments 161
6.2.2 Intraparticle diffusion 163
6.2.3 Summary of kinetic runs 169
6.3 Development of a New Kinetic Model 169
6.3.1 Development of mechanism consistent with experimental evidence 169
6.3.2 Influence of coverage upon reactivity of reactant adsorbate 172
6.3.3 Derivation of new rate expression 180
6.4 Testing Of Model Adequacy 180
6.4.1 Fitting adequacy 180
6.4.2 Temperature dependency of the parameters ...187
6.4.3 Agreement between coverages observed by infrared and coverages predicted by the model 191
6.4.4 Measurement Of Batch Conversions 195
6.5 Statistical Discrimination Between Alternative Models 199
6.5.1 Kinetic modelling in heterogeneous catalysis 199
6.5.2 Correlation of kinetic data with other published models for dehydration of alcohols .204
6.5.3 Correlation of improved published models ...217
6.5.4 Final model selection and considerations on the form of the autoinhibiting dependence ..226
7. CONCLUSIONS AND RECOMMENDATIONS 231

7.1 Conclusions 231
7.2 Recommendations 234
REFERENCES 236
NOMENCLATURE 249
APPENDIX 250

List of Figures

Figure Page

2.1 Model of Peri ~~on~~ arrangement of OH groups on alumina6

3.1 Recycle Reactor Material Balance....................51

3.2 Geometrical Configuration of Reactor Cells.........53

3.3 Sublimation Rates of Naphtalene in Various Reactor Prototypes..................................59

3.4 Comparison of Mixing Behaviour of the Reactor with Ideal CSTR.....................................65

3.5 Compensation of Gas-phase Absorbance Between Reference and Sample Cells..........................66

3.6 Typical Thermal Response of T1 to the Preheater Load. 69

3.7 Calibration Plot of Gas-phase Absorbance Compensation without the Window Heaters..................70

3.8 Calibration Plot of Gas-phase Absorbance Compensation with the Window Heaters.....................74

4.1 Photograph of Reactor System.......................77

4.2 Flow Diagram of Feeding Unit.......................78

4.3 Flow Diagram of Reactor Loop Piping...............85

4.4 Photograph of Infrared Cell Compartment...........87

4.5 Photograph of Cell Assembly and Catalyst Sample Holder...95

5.1 Geometrical Arrangement of Thermocouples in the Reactor...102

5.2 G.C. Calibration Plot of Propylene...............113

5.3 G.C. Calibration Plot of Water...................114

5.4 G.C. Calibration Plot of Isoproppanol............115

6.1 Infrared Spectra of Alumina Under Reaction Conditions 149

6.2 Mechanistic View of Surface Reaction.............152

6.3 Influence of Carboxylate Species.................154

6.4 Influence of Water.................................156

6.5 Poisoning Effect of Pyridine.......................160

6.6 Evaluation of Pore Diffusion.......................167

6.7 Interaction of Adsorbed Reactant Molecules as Function of Their Relative Coverage...............175

6.8 Overall Surface Activity as Function of Alcohol Fractional COverage..............................177

6.9 Comparison Between Experimental and Predicted Reaction Rates at 231.2°C..........................183

6.10 Comparison Between Experimental and Predicted Reaction Rates at 246.5°C..........................184

6.11 Comparison Between Experimental and Predicted Reaction Rates at 260.3°C..........................185

6.12 Comparison Between Experimental and Predicted Reaction Rates at 274.0°C..........................186

6.13 Arrhenius Dependency of Model Parameters..........190

6.14 Comparison Between Measured and Predicted Fractional Coverages of the Surface..................193

List of Tables

Table Page

2.1 IR Spectra of Hydroxyl Groups on Alumina............7

2.2 Possible OH Configurations on Alumina..............11

2.3 Isotopic Effects in the Dehydration of Alcohols....36

3.1 Simulated Mass Transfer Performance of the Reactor.56

3.2 Improvement of Mass Transfer Coefficients..........62

5.1 Typical Properties of Alon.........................99

5.2 Least Squares Fitting of G.C. Calibration Data for Isopropanol.................................116

5.3 Least Squares Fitting of G.C. Calibration Data for Propylene..................................117

5.4 Least Squares Fitting of G.C. Calibration Data for Water.....................................120

5.5 Comparison of the Two Syringe Pumps..............126

5.6 Comparison of the 50 and 20 CC Syringes..........127

5.7 Linearity of the Syringe Dial Settings...........129

5.8 Internal Consistency of the Alcohol Material Balance. 137

6.1 Summary of Kinetic Data..........................170

6.2 Derivation of New Rate Expression................181

6.3 Model Parameters.................................189

6.4 Published Simple 3-Parameter Kinetic Models for Dehydration of Alcohols.........................206

6.5 Correlation of Some Published Kinetic Models with Rate Data At 231.2°C........................209

6.6 Correlation of Some Published Kinetic Models with Rate Data At 246.5°C........................210

6.7 Correlation of Some Published Kinetic Models with Rate Data At 260.3°C........................211

6.8 Correlation of Some Published Kinetic Models with Rate Data At 274.0°C....................212

6.9 Modified Langmuir-Hinshelwood Models..............218

6.10 Correlation of Modified Kinetic Models with Rate Data At 231.2°C....................220

6.11 Correlation of Modified Kinetic Models with Rate Data At 246.5°C....................221

6.12 Correlation of Modified Kinetic Models with Rate Data At 260.3°C....................222

6.13 Correlation of Modified Kinetic Models with Rate Data At 274.0°C....................223

6.14 Kinetic Models For Various Forms of the Autoinhibition Dependency....................228

1. INTRODUCTION

One of the important objectives of catalytic research is to obtain understanding of reaction mechanisms. A practical reason for searching for the 'true' mechanism is that, in reactor design, extrapolation to new or more favourable operating conditions is much more safely done when the mechanism is known. Classically, the measurement of the kinetics of a homogeneous chemical reaction has been used to deduce the mechanism of the reaction. In heterogeneous catalyis, one is generally ignorant of the surface concentrations at which the catalytic processes take place. Consequently kinetic studies alone are not so useful in providing information on the mechanism, and they can serve only to eliminate some possible reaction schemes. In addition one major difficulty that arises is that more than one set of mechanisms that fit the observed data quite well can often be proposed. To eliminate and/or understand plausible reaction mechanisms, it is necessary to obtain experimental data by independent means. For this reason, other methods such as tracers, infrared and various spectroscopic techniques to study surfaces have been used to infer reaction intermediates.

Ideally, one would like to observe the catalyst surface at the molecular scale. Infrared spectroscopy is a powerful tool to examine the bonds that form between reactants or products and catalysts during a chemical reaction. Like the reaction kinetics, the infrared spectra are influenced by the conditions at which the spectra are taken. There is no guarantee that the spectra during reaction are similar to the spectra obtained by chemisorption during adsorption or desorption experiments. To better understand surface behaviour on a working catalyst, the infrared spectra must be taken during the reaction. Thus, a combination of simultaneous kinetics and infrared spectral analyses would be expected to provide more information on reaction mechanisms than by either method alone.

The first aim of this work was to develop a reliable apparatus to enable the simultaneous measurement of infrared spectra and kinetics. Important design considerations that have been frequently overlooked in older studies are analysed in chapter 3 of this work. Details on the construction of the actual infrared-cell recycle reactor system are presented in chapter 4, while useful as well as important operating refinements of the reactor are given in the folowing chapter.

The heterogeneous alumina-catalyzed dehydration of isopropanol was chosen as a model reaction to demonstrate the attributes of the new reactor. It was intended to arrive at a kinetic model that incorporates some key features displayed by the catalytic surface during reaction and as revealed uniquely and independently by infrared.A critical review of this reaction system and related subjects is provided in chapter 2 to-gether with criticisms.

2. LITERATURE SURVEY

2.1 Properties Of Catalytic Aluminas

Aluminas have been widely used as adsorbents and catalysts . In industrial catalytic processes, aluminas are mostly used as catalyst supports(1), particularly for noble metals in catalytic reforming. Aluminas are able to activate hydrogen-hydrogen, carbon-hydrogen and carbon-carbon bonds with varying efficiency. From knowledge of both the structure and the surface of aluminas, it is hoped that a better understanding and interpretation of reported chemisorption and catalytic data can be obtained.

2.1.1 The crystalline structure of catalytic aluminas

Alumina ,Al_2O_3, occurs in various crystallographic modifications among which the γ- and η- phases are the most important catalytically. These modifications have been studied in detail by Lippens(2-3). Both γ- and η- AL_2O_3 possess defect spinel lattices which are slightly tetragonally distorted(4). The unit cell is built up by 32 oxygen atoms and only 21 1/3 aluminum atoms arranged in the 16 octrahedral and 8 tetrahedral positions in the spinel structure. According to Lippens(2), the oxygen lattice is made of a cubic close-packed stacking of oxygen layers. In a single crystal diffraction study, Lippens and de Boer(5) found that the oxygen lattice of γ-alumina should be fairly well ordered. Consequently the disorder in γ-alumina is mainly determined by the disorder in the configurations of the aluminum cations. In spinels like $MgAl_2O_4$, the aluminum cations occur in octrahedral sites and the magnesium cations in tetrahedral sites. An excellent description of the spinel structure can be found in the book by Galasso(6) where the position of each individual atom of the ideal spinel $MgAl_2O_4$ is illustrated. In defect spinels like Al_2O_3 the octahedral sites are preferentially occupied and introducing a notation in which tetrahedral and octrahedral Al are given as [Al]t and [Al]o, the aluminas can be represented as $[Al_{2/3}]t[Al_2]oO_4$ (7). The main structural differences between the various modifications of alumina are probably the different ratios of [Al]t :[Al]o as well as the differences in packing density of the oxygen lattice (8).

2.1.2 Surface models of catalytic aluminas

It is generally believed (9) that the alumina surface terminates in oxygen anions rather than cations because of their greater polarizability . Accordingly the outermost aluminum atoms lie below the outermost oxide plane. For energetic reasons, water forms hydroxyl groups on the surface of oxide catalysts. As dehydration proceeds upon heating,

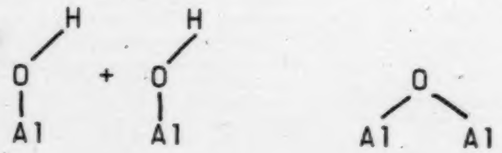

(2.01)

water molecules are eliminated by recombination of surface hydroxyl groups (10).

This process exposes aluminum and oxide ion sites in the surface. The nature and properties of these generated sites will be discussed in 2.1.3.

One of the most important studies of the alumina surface structure was made by Peri (11-13) using gravimetric and infrared data as a guide, in a computerized simulation of the dehydration of a fully hydrated surface on exposed (100) crystal planes. During dehydration adjacent OH ions are assumed to combine at random, but only about two thirds of the OH ions can be removed without disturbing local order (no two or more adjacent sites are left vacant). Further dehydration requires the creation of oxide and vacancy disorder. Random removal of all hydroxyl pairs leaves the surface as illustrated in Figure 2.1. Five different types of hydroxyl groups having from zero to four nearest oxide neighbours are predicted and their corresponding infrared vibrational frequencies are shown in Table 2-1. The presence of free hydroxyl groups on the surface has been shown by deuterium exchange as well as by infrared spectroscopy (14-15). The environmental differences of the OH groups were assumed to lead to different acidic properties of the hydroxyl groups. Peri (12) suggested that the low frequency hydroxyls (3700 cm^{-1}) were the most acidic, and the high frequency hydroxyls (3800 cm^{-1}) the least acidic ones. However, the exchange of deuterium with the latter is appreciably higher than that of the other hydroxyls (14-15). The

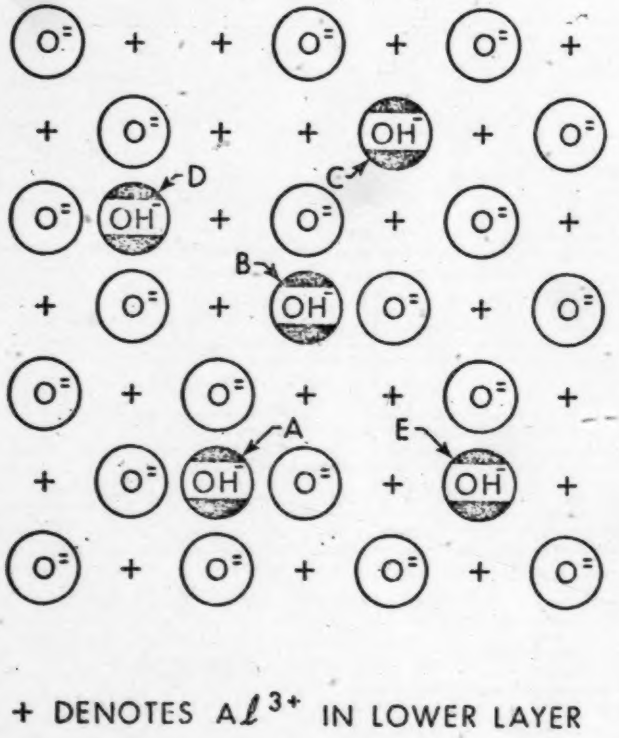
O=
OH-
A
B
C
D
E
+ DENOTES Aℓ3+ IN LOWER LAYER

Figure 2.1 Model of Peri on arrangement of OH groups on alumina

Table 2.1 IR Spectra of Hydroxyl Groups on Alumina

Band	Wavenumber, cm^{-1}	No. of Nearest Oxide Neighbors
A	3800	4
B	3780	3
C	3744	2
D	3733	1
E	3700	0

*with reference to Figure 2.1

assignment of the observed OH-stretching bands remains ambiguous and renders a discussion of the nature of surface sites rather difficult. These contradictions probablypoint to the two weakest points in Peri's surface model.

First, the surface of aluminas is much more complex and crystal faces other than the (100) face might also be exposed (16-17). His model can in fact only be applied to square lattices in which only equivalent OH configurations occur; therefore it is not applicable, for example, to the (111) face. This implies that the assignment of the OH-stretching vibrations by Peri does not take into account the different bonding character of the surface OH ligands in the various possible configurations. The second weakness (18) lies in the assumption that the number of nearest oxide neighbors in the surface is the dominant factor that determines the OH-stretching frequency. It is argued (18) that inductive effects usually are not effectively transmitted through more than two bonds and since the influence of an anion nearest neighbor in the surface has to be transmitted through four bonds, their effect upon the OH-stretching frequency should be minor.

In a series of papers, Zecchina (19), Borello et al. (20) and particularly Morterra et al. (21) have pointed out that the coordination of surface OH groups should be an important factor in determining the OH-stretching frequency. Morterra et al. (21) assigned the OH-stretching bonds in the range, 3760-3800 cm^{-1}, to OH groups belonging to the coordination sphere of tetrahedrally coordinated Al^{+3} cations and those in the range 3700-3750 cm^{-1} to OH groups shared by an octahedrally and tetrahedrally coordinated Al^{+3} cation,

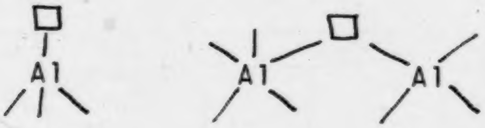

(2.02)

where the square represents an OH group. This new approach was developed in detail in a recent review by Knozinger (18). All possible types of OH configurations occurring on the three faces (111), (110), and (100) of aluminas were considered and are summarized below:

1. *Type Ia:* OH group coordinated to a single tetrahedral Al^{3+} cation
2. *Type IIa:* Bridging OH group which links a tetrahedral and an octahedral cation
3. *Type IIb:* Bridging OH group between two cations in octahedral positions
4. *Type III:* OH group coordinated to three cations in octahedral positions
5. *Type IB:* OH group coordinated to a single octahedral cation.

Accordingly a maximum of five different OH configurations should be expected on the alumina surface. Knozinger also used in his review a concept related to the strength of the electrostatic bonds between aluminum and oxygen ions originally introduced by Pauling (22), to estimate the net charges at a surface oxygen atom and a surface OH group in the various configurations. Earlier Jones (23) had demonstrated that the stretching vibration frequency of OH groups depended on their net charge. This enabled Knozinger to assign the detected OH bands with decreasing wavenumber to the corresponding configurations with increasing positive charge. The appearance of five distinct IR bands can now be better explained by the existence of five possible configurations of OH groups in the surfaces of spinel structure. Table 2-2 summarizes the results of his analysis , one more general and satisfying than that of Peri. In fact, taking the recent approach of Knozinger, only one band (Ib configuration) should be obtained in the case of the (100) face of the -alumina taken by Peri for deriving his surface model. The relative basicities and protonic acidities of neighbouring OH ions has also been described as the governing factor (18) during the regular dehydroxylation of the surface. The hydroxylation of the surface in the presence of residual water is clearly understood by comparing the respective net charges of the oxygen anions and of the hydroxyl groups. Following Pauling's electrostatic valence rule (22), the net charge in a stable ionic structure should be equal or nearly equal to zero and on Table 2-2, this requirement is always better approximated when OH groups instead of oxygen are the surface ligands.

Some evidence in support of the adequacy of Knözinger's

Table 2.2 Possible OH Configurations on Alumina

Crystal face	Configuration	Coordination Al(VI)	numbers Al(IV)	Net charge at O	Net charge at OH	OH frequency cm^{-1}
(111)	III	3	--	-0.5	+0.5	3700-3710
	IIb	2	--	-1.0	0	3740-3745
	IIa	1	1	-0.75	+0.25	3730-3735
	Ia	--	--	-1.25	-0.25	3760-3780
	Ib	1	--	-1.5	-0.5	3785-3800
(110)	IIb	2	--	-1.0	0	3740-3745
	Ia	--	1	-1.25	-0.25	3760-3780
	Ib	1	--	-1.5	-0.5	3785-3800
(100)	Ib	1	--	-1.5	-0.5	3785-3800

surface model will now be reported. One type of hydroxyl group, namely that exhibiting the highest stretching at 3800 cm^{-1} on alumina is sufficiently basic to react with CO to form a bicarbonate ion (24-25). Similarly, Amenomiya and co-workers (26) by using $C^{18}O_2$ showed recently that the oxygen of alumina surface corresponding to the hydroxyl groups at the highest frequency is exchanged readily with carbon dioxide, probably through bicarbonate and/or bidentate carbonate ions even at room temperature, while the oxygen atoms of other hydroxyl groups are exchanged only at high temperatures. According to Knozinger's model, the ease of removal of OH groups should parallel their basicity (i.e. their net negative charge) and in agreement with Amenomiya's results, these labile OH groups (high frequency stretching) correspond to the Ia and Ib configurations of Table 2-2.

When chemisorbed pyridine is treated at more than 400°C, new IR bands develop (1634 cm^{-1}, 1553 cm^{-1}, 1368 cm^{-1} and 1294 cm^{-1}) which have been assigned by Knözinger et al. (27) and very recently by Morterra et al. (28) to an pyridone species. Their formation through a nucleophilic attack of a surface OH group absorbing at 3780 cm^{-1} onto the 2-position of the aromatic ring was postulated. In fact, the 3780 cm^{-1} bond is not reformed at any evacuation temperature. This tends to confirm the higher basicity of the high-frequency hydroxyl groups in conformity with Knozinger's model.

Finally, using infrared spectroscopy Chukin (29) recently showed the existence of NH_4^+ ion on alumina when contacted with ammonia and that these species were formed by interacting with the low frequency acidic OH groups. The other OH groups were not influenced by the presence of ammonia and cannot be considered as Brönsted acidic centres. In the same paper, the Bronsted acidity of the low frequency vibrating hydroxyl groups (3665 cm^{-1}) was confirmed by their exchange with sodium ions.

2.1.3 The active sites of catalytic aluminas

The activation of catalytic aluminas occurs during their dehydroxylation at high temperature (300 - 700°C). According to Knozinger , the elimination of neighboring OH groups will tend to minimize the charge defects created by the removal of either a proton from a surface oxygen or an OH group from a coordination site in a given crystal plane. This regular dehydroxylation process forms CUS (coordinately unsaturated sites) ,oxygen anions (Lewis basic sites), and anion vacancies which expose CUS aluminum ions (Lewis acid sites). Numerous thermogravimetric analysis data are available in the literature on the dehydration of both γ- and η-Al O . The percent monolayer coverage as well as the OH groups retained on the surface have been shown as a function of the dehydroxylation temperature in figure 9 of (18). It is apparent that comparable degrees of dehydroxylation at similar temperature were obtained in the data reported in the various sources (13,30-35). Later, this study on the kinetics of dehydration of isopropanol (in the presence of water) will be performed around 500 K; therefore, it is of particular interest to expect a fractional monolayer coverage of roughly 0.5 under these conditions. This coverage corresponds to roughly 10^{14} cm^{-2} Lewis acid and Lewis base sites on the exposed surface. From specific poisoning experiments, the number of catalytically active sites is generally one or two orders of magnitude lower for many catalytic reactions (39-42). As a result, both Lewis acidic and basic sites produced during the regular dehydroxylation process are unlikely to be involved as active sites. This weakness certainly constitutes one of the main shortcomings of the more or less idealized models of the surface described in the literature. They all fail to predict both structural and energetic properties required for an active site. Alternatively, the creation of special site configurations may be responsible for the catalytic activity of transition aluminas. It is well known, that for stoichiometric reasons, not all of the cation positions can be occupied in the spinel lattice. On the other hand, it is not known how the different planes of the crystal lattice alternate on the exposed alumina surface. Such irregularities may appear as corners at the boundaries of adjacent crystal planes. Both situations could lead to the formation of several unusual defect site configurations of low probability.These provide the catalytic activity of aluminas and such populations cannot be predicted from idealized surface model considerations. The density of the defect sites created during dehydroxylation can be expected to be much lower than that of the lattice sites and to equal roughly the experimentally determined number of active sites for various catalytic reactions (18).

2.1.4 Acid-base and redox properties of catalytic aluminas

More generally, oxides like alumina expose cations, oxygen anions and hydroxyl groups.The surface coordinative unsaturation of these groups is considered to cause the activity or reactivity of the various surface sites (43). Alternatively, many workers describe the surface properties of oxides in terms of surface acidic and basic sites (44) and even reducing and oxidizing sites. Various physical chemical methods are available to determine acidity (45), but the values from the different methods do not agree and even differ widely. Moreover,several methods do not allow one to distinguish clearly between protonic and aprotonic centres(spectroscopic methods may permit differentiation between electron acceptor and proton donor centres). Pyridine as a base may donate an electron pair or accept a proton and thus,may interact with either type of center. The use of infrared spectroscopy has the advantage that the band character resulting from each type of interaction is reasonably characteristic (46). While the silica-alumina catalysts display strong Brönsted acidity by this method (46-48), the absence of Brönsted acidity and the existence of Lewis acidity has been verified on pure alumina (48-50). Using acid-base indicators, Pines and Haag (51-52) have shown that the seat of acid activity in η-alumina consists of Lewis, not Brönsted acidity. Acid-base properties are demonstrated by the capability of chemisorbing basic molecules such as amines, N-heterocycles, nitriles, ketones as well as acidic molecules such as CO_2 , BF_3 , carboxylic acids and phenol. Details of specific studies on alumina and their limitations were reviewed extensively by Knozinger (39). One drawback is the difficulty in discriminating between surface sites that purely adsorb the probe molecule and those which are actually involved as active sites in a particular catalytic process. The possibility of "multicenter sites" (acid-base pair sites) which actively interfere in catalytic elementary processes and which are modified by either acidic and/or basic molecules,also exists.

In addition to its large numbers of acid and base centres, alumina is also known for its activity in catalytic redox processes. In his pioneering work, Greenler (53) found that alcohols were oxidized at elevated temperatures on the alumina surface even with carefully controlled absence of oxygen. The oxidized species of alcohol formed on the surface were identified as aluminum carboxylates by infrared spectroscopy. It appeared that one of the oxygen atoms of this complex originated from the oxygen surface lattice. Independent ESR measurements made later by Ono and Keii (54) confirmed Greenler's discovery. The presence of reactive oxygen atoms on alumina was also shown by Basset (55) who reported that the number of these highly reactive oxygen atoms is 0.1 atom/nm^2. Further evidence of the oxidizing capability of alumina was provided by Parkyns (56), when he studied the adsorption of CO on alumina. The resulting infrared spectra displayed characteristic bands of adsorbed CO_2.

Oxidizing and reducing properties of alumina are manifested also in its ability to oxidize anthracene, perylene and phenotiazine to the corresponding cation radicals (57-59) and to reduce tetracyanoethylene, di- and trinitrobenzenes to the corresponding anion radicals (59-61). Because of the one-electron transfer process with the surface, the resulting species are spin-unpaired and give strong resonance absorption when investigated by ESR spectroscopy. The existence of one-electron accepting centres (oxidizing) and electron donating centres (reducing) is suggested by these processes. Previously, Lewis acid and base centres have also been defined to be acceptors or donors of electrons, but in these cases, a simultaneous transfer of an electron pair occurs. Nevertheless the fact that both types (redox and acid-base) of surface centres are electron-acceptors and electron-donors has brought up the idea that the same centres could play the role of acidic centres with one adsorbate and the role of oxidizing centres with other substrates. This concept of the double nature of Lewis centres was first suggested by Schwab and Kral (67).

Although this duality has been criticized by Flockart and Pink (68) as "undesirable and confusing", it will appear in the following that the distinction between the sites involved in acid-base reactions and those in redox reactions is not obvious.

Ghorbel et al (69) have found that in the case of alumina, oxidizing and reducing centres are the same centers as the acidic and basic sites taking part in the acid-base catalyzed reaction , isomerization of 1-butene into 2-butene. They discovered that the reaction was poisoned both by ammonia and phenotiazine (which are poisons for acidic and oxidizing sites, respectively) and by acetic acid and TCNE (poisons for basic and reducing sites, respectively). Their conclusion was that the reaction required the simultaneous participation of two centres: acid centres with oxidizing nature and basic centres with reducing character. In relation to the dehydration of alcohols on alumina Figueras Roca (70) found a strong inhibiting effect of TCNE. They concluded that this type of reaction requires the simultaneous presence of acidic and basic (reducing) sites. In another paper Knözinger and Müller showed that the spin concentration of the perylene cation on alumina surfaces can be reduced significantly by pyridine adsorption. This result also suggests the participation of Lewis acid sites in the radical cation formation.

A different opinion was expressed by Marczewski and Malinowski (71) who studied the effect of preadsorption of 2-

chloro - 4 nitroaniline (a Hammett indicator strongly adsorbed on basic centres corresponding to (H >17.2) on the ESR signal of TCNE anion radicals. They concluded that in the case of alumina, basic and reducing centres coexist independently since the adsorption of the mentioned indicator did not change the appearance of the ESR signal due to $TCNE^-$ anion radicals.

The existence of interdependent electron- donor and acceptor sites on alumina has been demonstrated by Flockart and coworkers(61). A strong increase in the intensity of trinitrobenzene radical anion was observed when perylene was preadsorbed. An analogous behaviour occurs when the sequence of the adsorption compounds is reversed; the signal of perylene cation radicals was enhanced by the addition of 1,3,5,-trinitrobenzene. Designating by A an electron-acceptor centre and by D an electron donor site, the electron-donating capability of D is insufficient to convert trinitrobenzene into a radical anion. When the electron coming from chemisorbed perylene on centre A is present, it reinforces centre D to the point where electron transfer occurs as depicted in (2-3).

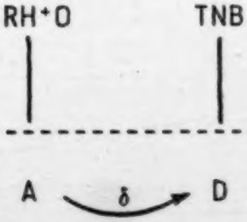

(2.03)

These results show that on alumina (and other oxide surfaces), electron-donor and acceptor sites exist in close proximity and that they are interdependent. The coordinative acid-base sites on alumina are possibly associated with an abnormally exposed aluminum ion and a defect centre containing oxide ions.

2.2 Infrared Studies Of Adsorption Of Alcohols On Alumina

Infrared spectral studies of the adsorption of alcohols on alumina surface using the in situ technique have been reported previously and three different types of surface species were observed:

1. molecular alcohol adsorbed via H bonds (62-64)
2. alkoxide groups formed by dissociative adsorption (36-38,53,62,63,65-66)
3. carboxylate structures formed by oxidation of the alcohol (62,63,53,65-66,71,72)

The molecular adsorption of alcohols has been well documented by Knozinger (73). NMR studies showed that the hydroxyl group of the alcohols interact directly with the oxide surface (74). This is confirmed by the absence of the free alcoholic stretching vibration on the infrared spectra of adsorbed alcohol. The simultaneous perturbation of the free surface hydroxyl groups can be most easily interpreted by the reaction of H-bonds between the alcoholic group of the adsorbed molecule and the surface OH groups as proposed in (2.04) by Kagel (62) and by Deo et al.(63). These species, which display an infrared spectra similar to its liquid counterpart is weakly H-bonded to the surface since it is readily desorbed hy evacuation at room temperature. Consequently, the relevance of such labile species in the dehydration of alcohols can be almost ruled out, because their presence at reaction temperature is very unlikely.

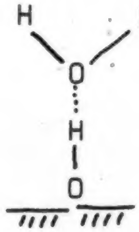

(2.04)

2.2.1 Alumina alkoxide structures

By comparison of the IR spectra of adsorbed phases with those of solid alkoxides, Greenler (53) first suggested the presence of surface alkoxides groups upon adsorption of ethanol or methanol. Similar results were obtained later with 1-propanol (62,38), 1-Butanol (62,38) and benzyl-alcohol(65). In the case of isopropanol, of particular interest in this work, the presence of alkoxide species was also postulated by Treibmann and Simon (66). Their evidence can however be questioned. It was clearly established elsewhere (17) that in aluminum isopropoxide the aluminum-oxygen-carbon linkage gives rise to a specific absorption band at 1033 cm^{-1}. In practice, the substantial lattice absorption of the alumina support in this region makes the observation of the 1033cm^{-1} band very difficult, and this interference was not mentioned by Treibmann and Simon. On the other hand, with the exception of this 1033 cm^{-1} absorption band, the spectra of liquid isopropyl alcohol and aluminum isopropoxide are not easily differentiated and so, this matter remains controversial. Similarly, Chuang (75) proposed the presence of alkoxide in the cases of 2-propanol, 2-butanol and 3-pentanol without strong spectroscopic evidence. Because of the absence of the characteristic bands of their respective alkoxides, other authors (65) disclaimed the formation of alkoxides on adsorption of isobutanol, cyclohexanol and t-butanol.In their study, the chemisorbed species, relatively strongly bonded to the surface, displays a sequence of bands similar to those of the corresponding liquid alcohols. However, because of their relative stability and low concentration on the surface, these chemisorbed species cannot be mistaken for physically H-bonded species and their quick disappearance at temperatures equivalent to the onset of the dehydration reaction suggests their participation in some intermediate stage of the reaction.

In summary, depending on the substrate used, two kinds of chemisorbed entities appear to be formed on the alumina surface. For the more simple primary alcohols, alkoxide species have been observed without ruling out the presence of other chemisorbed entities. With secondary and tertiary alcohols, adsorbed species not necessarily identifiable with alkoxides are usually observed. Quite judiciously, Knözinger

(73) pointed out that in parallel with the formation of alkoxide species during adsorption, the corresponding alcohols yield ether, at least at low temperatures . Thermochemical investigations of the alkoxide stability show analogous distinctions (76). In the absence of contrary evidence it is quite plausible that the surface alkoxides observed to be present are directly concerned with the selectivity during dehydration of alcohols on alumina. We should also be aware that the different ratios of -OR radicals to Al atoms between surface alkoxides and aluminum alcoholates may greatly complicate the interpretation of infrared spectra.

The question concerning the sites involved in the formation of alkoxides is crucial to the interpretation of their role. Again no unanimous agreement exists on this subject. Two possible routes for the formation of alkoxides by dissociative adsorption have been proposed:

1. a hydroxyl proton may be split off to form a surface OH group, while the alkoxide residue occupies an oxygen vacancy in the surface (Lewis center) as in (2.05);

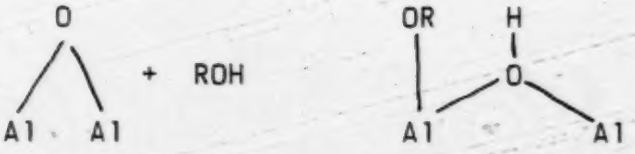

(2.05)

2. the C-O bond of the alcohol may be broken, the resulting hydroxyl group filling an oxygen vacancy on the surface

while the alkyl residue adds to an adjacent oxygen ion. The somewhat lower energy of rupture of the C-O bond in the free alcohol favors the second alternative. Recent infrared results (75) with ethanol using an alumina surface enriched with O^{18} favored the second possibility. In both cases however, the alkoxide formation necessitates acid-base pair sites (incompletely coordinated surface aluminum ions adjacent to a surface basic oxygen). In the previous schemes, the alkoxide reaction was considered dissociative in nature,however ,undissociated intermediate alkoxides as shown in (2.06) have been proposed by Bremer (17).

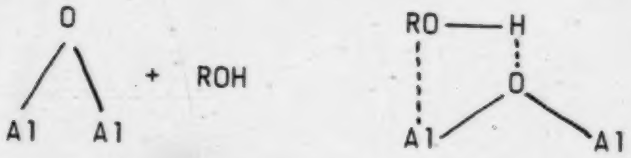

(2.06)

If such species do exist, their spectral characteristics should lie between those of alcohols and alkoxides. This may explain the ambiguities encountered in the interpretation of infrared spectra of chemisorbed alcohols. The chemisorbed entities in (2.5) were considered by Bremer as the essential intermediate in the dehydration reaction; his argument was based on the concept that more conventional alkoxides were too stable to decompose into olefin and water. It is ,unfortunately, conceivable that the alkoxide stability will be dependent on the substrate molecule and thus, varying degrees of dissociation into surface alkoxides may be expected for different alcohols. Analogously, the heterogeneous distribution in strength of the acid-base pair sites of a surface may also give, more or less, dissociated alkoxide species for the same alcohol. These differences may help to explain why the thermochemically more stable aluminum alkoxides of the primary alcohols have been the only ones observed unequivocally by infrared measurements. In addition to the energetic factor, from a steric standpoint it is easier for the normal alcohols, because of their less bulky hydrocarbon chain, to coordinate on the exposed aluminum cations which lie below the oxygen anion outer layer, than for the more highly substituted alcohol molecules to do so.

The proposition that alkoxide-like structures are intermediates in the monomolecular dehydration of alcohols remains speculative and other views have also been advanced. Earlier, the physically H-bonded alcohol species (I) was stated to be too weakly bonded to the catalyst to be considered as a possible reaction intermediate. The stability of this latter species may be increased by additional bonding to the surface as shown in species (2.07).

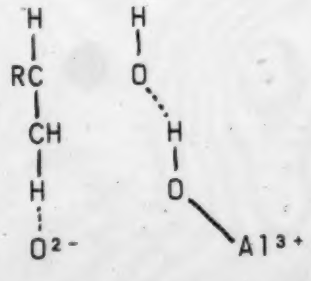

(2.07)

the alkoxide reaction was considered dissociative in nature, however, undissociated intermediate alkoxides as shown in (2.06) have been proposed by Bremer (17).

In fact such two-point adsorption species have been proposed as intermediate complexes for the monomolecular dehydration of alcohols by Knozinger (73) and by Chuang and al.(78). At this point, one realizes that the infrared technique alone is not sufficiently sensitive to permit differentiation of the subtle differences between the vibration frequencies of all the postulated intermediate reactive species. More on this topic will be presented in the next section of this chapter where kinetics, poisoning and isotopic effects are combined with infrared observations.

2.2.2 Carboxylate structures

These are the most stable species formed by the interaction of alcohols on alumina. They are formed by oxidation of the alcohols above 170°C and have been observed by infrared for methanol (53,72), ethanol (53, 66, 69, 72), 1-propanol (62, 65, 79), 1-butanol (62, 79), 2- propanol (66, 72), benzyl alcohol (80) and isobutyl alcohol (80). Moreover, no indication of a surface carboxylate was found by Knözinger, et al.(65) in the case of t-butanol. In view of their high stability up to 500°C, these surface carboxylates are unlikely to be involved as intermediates in surface reactions below 300°.The infrared identification of these species is based on the similarity of their absorption bands to those of aluminum formates and acetates (53). The splitting of the vibrational absorption bands of COO^- during the adsorption of alcohols on alumina enriched with isotope O^{18} (79) indicates the participation of surface oxygen atoms of the catalyst in the carboxylate structure formation. Alkoxide species were observed to transform into carboxylate compounds by elevating the temperature (53, 62). An exellent paper by Fink (72) gives a satisfactory interpretation ofn the nature and mechanism of formation of carboxylates. At the beginning of the dehydration reaction of isopropanol, when carboxylates are formed, Fink also detected some dehydrogenation products (acetone). He concluded that since acetone readily forms carboxylate species,the latter originate from acetone-like species. The reaction scheme is depicted below and was later confirmed by Chuang,et al. (78).

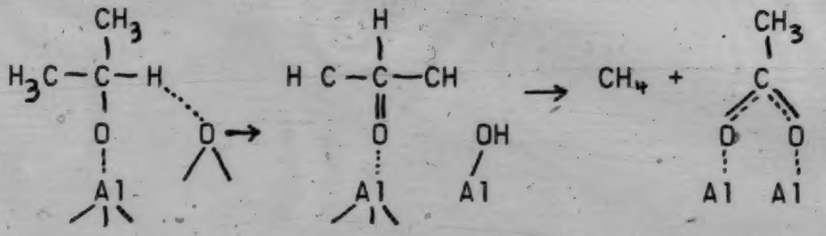

(2.08)

Both authors observed by mass spectral analysis the presence of hydrogen and methane. In the case of CO (72) ,bicarbonate species are formed analogously. Fink concluded that the OH groups having the greatest formal negative charge (the most basic OH groups) should be best favoured for these reactions. Recalling section 2.1.2 ,these OH groups correspond to the high frequency hydroxyl groups. The stability of the carboxylate species can be easily explained. The surface of alumina surface possesses electron donor centres as well as electron acceptor centres. The lowest energy state of the surface will be obtained when both electron donor (basic) and electron acceptor (acidic) sites are saturated by coordinative bonds, and the simultaneous saturation of the dual sites by the carboxylate structures satisfies these requirements. Although these species represent the most stable surface state, they are formed with a sufficient velocity only at high temperature because of some high activation energy probably related to the geometric requirements.

It may seem superfluous to extend the discussion concerning the carboxylate species since their high thermal stability tends to exclude them as possible intermediates in the dehydration reaction. Nonetheless, it seems likely that the activity of alumina towards different catalytic processes is lowered by the formation of these species on its strongest sites. According to scheme (2-6), both acidic and basic properties are required for their formation. Acid-base pair sites have been shown to be important in cracking reactions (77) and in double-bond isomerization of olefins (78) by specific poisoning experiments even though their chemical nature and their action in the activation of reactant molecules are not well understood (56). The formation of carboxylates on such sites should therefore alter the catalyst activity. It is not emphasized enough in the literature that various reactions on the same catalyst may well occur on chemically similar active portions of the surface, the difference being that sites of greater or lesser activity are necessary for the various processes. This argument parallels the well-known ones advancing the heterogeneity of catalytic supports (like oxides) which is not predicted by any simple surface model.

2.2.3 Adsorption of water

The catalytic activity of a wide variety of reactious and particularly the dehydration of alcohols is reduced in the presence of water. Water is a Lewis base that can be retained by incompletely coordinated surface cations according to (53) and as shown in (2.09),

$$H_2O + [Al^{3+}]_s \qquad [H_2O \rightarrow Al^{3+}]_s \qquad (2.09)$$

$$H_2O + [Al{-}O]_s \qquad [Al{-}OH]_s + [OH]_s \qquad (2.10)$$

or it can be dissociatively adsorbed on metal-oxygen pair sites(2.10),

Apart from these chemisorbed species, various types of H- bonded species have been recently discussed by Knozinger (81). These latter species are physically adsorbed at room temperature and can be removed from the surface by heating the catalyst to 150°C and should not be present above 200°C. Accordingly, under reaction conditions, the influence of water can be mainly depicted by the two above equations. Equation (2.09) can be related to the amount of reversibly chemisorbed water while equation(2.10) corresponds to the amount of irreversibly dissociated water held on the alumina surface. In section 2.1.3 it was showed that in the absence of water, the degree of hydration of the surface depends only slightly on the temperature. In the narrow temperature range of these kinetic studies (see Chapter 6) , it is reasonable to assume that the amount of water irreversibly held on the surface is constant. The influence of the presence of water during reaction probably corresponds to the process of equation (2.09) for the reversibly coordinated water molecules on the surface (82).

2.3 Dehydration Reactions Of Alcohols On Alumina

Many questions must be answered satisfactorily before the mechanism of a given reaction is said to be known. As was well expressed by Hall (83), "...the following should be answered at a reasonable level of refinement. What is the reaction scheme, as derived from chemical evidence or tracer experiments What are the reacting species What are their relative concentrations What are the modes by which they interact What are the relative values of the rate constants of the unit steps, and which is therefore rate limiting Given the last, what is the true activation energy of the reaction and what does the reaction coordinate look like As one proceeds to answer these questions, one at a time, the mechanism becomes known with increasing sophistication...". The reader is referred to the original article (83) for a detailed enumeration of the different methods and techniques necessary to the elucidation of the task at hand. The following section reviews the knowledge that is most relevant to the dehydration of alcohols on alumina.

2.3.1 Reaction scheme

The dehydration of alcohols on alumina catalysts lead to the formation of ethers, olefins and water. An extensive survey of alcohol dehydration was published by Pines and Manassen for work done prior to 1966 (84). A parallel consecutive scheme is generally accepted which may be written:

$$\begin{tikzcd}
 & E + W \arrow[dl, shift left] \arrow[dr] & \\
2A \arrow[ur, shift left] \arrow[dr] & & A + O + W \arrow[dl] \\
 & 2O + 2W &
\end{tikzcd} \qquad (2.11)$$

A, E, W and O representing alcohol, ether, water and olefin respectively. Both kinetic analysis (85) and the use of labelled isotopes (86) have provided evidence for this scheme in the case of ethanol. Under normal conditions, the equilibrium is far to the right for all the steps although it is not clear whether the reversible ether formation reaction is in equilibrium. This reaction scheme (2.11) has been verified with unbranched primary alcohols up to n-hexanol by Knozinger and Kohne (73). For secondary alcohols such as isopropanol, isobutanol and also t-butanol (73,87,88), the formation of olefins is predominant. The dehydration of isopropanol results in only small amounts of isopropyl ether with simultaneous formation of propylene. For alcohols of higher molecular weight, the secondary isomerization of the primary olefins formed follows the dehydration process (89). Isopropanol is therefore very suitable for kinetic studies since dehydration of olefin is the predominant primary step and the propylene produced is not affected by consecutive isomerization steps. The reaction scheme is then simply written:

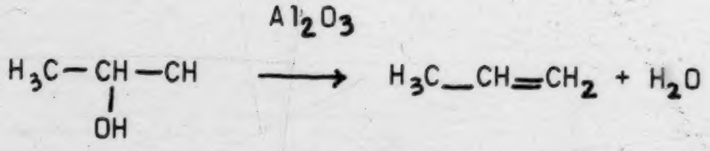

$$H_3C-\underset{\displaystyle OH}{\underset{|}{CH}}-CH \xrightarrow{Al_2O_3} H_3C-CH=CH_2 + H_2O \qquad (2.06)$$

2.3.2 Earlier postulated mechanisms

Widely different views concerning the mechanism and the nature of the sites involved in the dehydration process have been postulated and are reviewed in detail in (17,73,75). Actually, ionic, radical and covalent intermediate complexes were proposed:

1. The carbonium ion mechanism requires the proton addition from Bronsted acidic centres to the alcohol molecule. This picture is very unlikely as discussed by Chuang in his thesis (75) due to the lack of proton acidity of the surface and kinetic isotope effects contrary to the expectations of a carbonium ion mechanism.
2. Vasserberg suggested a free-radical mechanism (91). Free radicals from compounds having extremely strong electron-donor properties have in fact been detected on aluminum oxide surfaces by U.V. and ESR studies (see

section 2.1.4). These donor properties are not so pronounced in alcohols as in the aromatic compounds studied. Besides, since free radical mechanisms proceed preferentially in apolar media, whereas the surfaces of metal oxides must be regarded as polar (92), this route seems rather unlikely.

3. A covalently bound adsorptive complex is the most probable intermediate complex. The monomolecular dehydration process requires the rupture of the C_β-H and C_α-O bonds in the alcohol molecule since β-eliminations always appear to occur if the molecule contains β-hydrogen atoms (84,95).

Eucken and Wicke have demonstrated that in the case of a deuterated alumina surface, one of the hydrogen atoms of the produced water comes from the catalyst surface (94). Therefore, the water molecule may already be substantially formed in the adsorption complex under the conditions of catalysis according to the principle of least structural change. As a result a two-point adsorption of the alcohol molecule involving both acidic and basic centers (84) has been generally adopted.

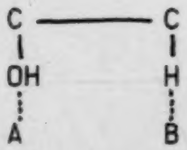

$$\begin{array}{ccc} \mathrm{C} & \text{———} & \mathrm{C} \\ | & & | \\ \mathrm{OH} & & \mathrm{H} \\ \vdots & & \vdots \\ \mathrm{A} & & \mathrm{B} \end{array} \qquad (2.13)$$

Thereafter, much effort was devoted to ascertain which two of the three atom configurations of the alumina surface were involved in the dehydration process (OH groups, oxygen anions, or aluminum cations). Some references to each alternative are now given:

1. Al cations - Oxygen anions (89,95,96);
2. Al cations - Hydroxyl groups (17);
3. Hydroxyl groups - Oxygen anions (73,90).

A clear answer to this particular problem has not yet been found. Controversy remains regarding the participation of the coordinately unsaturated aluminum cations generally described as Lewis acid centres. To clarify this point, numerous poisoning experiments were conducted by using nitrogen bases such as ammonia, pyridine, etc., to poison these sites. Unfortunately the conclusions from these studies are contradictory. On one hand, it is claimed that the dehydration activity of the alumina catalyst is hardly influenced by these poisons (97-99). On the other hand, it has been stated by Bremer (17) that the dehydration activity is proportional to the Lewis acidity of various aluminas, which was measured by the chemisorption of basic molecules such as ammonia and pyridine, thereby suggesting the participation of Lewis acid sites in the reaction. Similarly, Soma and his co-workers (100) deduced from their dynamic treatment that a surface alkoxide species formed on Lewis acid sites is the intermediate in olefin formation. If their view is correct, one would expect a strong poisoning effect by pyridine. More detailed studies are necessary to resolve these discrepancies. In fact the interpretation of data from specific poisoning experiments is subject to pitfalls and ambiguities.

Apart from the fact that catalysts, reactants and operating conditions differ in each study, some arbitrariness is always introduced in stating that a particular poisoning agent interacts with an active site of a defined chemical nature. For instance, the number of hydroxyl groups or aluminum cations or oxygen anions is certainly much greater than the number of the true active sites as discussed in section 2.1. Furthermore, in the presence of reactants and products the expected poisoning molecules may be displaced from the surface, their effect being nullified. Also, their influence may be quite different depending whether the poison is preadsorbed or fed with the reactant under reaction conditions. More about these potential difficulties can be found in the excellent review of Knözinger (39). So far, poisoning studies have led to an incomplete and ambiguous picture of the mechanism of alcohol dehydration on alumina.

2.3.3 Detailed isotopic effects

Mechanistic information about the time sequence of bond splitting can also be obtained from kinetic isotope effects. The isotope effect can be used to identify a rate determining step if the reacting bond in question is isotopically substituted. For the alcohol dehydration on alumina, these effects have been extensively studied (101,106) and are summarized in Table 2-3.

Since CH_3OH and CH_3OD or CD_3OH and CD_3OD are dehydrated at equal rates, the rate determining step was ascribed to

Table 2.3 Isotopic Effects in the Dehydration of Alcohols

Deuterated Alcohols	Catalyst	T(°c)	Rate Ratio H/D	Reference
CH_3OH/CH_3OD	Al_2O_3	130-180	1.0	101
CD OH/CD OD	Al_2O_3	130-180	1.0	101
$(CH_3)_2CHOD$	Al_2O_3	300	1.4	102
	ZrO_2	300	1.13	
	TiO_2	300	1.24	
	SiO_2	300	1.47	
$(CD_3)_2CHOH$	Al_2O_3	300	1.44	102
	ZrO_2	300	1.37	
	TiO_2	300	1.25	
	SiO_2	300	1.04	
$(CD_3)_2CDOD$	Al_2O_3	160	4.06	105
	SiO_2/Al_2O_3	160	1.0	
$(CD_3)_3COH$	Al_2O_3	150	2.42	103
$(C_2D_5)CH(OH)CH$	Al_2O_3	150	2.70	103
$(CH_3)_2CDCH_2OH$	Al_2O_3	150	3.44	103
$(CD_3)_2CDCH_2OH$	Al_2O_3	150	3.44	103

the rupture of the R-OAl bond of an alkoxide (101). In the case of olefin formation, the removal of a β-hydrogen suggests that the cleavage of the C-H bond is probably involved in the rate-determining step. Since the isotope effect is identical for $(CH_3)_2CDCH_2OH$ and $(CD_3)_2CDCH_2OH$ on Al_2O_3 at 150-210°C (103), the secondary effect of the CD group is assumed to be negligible. It was also found that the extent of the isotope effect, as well as the activation energy of dehydration increases in the order,

tert-alcohol < sec-alcohol < primary alcohol.

This sequence suggests that the isotope effect increases as the ionic character of the activated complex decreases, because the alkyl group is known to be electron-donating. The activated complex of alcohol dehydration on Al_2O_3 was written (103) according to an E2 mechanism of elimination as per (2.13). The relative bond loosening of the C_α-O and the C_β-H bonds may vary over wide ranges (107) depending on acid-base strength of catalyst and substrate. Thus, asymmetric transition states (108) with the proton near C_β and the C-O bond nearly completely broken (E1-like transition state, favored by strong acids and substrates that undergo ready C-X cleavage to give carbocations) and with the proton near the base and the C-O bond nearly unaffected (E1cb-like transition state favored by strong bases) are possible. The size of the isotope effects for all the alcohols studied suggests an E2-like mechanism which at low temperatures contains ionic contributions. As the temperature increased, the isotope effects were observed to decrease much faster than theoretically predicted. It was therefore proposed that the ionic character of the transition state (E1) becomes more and more pronounced as the temperature is increased.

The dependence of the isotopic effect on the acidity of the oxide catalyst has been demonstrated (102) (see Table 2-3). Koechloefl,et al. concluded that the mechanis changes from E2 to E1 in the above series of catalysts and parallels the acidic nature of the catalyst. Finally, Yamaguichi and Tanabe (105) examined the isotope effect with isopropanol-d and found little effect on silica-alumina at 160°C, in contrast to the isotope effect on alumina at 160°C. Strong Bronsted acidic groups are known to be present on silica-alumina surface and it is likely that the C-O cleavage is involved in the rate-determining step in conformity with an E1-type carbonium ion intermediate.

2.3.4 Stereochemistry of dehydration

As in liquid phase solution, trans-eliminations through a trans-planar transition state seems to be preferred on alumina. Valuable information on this problem is obtained by the choice of model substrate alcohols of suitable structure (84). The predominance of the trans-elimination by β-elimination for aliphatic alcohols has been demonstrated (109,110). Thermodynamically, trans-2 butene is the more stable isomer, but cis-2 butene is preferred as the primary kinetic product. Based on experimental studies of the product distributions, the Arrhenius parameters, and the reactivities of a series of aliphatic alcohols, a new transition state has been proposed recently (111) which explains the transelimination as well as the cis-preference. The alcohol is adsorbed by interaction with a surface hydroxyl and oxide pair (IV). The transition state develops (V) in which formation of a molecule of water is occurring with the formation of a double-bond between the C and C atoms. Successful transition to the alkene occurs when the -hydrogen is removed, a process which can take place if this atom approaches sufficiently

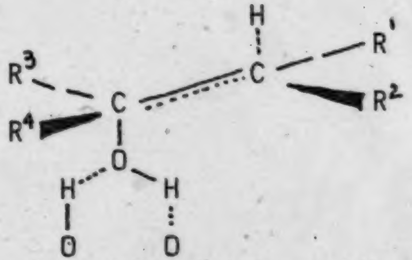

(2.14)

close to a suitable basic site on the surface. Indeed a H-bonded surface intermediate having a partial double-bond character before dehydration and desorption of the olefin take place has been observed by infrared by Deo,et al. (78) for 3-pentanol. Since rotation about the C_α-$C_\beta$axis is precluded by the developing double-bond, it is necessary for the whole transition state structure to move relative to the surface in order to induce the removal of the β-hydrogen. When this occurs, the elements of water are removed from the alcohol in a trans-elimination which is demanded by the nature of an E2 process (112). The approach of the -hydrogen towards a basic site by inclination of the plane defined by the O-C_α-C_β-H plane will be sterically restricted by the presence of alkyl groups at the C_α and C_β positions. Knözinger suggested that the inclination to the surface will occur more effectively to the side of the transition state structure that leads to the lower steric hindrance. This is most favored when the bulky groups are in a cis-conformation so that the transition structure can incline to the surface on the other side. The general preferential formation of the cis-alkene in dehydration reactions is thus explained. The main advantage of the Knözinger- postulated transition complex over the cyclic transition-state proposed by Notari (113) remains in its capacity to explain the experimentally observed stereospecific trans-β-elimination reactions of concerted type (106,114). In a more recent paper, Knozinger and his co-workers (115) add impressive support to their ideas concerning the transition state.

2.3.5 Kinetics of alcohol dehydration on alumina

To more completely understand the mechanism of a heterogeneous catalytic reaction, a knowledge of the reaction kinetics is necessary. Döhse and Kalberer (116) were the first to report the inhibiting effect of water upon the reaction and this was confirmed in all subsequent studies. The olefin formation from alcohols has frequently been explained by a single-site adsorption Langmuir-Hinshelwood model (117-120). The resulting Langmuir-type equation (2.15) includes a term for the inhibition of water. Butt and co-workers (121)

$$r = \frac{kK_A P_A}{1 + K_A P_A + K_W P_W} \qquad (2.15)$$

could also describe their conversion isotherms of the parallel consecutive reaction scheme for the ethylene-ether-ethanol interconversion by means of the same rate equation. On the contrary the kinetics of the dehydration of cyclohexanol (122), isobutanol (115) and Isopropanol (124) were best fitted with a dual-site mechanism equation (2.16) with surface reaction as the rate controlling step. In other studies at sufficiently low temperatures

$$r = \frac{kK_A P_A}{(1 + K_A P_A + K_W P_W)^2} \qquad (2.16)$$

and small conversions where the inhibiting influence of water can be neglected, the rate of reaction is independent of the alcohol pressure over a wide range; the reaction behaviour is thus zeroth order (125-128) and this was verified for the dehydration of aliphatic as well as cyclic alcohols. Because equation (2.16) does not result in a zero-order rate law at high reactant pressure, some discrepancy exists in the experimental findings. A shortcoming of the previous papers is that the number of rate equations tested was limited to one or two. It is also known that a clear discrimination between kinetic models depends strongly on the range of investigation of the experimental variables as well as on the appropriateness of the statistical methods used in analyzing the data (123,130,131). Consequently, there is always the possibility that better equations for describing the experimental data have been overlooked.

Kinetic experiments on the dehydration of isopropanol over alumina were almost perfectly correlated by a dual-dissimilar sites Hougen-Watson equation (2.17) (90)

$$r = \frac{kK_AP_A}{(1 + K_AP_A)(1 + K_wP_w)} \quad \begin{matrix}A\\W\end{matrix} \qquad (2.17)$$

In studying the dehydration of t-butanol (125) and cyclohexonol (126), the inbibiting effect of water was empirically correlated by equation (2.18) where r and r are the reaction

$$r = r_o \frac{\sqrt{P_A}}{\sqrt{P_A} + bP_w} \qquad (2.18)$$

rates under the given conditions and for zero-order, respectively. This expression corresponds to a dissociative adsorption of alcohol on two similar sites and a molecular adsorption of the poisoning water on one of the two centres. This is in conflict with the reaction mechanism proposed by the same author in his earlier investigations where alcohol was molecularly adsorbed. The kinetics of the t-butanol dehydration (132) leads also to rate equations (2.19) and (2.20) for which a dissociative adsorption of the alcohol and a molecular adsorption of water must be assumed.

$$r = \frac{k\sqrt{K_AP_A}}{1 + K_wP_w + 2\sqrt{K_AP_A}} \qquad (2.19)$$

$$r = \frac{k\sqrt{K_AP_A(1 + K_wP_w)}}{1 + K_wP_w + \sqrt{K_AP_A(1 + K_wP_w)}} \qquad (2.20)$$

In kinetic studies, the question of behaviour of chemisorbed molecules on a surface, in particular the choice between models involving localized or mobile adsorption, is important in establishing the mechanism of heterogeneous catalysis (133). Because adsorption is a dynamic process, the adsorbed molecules may return to the gas or they may migrate to other sites on the solid surface while in the adsorbed state. This surface movement is certainly of great importance in catalysis (134,135). The mean free life of a molecule in the adsorbed state will depend essentially on the bonding energy (adsorption heat) and the temperature of the catalyst. Accordingly, a strongly held molecule will tend to remain fixed on the same surface site for a longer period, but its greater adsorbed life also increases its probability of migrating while adsorbed. These reverse effects do not allow us to predict with confidence the occurrence of surface migration. In a simple way, surface migration will be important when the energy barrier Es between adjacent adsorption sites is small compared to the average energy of the adsorbed molecule.

In relation to the dehydration of alcohols, surface diffusion has been advanced as an explanation for unusually large effectiveness factors measured for the dehydration of primary alcohols on silica-alumina catalysts (136). Masanume and Smith (137) found that surface transport of ethanol on silica gel at temperatures up to 175°C predominated over gas phase diffusion. Some evidence for significant surface diffusion in the dehydration of isopropanol at 200-250°C on γ-alumina was also presented by Bienert and Gelbin (138). More recently in a series of papers using a differential isotopic method with C^{14}, Vasserberg et al. (139-140) have demonstrated the surface mobility of chemisorbed alcohol during its dehydration on aluminum oxide and aluminosilicate. In addition, they did some poisoning experiments and concluded that the number of active centers was of the order of 10^{12} sites/m^2. Since the total number of alcohol molecules reacting in the adsorbed layer was up to two orders of magnitude greater than the number of active sites, it was concluded that chemisorbed isopropanol molecules migrate. In view of these data, it appears wise to consider the possibility of surface migration in any evaluation of a reaction mechanism and intraparticle effects for our reaction system.

3. DESIGN CONSIDERATIONS FOR SIMULTANEOUS INFRARED AND KINETIC STUDIES

3.1 Infrared Spectroscopy Of Adsorbed Species

Up to now, among the various spectroscopic tools, IR has proved to be the most useful technique to obtain information concerning the nature and structure of adsorbed species. Absorption bands of surface compounds can be identified if their lifetime on the surface is longer than approximately 10^{-13}s. The early work of Eischens and his collaborators (141) showed that conventional transmission infrared spectrophotometers could be used to record spectra of species at the surfaces of oxide powders or of metals dispersed on oxide powder supports. The successful extension of surface infrared spectroscopy from these early applications to a wide variety of adsorbates and catalysts is attested by the many books and reviews that have appeared subsequently (142-144). Practical aspects of sample preparation and cell construction have been considered by Parkyns (145). The main advantage of the pressed disk method is the large surface area available within the infrared beam, resulting in large concentrations of adsorbed species even at low surface coverages. A typical oxide disk may weigh about 20 mg/cm^2 and possess a specific area of 100 m^2/g. The total surface area in a sample of one cm^2 would then be 2 m^2 ,so that many adsorbents can be used to give sufficiently intense absorption bands for measurement with conventional spectrophotometers. However, the sensitivity of transmission experiments cannot be increased indefinitely by increasing the sample thickness. A limit is set by the absorption and scattering of radiation by the adsorbent itself, so that with increasing sample thickness the adsorbate absorption becomes a larger fraction of a smaller amount of available energy. In particular, the absorption of light by the alumina lattice limits its use by the transmission technique to wavenumbers above 1000 cm^{-1}. Some other commonly encountered difficulties covering the infrared identification of surface species on metal oxides using the standard static "in situ" technique are described by Bozon-Verduraz (146).

With this technique a great deal of important information about the chemisorbed species, such as structure and bonding state of each individual substrate participating in a catalytic process, has been determined for many reaction systems . Nevertheless, such static studies of the adsorbed phase generally performed at room temperature may not provide the kind of information which enables one to follow the evolution of adsorbed species in the course of the catalytic reaction. This is a major limitation of the technique . Therefore, an IR method to study the dynamic behaviour of chemisorbed species and also to measure the overall rate of reaction simultaneously, should provide an effective means of looking at the catalytic surface. A number of simultaneous infrared and kinetic studies have been reported in recent years (75,147-152) and these represent most of the work done to implement this new technique. However, it was felt that, although the different IR reactor cells designed in the past could provide valuable information for some of the systems studied, their use as a practical laboratory catalytic reactor was limited to a narrow range of conditions. Such important factors as contacting between gas phase and catalyst, isothermality in the reaction zone, accurate elimination of spurious gas phase absorbance were either not thoroughly considered or only suitable to the narrow range of experiments investigated. Consequently this study has the objective of designing an improved version of an infrared cell-recycle reactor which can be used as a practical tool by the heterogeneous kinetist, while enabling him to obtain additional information by means of infrared spectra of the catalyst surface recorded during the reaction.

3.2 Design Factors

This section reviews, in more detail, the design factors that should be considered in the development of a new reactor. This should facilitate wider use of this novel technique. Consider first those factors directly associated with obtaining spectra of the adsorbed layer before discussing other factors that are specifically related to the procurement of intrinsic rate data.

3.2.1 Infrared design considerations

With double-beam instruments, when recording spectra at elevated temperatures, it is not possible to exclude emission from the sample. This leads to a strong distortion of the spectra due to the fact that the sample and the radiation detector are at different temperatures, giving rise to an additional thermal flow between them caused by the emission of the sample. This has been shown experimentally for solid samples having different absorptive capacities (153). Eberly (154) was the first one to report the separation of these fluxes by using a spectrometer in which the beam was modulated before the passage of the infrared beam through the sample, in contrast to conventional instruments. As a result, the unmodulated radiation from the heated sample is not recorded by the detector of the instrument. The Perkin-Elmer model 621 used herein was specially equipped with a pre-sample chopper, which excludes the effect of emission from the samples at different temperatures by allowing the filter to pass only the modulated signal.

Another important discrepancy is caused by the presence of the gas phase surrounding the catalyst during reaction. Using the ideal gas-law and a cell pathlength of 10 cm, the number of gas molecules crossed by the IR beam is estimated to be 10^{18}-10^{19} molecules per cm^2 of IR beam.The number of molecules in the gas phase may, as a result, easily be one or two orders of magnitude greater than the number of molecules of the same component chemisorbed on the catalyst surface. A general but practical implication is that unless the adsorbed state and the gaseous state of the same compound possess quite different absorption bands (which has been the case in most implementations of this technique (90,147,152)), the investigator will not be able to differentiate between the absorption (of the infrared radiation) by the gas phase and that by the adsorbate. Accordingly, the sample cell is usually matched with an "identical" reference cell without catalyst in it which presumably compensates for the background spectra resulting from the gas phase. Unfortunately, variations in pressure and/or temperature between sample and reference cells can alter the gas densities enough to prevent matching of absorption bands attributable to the gas phases in the two cells. When the catalyst wafer is placed transverse to the flow of gases through the IR-cell reactor, the flow patterns within the cell can also lead to temperature and concentration gradients along the axis of the IR beam, and differences between the front and rear surface concentrations on the wafer. Under reaction conditions, this inability to eliminate the background spectrum of the gas phase limits the sensitivity of the technique ,especially, with the low surface coverages encountered at reaction temperatures. The new cell attempts to eliminate many of these objectionable features and its performance will be assessed in section 3.3.

3.2.2 Kinetics design considerations

Three relatively recent reviews (155-157) provide the reader with adequate background on the status of laboratory catalytic reactors for studying kinetics. It is demonstrated that "gradientless reactors" are extremely convenient and that they offer the best characteristics for studying the kinetics of heterogeneous catalytic reactions. Figure 3-1 illustrates the material balance analysis of a reactant in a recycle reactor based upon simple first order kinetics. The integration for the inner limits is valid for any value of n, while the averaging is justified only for reasonably large values of n. At high recycle ratios, (usually n>20 (156)), the reaction proceeds at, or very close to, discharge conditions equivalent to those from the ideal continuous stirred tank reactor(CSTR). By increasing the RPM of the circulating blower, the mass velocity can be increased without changing F and consequenctly W/F, the overall space velocity remains unchanged. The opposite is also possible; namely, keeping the RPM constant, the mass velocity will remain unchanged even if F, and with it the overall contact time or space velocity is changed. In both cases the recycle ratio n is changing but as long as it remains above about 20, it has no influence upon the kinetics. The high mass velocities used in recycle reactors are a factor in reducing the influence of interphase and concentration gradients. Sampling and analysis of the reacting mixture recycled within the loop are easy to implement and produce directly a

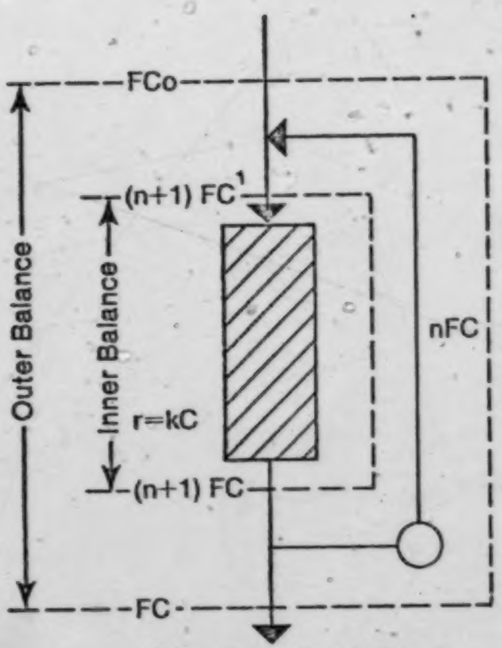
FCo
(n+1) FC¹
Outer Balance
Inner Balance
r=kC
(n+1) FC
nFC
FC

$$nFC + FCo = (n+1)\ FC^1$$

$$C_1 = \frac{nC + Co}{n+1}$$

$$\text{'t' Perpass} = \frac{W}{(n+1)F}$$

$$\text{'t' Overall} = \frac{W}{F}$$

Between Inner Limits

Integrating

$$-(n+1)\ F \frac{dc}{dw} = kC$$

$$-\int_{C_1}^{C} dc = \frac{k}{(n+1)F} \int_{0}^{w} dw$$

$$-\ln \frac{C}{C_1} = \frac{kw}{(n+1)F}$$

$$C = C_1\ e\ \frac{kw}{-(n+1)F}$$

Averaging

$$-r = \frac{(n+1)\ F\ (C_1 - C)}{W}$$

$$-r = \frac{F\ (Co - C)}{W}$$

$$-r = k\ \frac{C_1 + C}{2}$$

$$\frac{F\ (Co - C)}{W} = k\ \frac{C_1 + C}{2}$$

Figure 3.1 Recycle Reactor Material Balance

value of the reaction rate (see Chapter 5). An advantage of the external recycle reactor over other CSTR reactors, like the rotating- basket reactor arises from its well defined flow-path. The mixing may be perfect in both cases, yet the contact between the catalyst and the gas may be still poor or uncertain in the rotating-basket.

In this study, because of the infrared requirements for transparency, the differential catalytic bed is reduced to the geometry of a thin flat disk. This is shown on Figure 3-2 which was the of configuration used by previous workers. It is apparent that the flow patterns on the two sides of the pellet are not identical and the mass transfer characteristics are likely poorer on the stagnant rear face than on the impinged front face. A still more critical factor results from most of the reacting gases channelling through the gap between the sample holder and the internal cylindrical walls of the cell. The ensuing poor contacting between the gases and the faces of the catalyst wafer render difficult the gathering of true kinetic data. The low average mass transfer coefficients over the whole external catalyst area can make the reactor impractical for extensive kinetic studies.

Since the external area of the catalyst pellet is fixed at about 10 cm², it is relatively easy to assess the capability of the reactor to obtain intrinsic rate data before their falsification by external diffusion limitations. The external film resistance can be written:

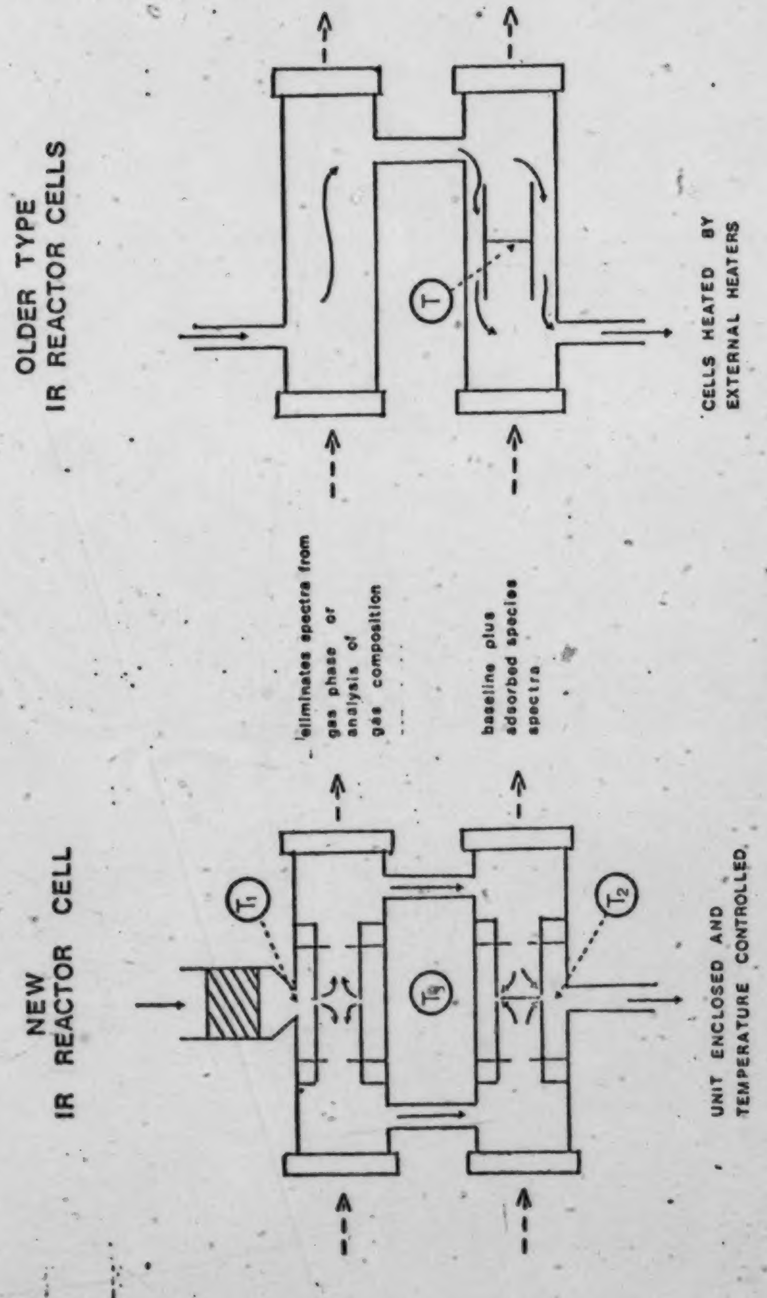
OLDER TYPE
IR REACTOR CELLS
T
CELLS HEATED BY
EXTERNAL HEATERS
eliminates spectra from
gas phase or
analysis of
gas composition
baseline plus
adsorbed species
spectra
NEW
IR REACTOR CELL
T1
T3
T2
UNIT ENCLOSED AND
TEMPERATURE CONTROLLED

Figure 3.2 Geometrical Configuration of Reactor Cells

$$r = k_g A (C_A - C_S) \qquad (3.01)$$

On the other hand, the rate of reaction in a recycle reactor is given by a simple mass balance:

$$r = F (C_{A_o} - C_A) = F C_{A_o} X \qquad (3.02)$$

In these design calculations, the film resistance is considered to be negligible, whenever the following criterion implying that the reactant concentration at the surface does not differ by more than 5% from the bulk concentration, is fulfilled:

$$C_A - C_S < C_A/20 \qquad (3.03)$$

A constant value of 10 cm/s will be considered to be representative of the average superficial mass transfer coefficient. At steady state the net rate of transfer of reactant molecules to the catalyst wafer is equal to the rate of chemical reaction. By combining equations (3.2) and (3.3) the following relation is obtained and evaluated for the specified above values:

$$X = \frac{k_g A}{k_g A + 20F} = \frac{100}{100 + 20F} \qquad (3.04)$$

Equation (3.4) shows within the previous assumptions the maximum level of conversion X, that can be obtained in relation to the volumetric gas flow rate to the reactor before the occurrence of significant external diffusion. Above this maximum level, significant diffusion limitations may be expected to falsify the kinetic data. This relation can be slightly modified when the total number of moles processed is changed by the reaction. The results of these preliminary design calculations are summarized in Table 3-1, which indicates for different levels of conversions the maximum volumetric flow rates (or molar flow rates) that can be processed through the reactor without significant external diffusion. For a reactor loop of 500 cc the corresponding average residence times in the reactor are indicated in the last column of Table 3-1.

The important conclusion obtained, providing that the value of 10 cm/s for the average mass transfer coefficient is reasonable, is that the reactor may be suitable to perform kinetic experiments at high levels of conversion and at the flow-rates commonly encountered in the laboratory. In section 3.3, experimental values of the average mass transfer coefficients for different geometries will be determined.

For many reaction systems, the apparent activation energy is high enough to make temperature the most critical independent variable in kinetic studies. In virtually all previous applications of the combined infrared-kinetics technique the conventional way of controlling the temperature of reaction was to wrap the cell body with a heater and to record the temperature with a thermocouple located close

Table 3.1 Simulated Mass Transfer Performance of the Reactor

X	F (cm^3/s)	F (moles/h)	t (s)
0.2	20	3.21	25
0.5	5	.804	100
0.8	1.25	.200	400

to the backside of the pellet, as shown in Figure 3.2. With this heating mode, the IR-transparent windows are much colder than the catalyst wafer and significant axial longitudinal temperature gradients will develop inside the cell in combination with the radial gradients caused by the higher temperatures of the walls in the reaction zone. The first drawback is that the temperature gradients in the reference cell and in the sample cell are not similar, preventing accurate compensation for the gas phase absorbance of the recirculating gases. In addition, the temperature of the catalyst may vary from point to point along the radial position preventing the procurement of true isothermal data.

To summarize, consideration of all of the above design factors led to the conception of a new geometrical configuration in which both the flowpath and heating sources have been modified. Its characteristic features are schematically depicted in Figure 3-2 . Different tests describing the performance of the reactor in relation to the general design limitations outlined will be described in the next section.

3.3 Tests Of Reactor Performance

3.3.1 Mass transfer characteristics

In the new configuration sketched in Figure 3-2, the recycling gases impinge upon both sides of the wafer to develop a highly turbulent field over the entire wafer surface before being removed by radial flow to the outer periphery of the pellet. Besides eliminating the stagnant zone encountered at the rear of the pellet in the earlier reactors , it was hoped that a substantial enhancement of the contacting between gases and catalyst would result. In the previous section, an arbitrary value of 10 cm/s for the average mass transfer coefficient was taken. More realistic values can be obtained by measuring the sublimation rates of a volatile solid in the same geometrical configuration. A prototype cell made of brass and identical to the proposed reaction cell was built. The catalyst pellet was replaced by a naphthalene flat disk of the same size. Air flows between 10 and 50 l/min were passed through the cell and the corresponding sublimation rates in mg/min were recorded. Since the cell geometry was held constant for a series of flow rates and was always maintained at room temperature, the coordinates of Figure 3-3 show the measured sublimation rates versus flow rate rather than Reynolds number. The exponent of the flow parameter (given by the slope of the lines) remain nearly constant over a wide range of conditions verifying that the flow regime does not change in the conditions investigated. The influence of changing the orifice size used to create the jets, and of the spacing between the orifice and the wafer upon mass transfer rates is shown on Figure 3-3. In addition to the above tests performed in the new geometry, sublimation rates were also examined for cell reactors involving the older geometry (152). The most important conclusion from these experiments is that the mass transfer is about four times faster in the new cell

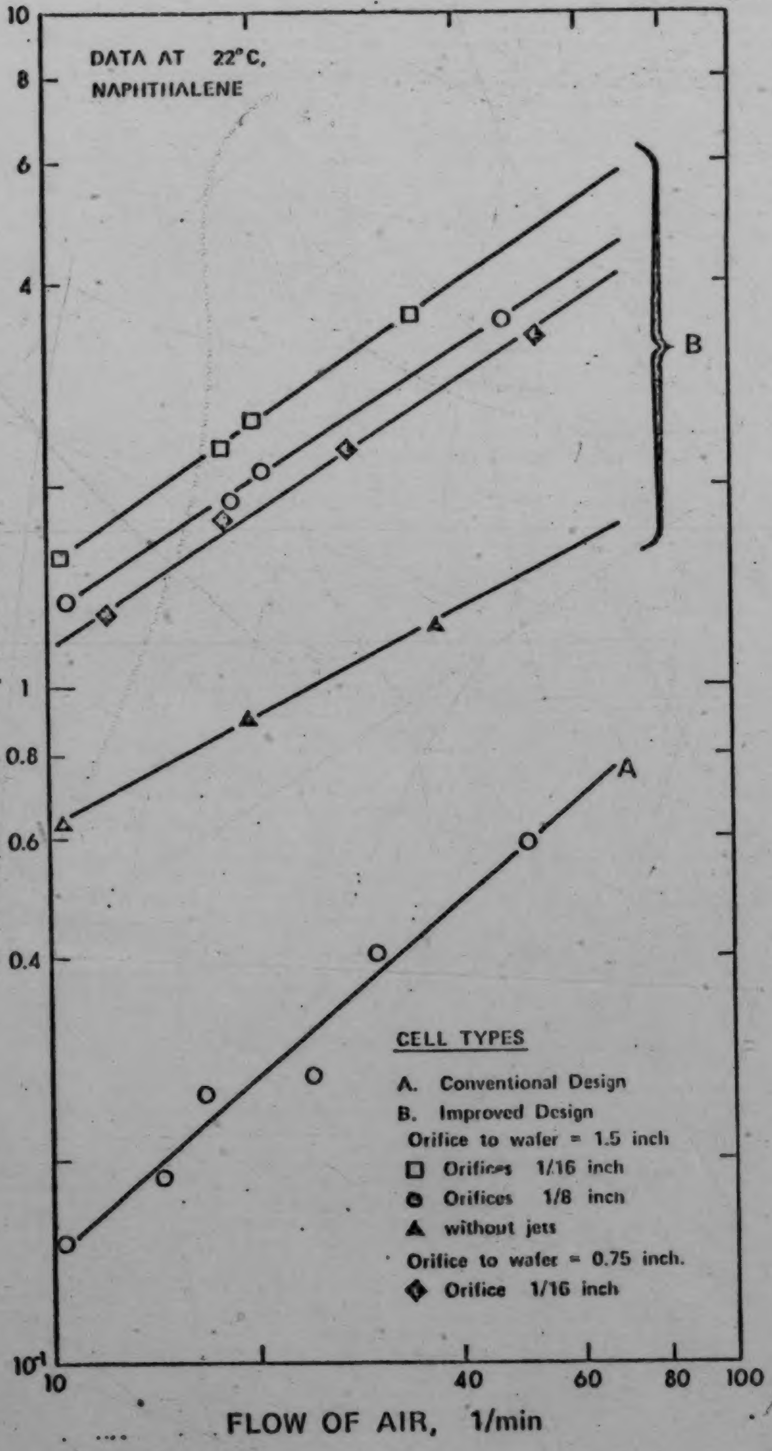

Figure 3.3 Sublimation Rates of Naphtalene in Various Reactor Prototypes

configuration when compared to the conventional axial-flow type. Although the contacting of the wafer can still be more than doubled by the insertion of drilled windows to create more turbulence, it was decided not to incorporate this design feature in the new reactor. It complicates the design and it was also observed that the local mass transfer coefficients at the centre of the naphthalene wafers where the jets directly impinge, were much higher than in the outer periphery of the disks. This point was demonstrated by the appearance of a hole at the centre of the disk after the sublimation experiments had been continued for an extensive time. Another important consideration was that in comparison to the very thin catalyst wafer (0.01 cm), the naphthalene disks (0.5-1 mm) have a much greater mechanical strength and can better sustain the additional stresses from the more energetic jets. Blank catalyst wafers were more readily broken in the mass transfer cell under the influence of the energetic jets and correspondingly thicker catalyst wafers would have to be used during reaction. With thicker wafers,the intraparticle diffusion effects may become much more significant than the effect of external diffusion thereby ruining the possible advantages of the impinging jets configuration.

In the sublimation experiments, the temperature was fixed at 22°C to allow the calculations of the average surface mass transfer coefficients following equation (3.05).

$$r = k_g A (C_{bg} - C_o) \qquad (3.05)$$

By further assuming that the mass transfer coefficient is almost proportional to the square root of the molecular diffusivity, the values obtained for naphtalene at 22°C could be corrected for the case of isopropanol at 250°C (reaction conditions).The corresponding values of the mass transfer coefficients are shown in Table 3-2.

The recycle pump normally operates at 1725 rpm and delivers a gas flow rate of approximately 20 l/min.By interpolation in Table 3-2, this corresponds to an average mass transfer coefficient of about 15 cm/s for the reacting isopropanol. During reaction, an additional degree of turbulence due to the rapid pulsations of the bellows pump, absent in the sublimation experiments, must contribute to further improve the contacting at the gas catalyst interface. The magnitude of this improvement could be assessed more accurately in further mass transfer experiments but at the present time an average surface mass transfer coefficient of 20 cm/s seems appropriate. Recalling the predictions on the mass transfer performance in the previous section, which were based on a value of 10 cm/s, we can still expect a better performance with the reactor. The capacity of the reactor to generate kinetic data at high conversion levels and at the most practical flow rates used in the laboratory without influence of external diffusion seems

Table 3.2 Improvement of Mass Transfer Coefficients

Configuration	Air Flow at 10 l/min	Air Flow at 50 l/min
Old geometry	2.0 cm/s	7.5 cm/s
New geometry	9.25 cm/s	23 cm/s

therefore substantiated.

In conclusion the new reactor IR-cell configuration demonstrates a fourfold improvement in gas-solid contacting. In general, the greater flexibility in the range of independent variables (concentrations, temperature) to be covered in the experiments should also result in wider variations in the observed dependent variable (rate of reaction). This last feature is a key factor in the discrimination between rival kinetic models.Of course this argument is valid only if no other more restrictive phenomenon (i.e. intraparticle diffusion) is in effect; this will be established in section 6-2.

3.3.2 Mixing characteristics

If the recycled flow within the reactor approximates perfect mixing, the outlet composition is indicative of the gas phase composition at any point within the reactor. To demonstrate that perfect mixing does occur, the step-response method was used. The inlet gas composition of acetone was changed instantaneously under non- reactive conditions while the concentration in the loop was measured continuously by monitoring the absorbance of the carbonyl band. Mathematically the characteristic change in the reactor composition for an ideal CSTR is given by equation (3-6),

$$C/C_o = \exp(-t/\bar{t}) \qquad (3.06)$$

which can be found in many textbooks. Figure 3-4 illustrates the response of the system to the step-change in acetone feed concentration and the expected response for the case of perfect mixing (CSTR).Substantial agreement between the two cases is indicated. Since the recycling rate and residence times used in Figure 3-4 are typical of the conditions where the experimental reaction rate data will be obtained, it may be expected that the reactor will be perfectly mixed under all conditions reported in this study.

3.3.3 Compensation for gas phase infrared absorption

As suggested in section 3-2, the difficulty in balancing the gas phase attenuation of the two beams has certainly limited the general use of the technique. For example, a pressure drop between the two cells necessitates heating the upstream cell to reduce its gas density to that in the downstream cell. Similarly, non-isothermal differences at constant pressure between the two cells must also be compensated.

Such imbalances between reference and sample cells required calibrations to establish the values of the reference cell temperature T1 required for a fixed reaction cell temperature T2 (see Figure 3.2(b)) to eliminate gas absorption spectra. Figure 3-5 shows how spectral bands in the 1200-1500 cm^{-1} region of gas phase isopropanol are altered by changing T1. In the early experiments, when the oven

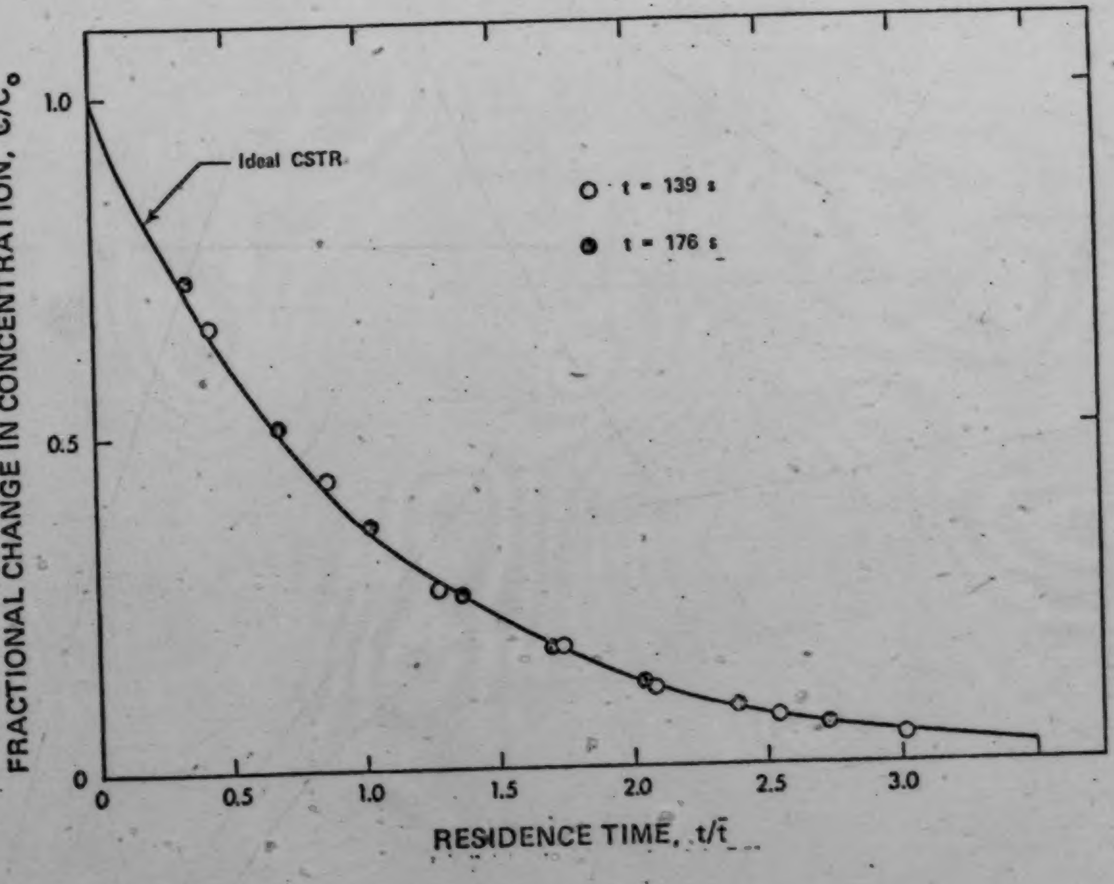

Figure 3.4 Comparison of Mixing Behaviour of the Reactor with Ideal CSTR

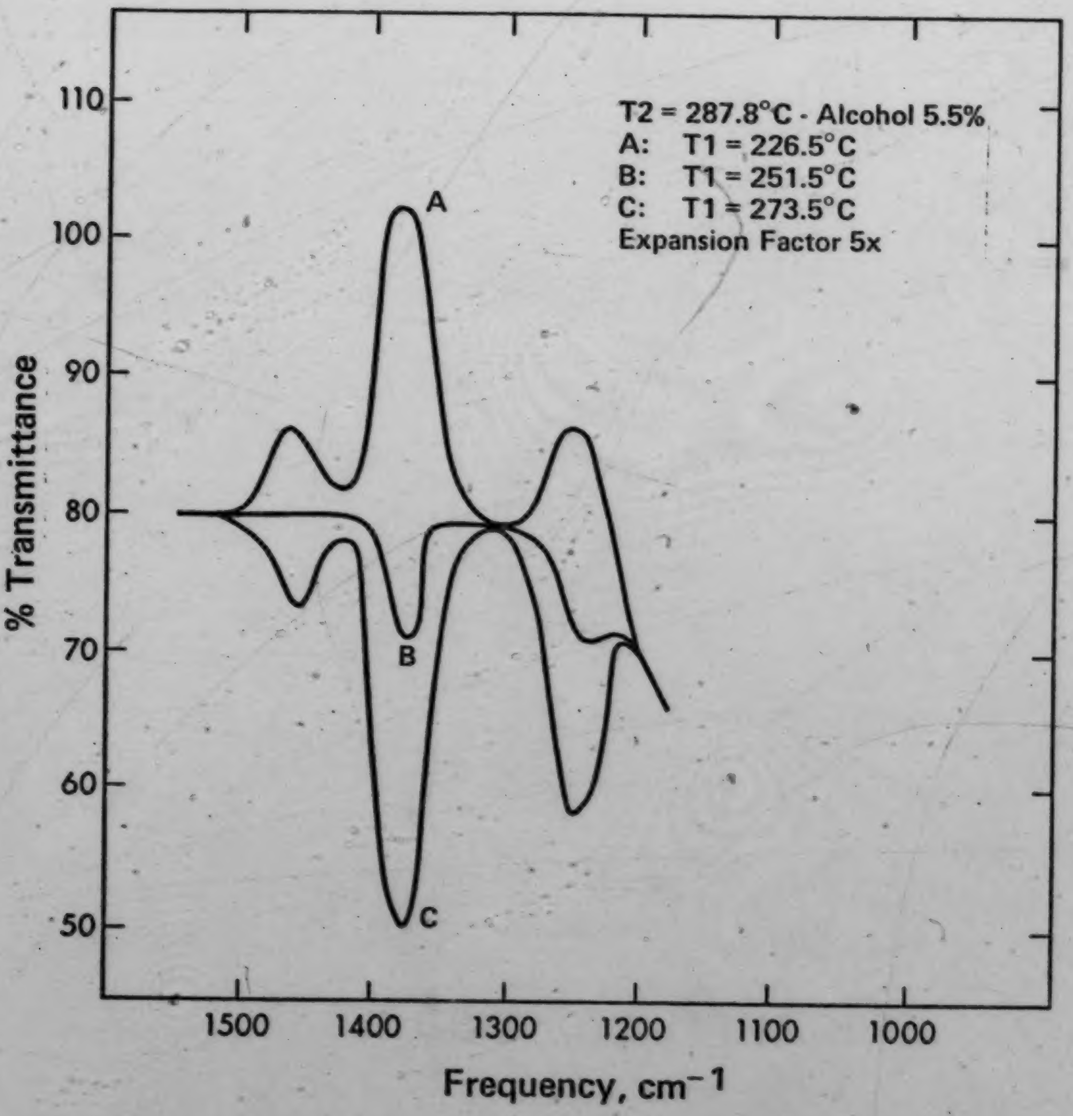

Figure 3.5 Compensation of Gas-phase Absorbance Between Reference and Sample Cells

temperature T3 was maintained at a constant level and while the gases were being recirculated (1725 rpm), it was found that apart from slight variations with composition, the recorded temperature T2 in the reaction zone was always about 50°C below the oven temperature. On the other hand, the changes in T2 were only negligible when T1 at the entrance of the reaction cell was varied over a wide range by manipulation of the heat load applied to the packed bed preheater. From these observations, it was apparent that heat losses from the recirculating gases in the vicinity of the infrared windows contributed substantially to a reduction in the temperature T2 in the reaction zone relative to the oven enclosure temperature T3. The temperature difference between T2 and T3 could only be reduced by decreasing the recirculation flow rate of the pump. This leads to the conclusion that significant axial temperature gradients (possibly up to 100°C) are established in the infrared cells at the high flow rates delivered by the pump. Under these conditions, attempts to balance the gas phase absorbance of the two cells became a tedious procedure. These complications had never been reported in previous applications of the technique. It was mentioned in section 3-2 that the total number of gaseous adsorbate molecules traversed by the infrared beam may easily exceed by an order of magnitude the number of molecules of the same adsorbate on the catalyst surface. Accordingly differences in the compensation of a few per cent (corresponding, for instance, to a 10°C difference between the two cells) can drastically alter the nature of the adsorbed layer spectrum, especially when both gaseous and adsorbed species absorb infrared radiation at the same frequencies.

In another type of preliminary experiment the thermocouple located in the reaction zone was connected to the Honeywell controller in order to maintain the associated temperature at a constant set point. This set point could only be maintained within regular oscillations of a few degrees because of the distance and heat barriers (Pyrex walls) between the source oven heaters and the sensing thermocouple. These instabilities were however of minor importance in the following analysis. The differential absorption spectra shown in Figure 3-5 were also recorded at various levels of T1 and for different concentrations of alcohol in the reactor loop. Figure 3-6 shows how the temperature T1 typically varies with the setting of the Variac controlling the preheater. At each concentration level of isopropanol, T1 changes almost linearly with the variac setting, and since the heat capacity of the gas mixture increases with alcohol concentration, higher settings of the Variac are required at higher concentrations to produce the same temperature at the entrance of the reference cell. In similar conditions Figure 3-7 represents a plot of the relative difference gas absorbance at 1380 cm^{-1} between the sample and the reference cells as a function of T1. Even if the exact compensation occurs for each series of experiments at one value of T1, we

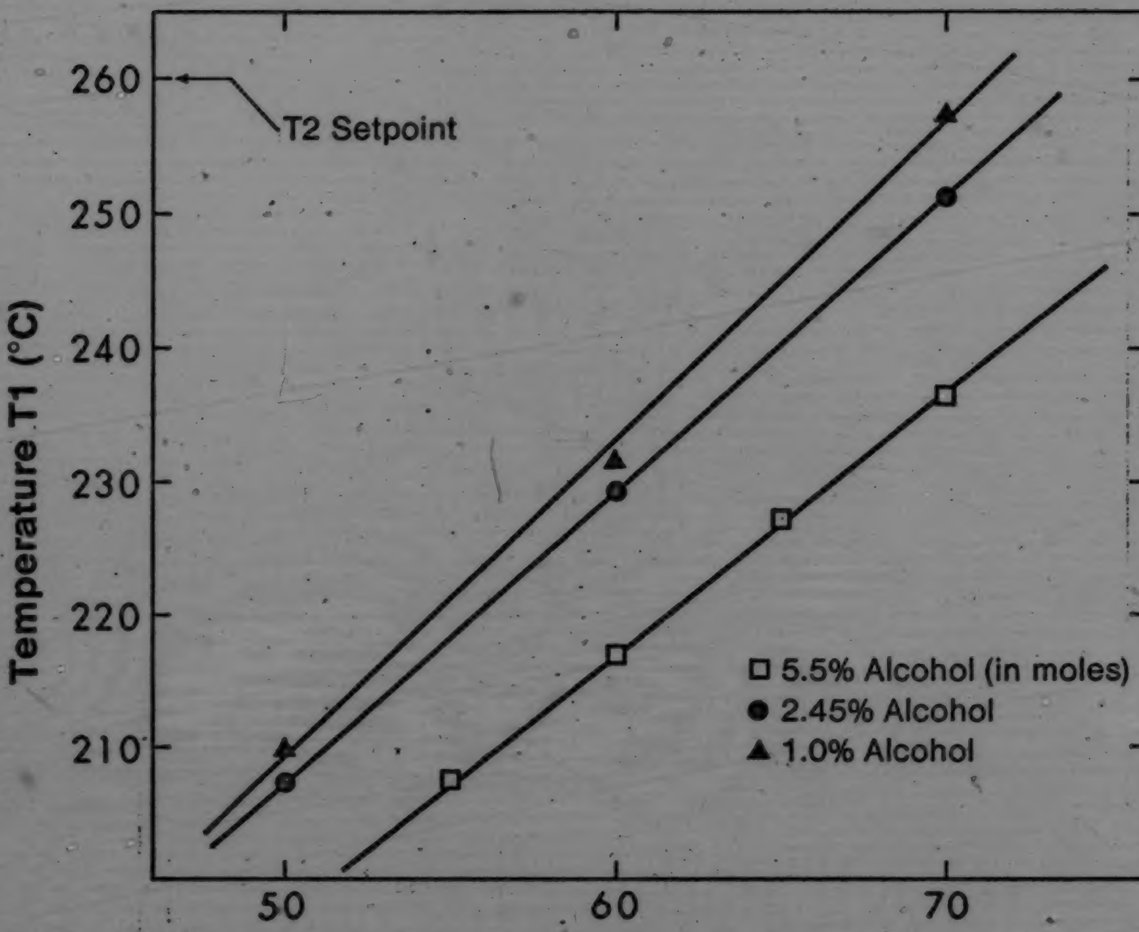

Figure 3.6 Typical Thermal Response of T1 to the Preheater Load

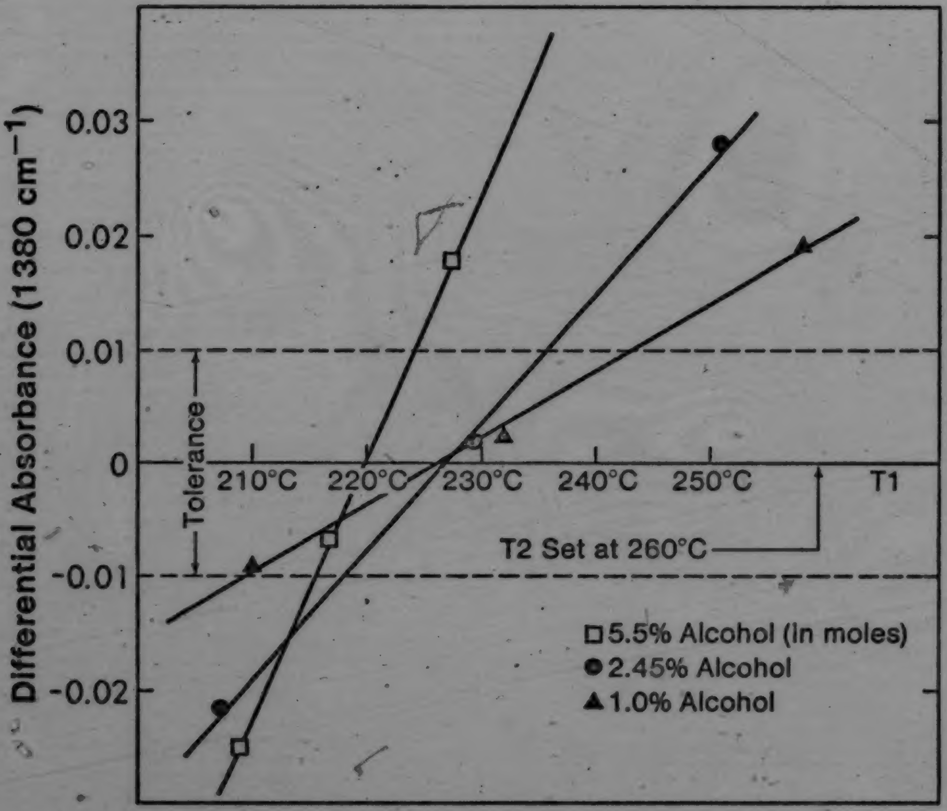

Figure 3.7 Calibration Plot of Gas-phase Absorbance Compensation without the Window Heaters

have indicated on the plot a tolerance level of ±0.01 absorbance unit because this is almost unnoticed on the catalyst spectra. During the calibration experiments however, the spectrophotometer was operated with an expanded ordinate scale (5x) in order to increase the sensitivity for measuring the difference in absorbance.

Figure 3-7 shows that satisfactory compensation is reached whenever T1 is 30 to 50°C below the constant value of T2 in the reaction zone. At these conditions the average density of molecules along the pathlengths of the two cells is nearly identical; this also means, in relation to the ideal gas law, that the average axial temperature in each cell is almost the same. Neglecting the temperature gradients in the reference cell, (T=T1 along the axis), the results show that the temperature in the vicinity of the windows of the reaction cell (where the recirculating gases enter) must be substantially lower than T1 since T2 at the center of the reaction cell is higher than T1. This confirms the occurrence of heat losses through the windows of the reactor. In addition, from Figure 3-7, the range of acceptable values of T1, according to the specified tolerance level, decreases with the concentration of alcohol as a consequence of the increases in the slopes of the straight lines. These problems had never been mentioned previously but independent manipulation of T1 has now been provided in the new reactor. Without this feature, unpredictable errors in the gas absorbance compensation would complicate the observed spectra and thus make the correct interpretation of the spectra of the adsorbed layer more difficult. The same kind of experiments as shown in Figure 3-6 and 3-7 were performed at two other values of T2 (230°C and 290°C) and the results were very similar to the results obtained at 260°C. The thermal behaviour of the reactor may now be regulated over a wide interval of temperatures. The final calibrations and operation procedures will be defined in the next subsection.

3.3.4 Isothermal reaction zone

It was mentioned in section 3.2 that in the previous infrared cell reactors, the combination of axial and radial temperature gradients as well as the poor contacting of the gases with the wafer would prevent the gathering of true isothermal kinetic data. In the new reactor configuration the more intimate sweeping of both faces of the catalyst wafer by the flowing gases should ensure that the reaction temperature remains uniform over the entire wafer surface and equal to that of the gases. It is also desirable that the temperature of the sensing thermocouple remains identical to the true catalyst temperature. This condition cannot be directly checked since the position of the thermocouple is just above the wafer and not in direct contact so as not to modify the flow patterns around the catalyst. Approximately, it can be inferred that when the heat transfer is minimized the difference in temperature between the recirculated gas and the wafer is also minimized. Whenever the difference between T3 (oven temperature) and T2 (reaction zone) is suppressed, the previous optimal conditions are approached. Unfortunately, as mentioned in the previous section, T3 was always higher than T2 by more than 25°C depending on the operating conditions; consequently, the gases are still gaining heat from the hotter Pyrex walls of the cell while the reaction zone. The true temperature of the wafer depends on how rapidly the temperature of the travelling gases is altered.

In order to eliminate these uncertainties, originating from the heat losses at the windows, additional heaters (described in detail in Chapter four) were placed around the ends of the two cylindrical cells. With this additional heating source, the temperatures T2 and T3 could be closely matched by adjustment of the input voltage to the new heater. In this final set-up, it now appears reasonable to identify the true temperature of reaction with T2. Simultaneously, because of their appropriate locations, the additional heaters compensate for the heat losses of the gases in the vicinity of the windows and thereby greatly reduce the axial temperature gradients along the two cells. This important consequence is made clear in Figure 3-8, which was obtained after conducting similar experiments to the ones described for Figure 3-7. The trends are again similar, except that with the new heaters in operation, the levels of T1 required for exact compensation of the gas phase absorbance almost match the common values of T2 and T3. During operation, it

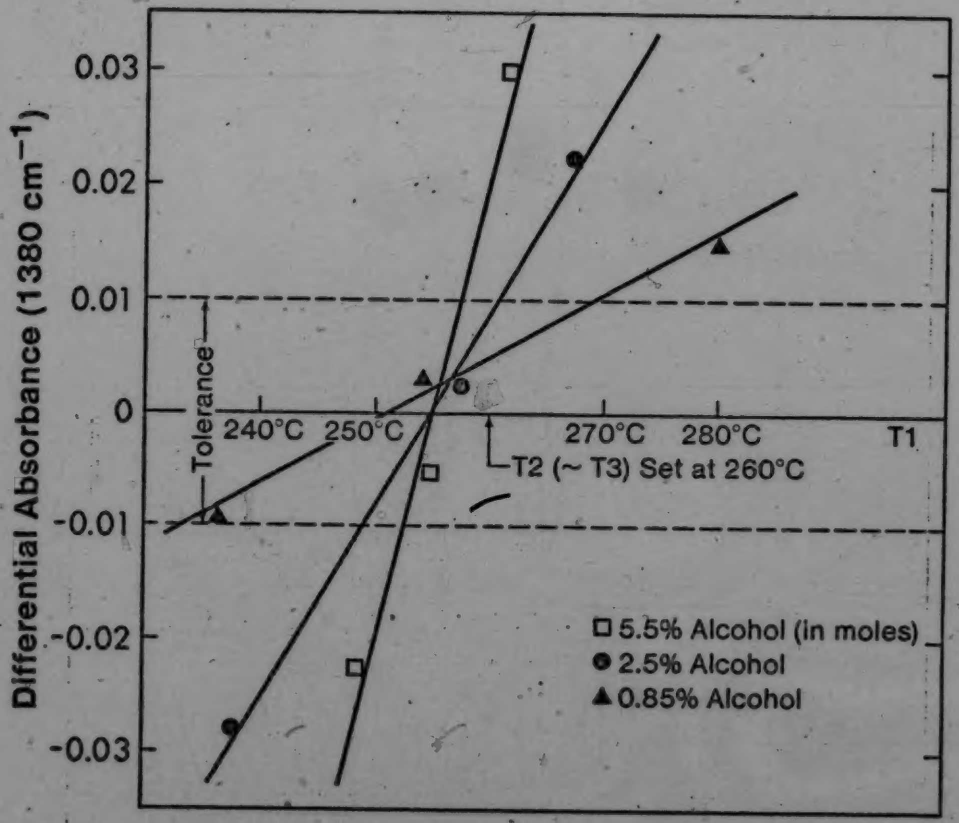

Figure 3.8 Calibration Plot of Gas-phase Absorbance Compensation with the Window Heaters

is now only necessary to keep T1 about 5°C below the reaction temperature to ensure a good compensation, and this facilitates greatly the operation of the reactor .The new reactor provides adequate means of compensation for non-isothermal axial gradients as well as good isothermality in the reaction zone.

4. CONSTRUCTION AND DESCRIPTION OF APPARATUS

The general appearance of the reactor system is shown in Figure 4.1. The equipment was mounted on a mobile trolley and consists mainly of two compartments, the pump compartment and the infrared cell oven compartment linked together by flexible stainless steel tubing. All temperature and flow accessory instrumentation has been mounted on the assembly unit for convenience. The apparatus is compact and occupies a floor space of about 1.4 m x 0.4 m, while its height does not exceed 1.2 m. To be operated, the system must be moved and connected to the gas chromatograph at the outlets of the gas sampling loop. The mobile infrared spectrophotometer can then be adjusted in proper position for adequate analysis. Finally, the various electrical outlets and thermocouples are connected to the main power system and the temperature recording unit. The various components of the experimental equipment will be described in detail in the following sections.

4.1 Feed System

With the exception of the nitrogen cylinder A, all components of the feed system on Figure 4.2 were mounted on the reactor unit. To provide a constant flowrate of the nitrogen diluent during constant upstream variable downstream pressure applications, a Matheson pneumatic flow controller C

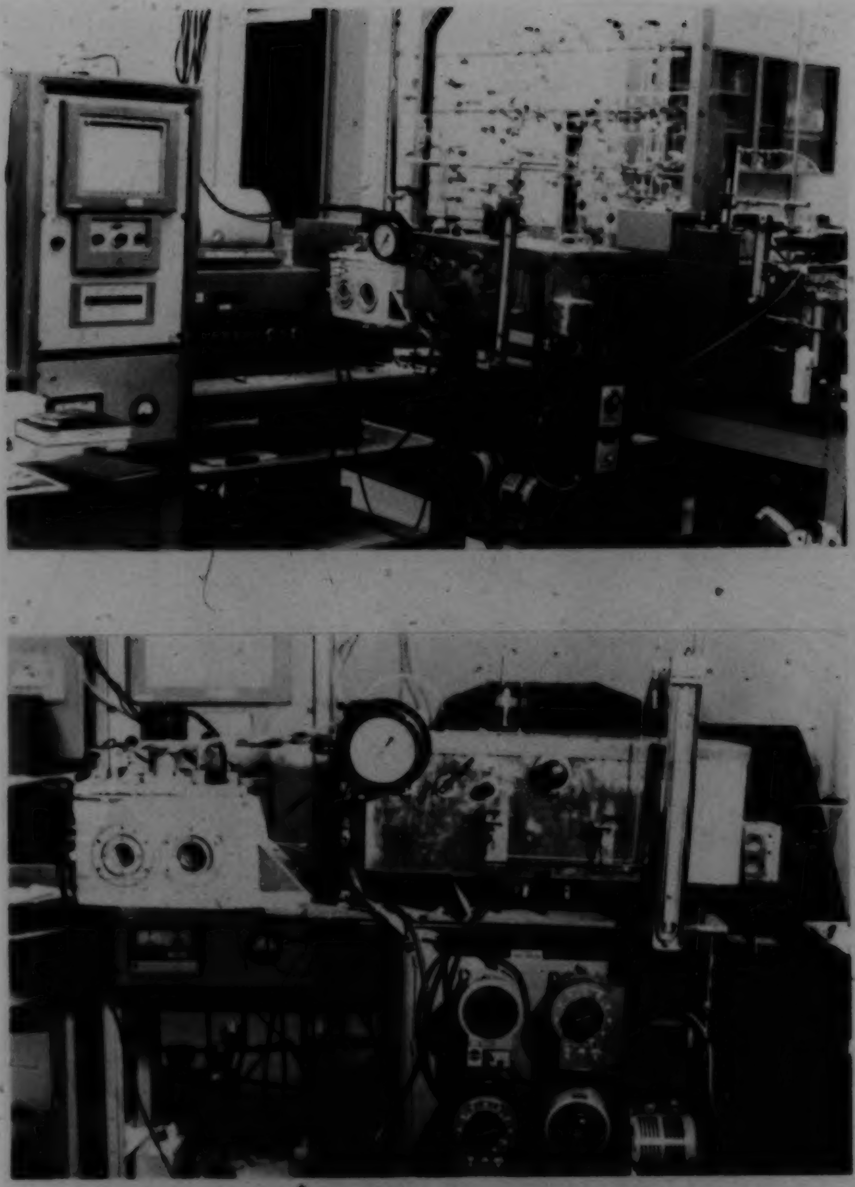

Figure 4-1 Photographs of Reactor System

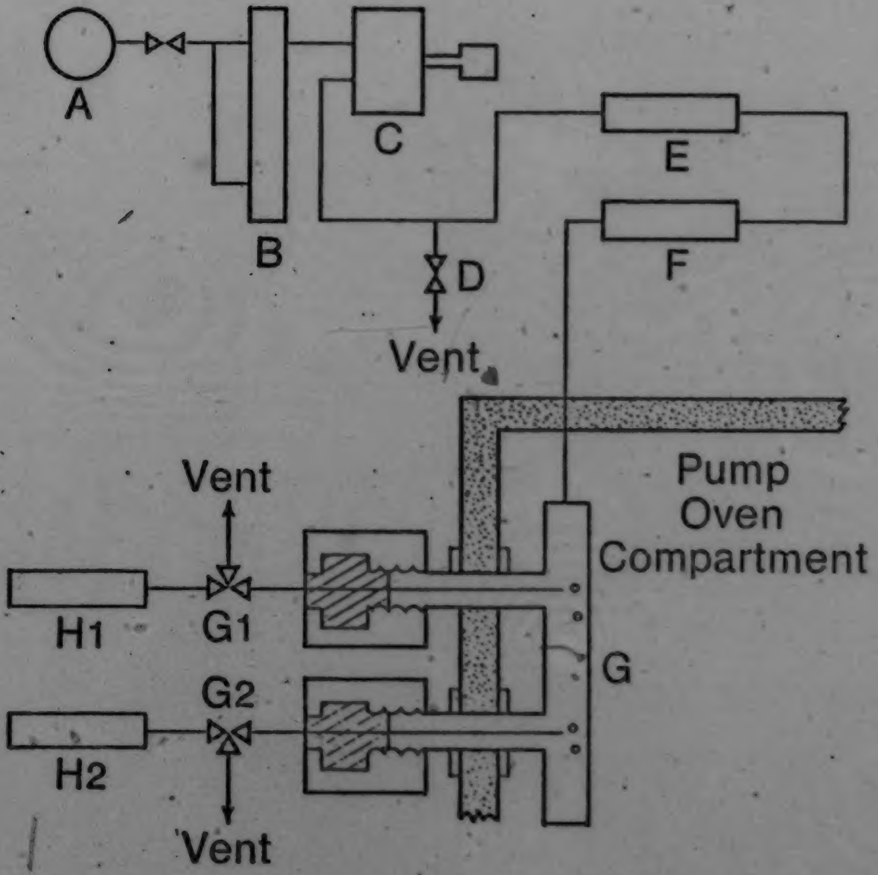
A
B
C
D
Vent
E
F
Pump
Oven
Compartment
Vent
H1
G1
G
G2
H2
Vent

Figure 4.2 Flow Diagram of Feeding Unit

(Model 8287) was incorporated in the feed line. The supply pressure to the controller was maintained nearly constant with a gas pressure regulator attached to the nitrogen cylinder. The specifications of the controller are such, that at a supply pressure of 50 psig, it can maintain a constant flow within 0.3% while the downstream pressure varies from 0 to 40 psig. The flowrate was indicated by a rotameter B installed in the controller supply line so that downstream pressure changes could not affect the reading. Interchangeable needle valves are available for different flow ranges and different sizes of rotameter tubes (600 and 601 in our study) were adapted to provide a better visual indication of the flow setting. The good reproducibility of the flow settings enabled a substantial amount of time to be saved. After the flow controller C, a side exit D was used in order to bypass the rest of the reactor for identifying occasional leaking parts. At other times, this side line could be used to introduce an additional gas component, i.e. propylene, whereas during normal operation this exit was closed. Oxygen-free nitrogen was obtained by passage over a supported Cu-CuO catalyst maintained at 300°C in column E. In addition, the nitrogen gas was passed through an ascarite and molecular sieve column F to remove traces of carbon dioxide and water vapours. Following that treatment, the diluent entered the pump oven compartment and was directed towards the vaporizer G where it was mixed with the liquid vapours ,i.e. isopropanol and water.

The vaporizer G is a 3/4 in O.D., 3 in long manifold made of stainless steel. Both ends are provided with connections to 1/4 in O.D. tubing ,serving as inlet for the diluent into the vaporizer and exit for the feed mixture to the reactor. The two 1/8 in O.D. side-arms of the manifold are for the introduction of two separate liquid compounds. The vaporizer was attached to the walls of the pump compartment by its two side-arms. The inside of the vaporizer was packed with glass wool to insure a good distribution of liquid and a steady flow of vapor. Although the oven was maintained at 150°C, a supplementary nichrome wire heater was wound on the outside of the vaporizer and wrapped with insulating blanket to provide heat to vaporize rapidly the incoming liquids. The entry of liquids to the manifold had to be modified and designed carefully to avoid the temperature gradients that develop in the liquid lines and cause surging in the vapor flow. This nonsteady-state behaviour is usually the consequence of too long a residence time of the liquid between the places where it starts to be heated and where it is finally flushed out of the vaporizer. This residence time was minimized by introducing the liquids through very fine and long hypodermic needles impinging directly on the hot inside walls of the vaporizer. Hamilton needles 3 in long and of various orifice sizes (KF.722-KF.731) were used. Their means of attachment to the apparatus is depicted schematically in Figure 4.2.

First, the female Luer lock ending of the needle was connected to one of the male Luer outlet ports of one of the two Hamilton inert 3-way valves,G1 or G2. A Swagelock 1/8 in nut and a rubber septum were slid along the needle stem permitting the needle assembly to be screwed tightly in its final position on the side walls of the oven. The squeezed rubber septum provided a good gas-tight seal . The two small valves G1 and G2 were very practical for the switching on and off of the liquid feeds and helped to minimize the stabilization time necessary before the establishment of steady-state in the liquid lines. Any unwanted entry of air into the system could also be avoided by proper manipulation of the valves. Flexible teflon tubing with Kel.F female Luer fittings provided a good seal and were used for connecting the various Hamilton gas-tight syringes (Catalog Numbers 1010,1020,1050) with the inert valves.

Finally, two Sage model 355 syringe pumps H1 and H2 (Sage Instruments, Inc., White Plains, New York) were employed to inject water, alcohol and other liquid reagents into the feed mixture. The plungers of the syringes are depressed by means of a slowly moving carriage working on a rack and pinion principle. A set of driving gears in the syringe pumps enables one to infuse liquids continuously at various speeds using any single syringe. According to the manufacturer a reproducibility of ±0.5% full scale is specified regardless of the changes in back pressure (i.e., within the limits of 700 mm Hg for a 50 cc syringe and 2600 mm for a 10 cc syringe). This is possible because of an electronic feedback circuit that regulates the permanent DC motor to drive the pump. The calibration results and the ability of the syringe to deliver a continuous stable flow will be the subject of a separate section in the next chapter, since in contrast to other published studies, we have spent substantial time and effort in determining the optimal conditions of use of this method of feeding. The key advantage of this method of infusing liquids to a catalytic reactor remains its greater versatility than other means. For example, when using a vapour saturating device, the range of compositions is limited by the volatility of the liquid reagent. Furthermore, it becomes impractical to feed simultaneously two or more liquids in one saturator because of the usual mutual solubilities of different compounds.

4.2 Recirculation System

The oven which enclosed most of the recycling loop was constructed of sheet metal on an angle iron frame with outside dimensions of approximately 65 by 34 by 24 cm. Between the inside and outside metal walls one half inch thick Cotronix boards provided adequate insulation. The oven was mounted horizontally on the movable trolley. On top of the removable lid a small electric motor was mounted and attached to a blade type fan by a shaft which extended through the lid. The purpose of the fan, which is located just above two 500 watt strap heaters lying on the bottom of the compartment, was to circulate the air within the oven. The oven temperature was regulated at about 170°C by setting the voltage to the oven heaters via a Variac and a period of approximately 3 hours was necessary to heat the oven from a cold start.

The circulation pump constitutes the most important single piece of equipment of the recycling reactor. A Metal Bellows Company model 118.HT bellows pump was driven by a 1/4 hp d.c. motor equipped with a variable speed controller. The pump drive shaft extended through the bottom of the oven wall and was coupled to the motor shaft . The pump, designed to operate up to 230°C, provided a continuous leak-free operation for two and a half years. Its great dependability and contamination-free operation eliminate many of the problems encountered in earlier recycle reactors. The capacity of the pump at atmospheric pressure and in open atmosphere is almost 28 l/min at a motor speed of 1725 rpm. The delivered flow rate decreases linearly with the operating pressure of the pump, down to zero at about 25 psig. The capacity of the pump also decreases linearly as the net difference between the discharge pressure and the suction pressure increases. The testing of these characteristics was done experimentally by incorporating an adequate throttling valve in the discharge line of the pump. The presence of a filter is recommended by the manufacturer to prevent the entrance of particulate matter into the pump thereby causing permanent damage to the stainless steel bellows. Three sintered stainless steel filters of size 7, 15 and 60 microns were tested and the respective capacities were reduced to 90, 70 and 50% of fulll capacity. On the basis of these results we selected the 60 micron filter in the final design. In other similar tests, it appeared that the use of 1/4 in O.D. stainless steel piping can create high enough resistances to the flow to reduce the capacity of the pump significantly. Accordingly, our final choice for the piping size in the recirculation loop was 3/8 in O.D. 316 SS tubing.

Figure 4.3 is a flow diagram of the major components of the reactor piping. At the exit of the vaporizer G, the feed mixture can be split into two portions. The main portion goes to the four-way valve SW1 (Whitey SS-43YF2) where it can be directed either to the entrance of the reactor loop or to simply bypass the reactor (as in batch operation). Similarly the smaller portion of the feed is routed to another suitching valve SW2 where it can either enter the reactor or bypass it via a GC sampling valve for feed analysis. The metering valve R1 (Nupro "S" series) regulates the amount of secondary flow diverted for GC analysis. After the feed enters the reactor loop near the pump discharge, it is first recirculated through a regulating valve R2 (Whitey SS-1RS6) which is normally fully open. However, various recirculation rates in the reactor can be obtained by proper throttling of R2 and a mercury manometer has been installed across the valve to monitor the recirculation rates. The gas mixture exits the oven and flows through the infrared compartment past the catalyst before returning to the pump oven

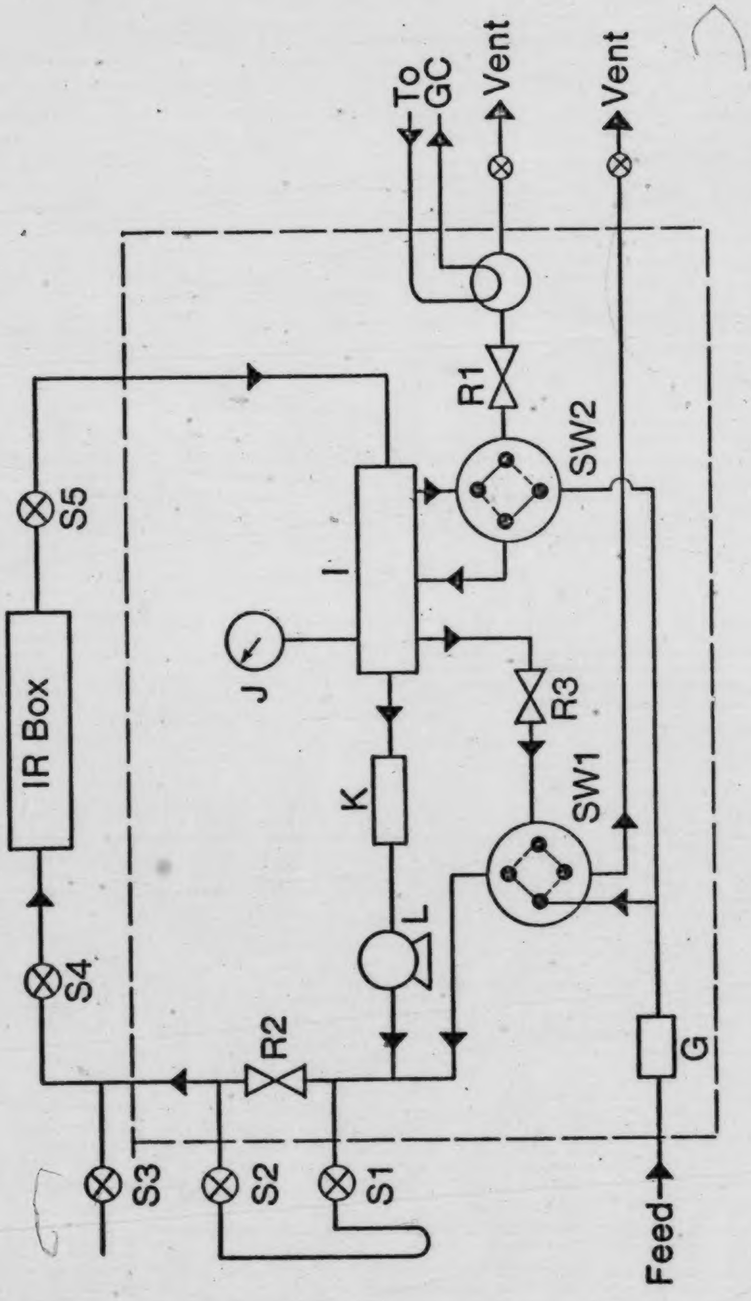
To GC
Vent
Vent
R1
SW2
S5
I
IR Box
J
R3
SW1
K
L
S4
R2
G
S3
S2
S1
Feed

Figure 4.3 Flow Diagram of Reactor Loop Piping

compartment. Several shut-off valves have been installed in the lines to greatly facilitate the detection of leaks in various sections of the apparatus . The gases enter a manifold I where all other external connections have been incorporated. In addition a pressure gauge J is mounted on the manifold for indicating the operating pressure in the reactor loop. Because of the low resistances to flow within the large connecting lines in the loop (3/8 in O.D.), the pressure reading approximates closely the true value of the pressure in the catalytic zone. Most of the flow proceeds towards the suction entrance of the bellow pump after passing through the sintered stainless steel 60 micron filter. After the manifold I, the exit gases are again split into two streams. The major part goes to SW1 through a 1/4 in O.D. line and another regulating valve R3. The purpose of this valve was to maintain a constant gauge pressure in the reactor loop throughout the entire study (i.e., at all flow rates and compositions). The other smaller portion of the outgoing gases passes through SW2 and is routed through the gas sampling loop for GC composition analysis. Before being vented, the two exit stream flows can be measured with soap bubble meters.

4.3 Infrared Cell Compartment

The infrared compartment of the new reactor can be seen in Figure 4.4. It consists of two major pieces; a 4 3/4 inch wide, 13 inch long and 8 inch deep rectangular tank and a

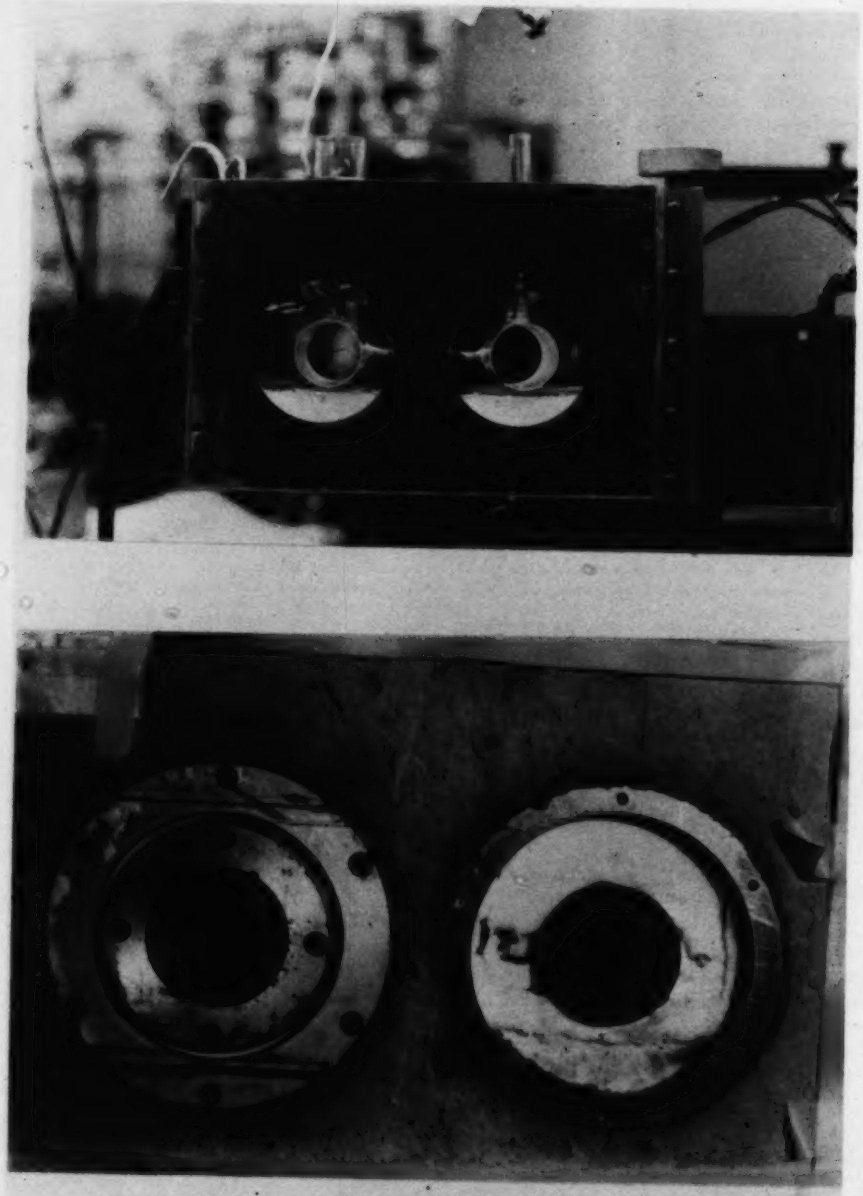

Figure 4-4 Photographs of IR Cell Compartment

dual cell assembly placed inside the tank. The tank was made of 1/8 inch aluminum sheets. To allow for the passage of the infrared beams and the positioning of the cell assembly, two 3 10/16 inch diameter holes were cut on each of the two largest vertical faces of the rectangular tank 5 inches apart. These holes were positioned so that their centers could be aligned exactly with the axis of the reference and sample beams of the infrared spectrophotometer. The holes were centered 3 5/8 inches from the base of the tank; the width of the tank fitted snugly in the analytical compartment of the spectrometer. The tank was mounted on the end of the main base plate of the movable trolley, as shown on Figure 4.1 and 4.4. The position of the tank could be shifted vertically to match the level of the infrared beams by means of the projecting arm seen on the left of Figure 4.4. The bottom of the tank was also covered with 1/2 inch thick cotronix insulating boards. Two flat 400 watts heating elements (OT-1004, Wiegand, USA) were installed in parallel just above the bottom insulation, covering almost the entire length of the tank. These strap heaters provided the main heat supply to the infrared oven and were connected to the outside by two ceramic connectors fixed into the sample side wall of the tank. In the middle of the same side wall a 1/4 inch hole was drilled in order to introduce various thermocouples inside the box.

We will now describe the sequential procedures required before the reactor could be placed in use. The lower part of the inner walls of the tank was covered with 1/2 inch thick Cotronix insulating blanket before introducing the Pyrex cell assembly into the infrared oven compartment (see Figure 4.4). The length of the cells was exactly 4 5/16 inches, 1/16 inch smaller than the inside width of the tank. To position the Pyrex cell unit in its final horizontal position, one aluminum external plate was slipped over each end of the cells and attached to the sides of the tank by six bolts. This operation is displayed in Figure 4.4 where we can see the six equidistant threaded holes of 3/32 inch diameter that were made along a circle 3/16 inch outside the outer circumference of the side walls cavities. The external plates were machined so that they could fit exactly into the circular gap (see Figure 4.4) between the 45 cm O.D. cylindrical Pyrex cells and the tank walls. An additional groove was machined to allow the external vertical face of each plats to be positioned almost exactly flush with the ends of the infrared cells. A 1/8 inch wide, 2 mm deep groove was machined to accommodate a Viton o-ring around each end of the cells (see Figure 4.4). When in place, the o-rings maintained the cells in their exact position and were slightly protruding to the outside. Four equidistant additional threaded holes were made along a circle at a 1 1/8 inch distance from the central axis of the plates. The function of these holes (see Figure 4.4) was to hold the covers of the infrared windows. The four identical aluminum window covers were 2 6/8 diameter disks 5/16 of an inch thick. A trough was cut from each disk for the incorporation of the 49.5 x 6.5 mm NaCl infrared transparent windows (Harshaw Chemical Company - Part number 04806). A hole with 1 3/4 inch diameter was cut from the bottom of the trough to allow the passage of the infrared beams. Four holes equidistant from each other were drilled along a wide 2 2/8 inch in diameter on the window caps. By employing four screws, the cover together with the NaCl window could be fastened onto the external plates. To provide a good seal, the window was pressed against the outside face of the o-rings by tightening the screws. Experience indicated that the Viton o-rings seals remained effective even after repeated pretreatments of the catalyst at 400°C. However, when the reaction cell had to be opened to change the catalyst wafer, the windows usually adhered to the o-rings and could only be detached after repeated flushing with acetone. The Viton o-ring could be removed from its groove without damage to the glass cell by propping it out carefully using a needle hook. In the present work the o-rings were renewed at each removal of the adjacent windows, so that when the catalyst was changed it was only necessary to replace the two o-rings of the reaction cell. The infrared windows were reemployed with occasional repolishing. Attempting to detach the windows too quickly without flushing with acetone resulted in small pieces of the NaCl windows remaining on the contact surface of the o-ring. This deterioration eventually prevented a good seal in subsequent use of the window.

Consequently, care is recommended in the removal operation and the experimenter should apply a minimum shearing stress between the window and the Viton o-ring in order to extend the life of the crystal.

The infrared dual cell assembly now in position in the infrared oven is shown separately on Figure 4.5. Its conception was based on the various design factors enumerated in Chapter 3. The assembly consists of eight individual Pyrex parts that were assembled in the glass shop. Because of its inertness towards many compounds, and particularly alcohols, Pyrex was selected for the construction material. The brittle point of Pyrex occurs at 550°C. Two of the eight components were identical cylindrical sections, 4 5/16 inch long and 45 mm O.D., to be used as reference and sample cells,respectively. On the reference cell a side arm was mounted at the centre and perpendicular to the cylindrical section, permitting entrance of the gases. To facilitate the glass blowing operation, the size of the arm was made smaller at the joint base (15 mm O.D.) for a length of approximately 2 cm. Above this short section, the size of the arm was expanded to 35 mm O.D. to preheat the recycled gases to the reaction temperature before entering the reference cell. The preheating requirements could be most effectively met by incorporating a heated packed bed in the entrance section of the cells, containing glass beads of 4 mm diameter to a depth of about 7 cm. The glass beads are supported on a perforated Pyrex disk slid within the entrance tube to the reduced section. An important advantage of this configuration has already been illustrated in Chapter 3 where the temperature of the gases at the entrance of the reference cell could be manipulated independently for the compensation of the gas phase absorbance. The temperature T1 could be monitored very accurately through the packed bed.

The exit side arm was mounted identically on the reaction cell except that its diameter was uniform (15 mm O.D.). The overall length of the entrance and exit arms was exactly 13 cm. Just above the junctions with the cells at the base of the two vertical arms, Kovar joints were attached in an inclined position. They enabled thermocouples to record the temperatures T1 and T2 at the entrance of the reference cell below the packed bed and at the outlet of the reaction cell just above the catalyst pellet. Two additional 6 mm O.D. Pyrex tubes connected the two cells. These tubes were located at 1.5 cm from each end of the two cells and were mounted parallel to each other in the same horizontal plane so that they could be aligned with their counter-parts. This geometry allowed the splitting of the flow between the two cells into two equal streams impinging on both faces of the catalyst wafer according to the design considerations elaborated in Chapter 3. To ensure proper final alignment of the two cells, a special mount was designed to support the individual cells in this position before the glass blower made the final connections. Use of two single loops of 5 cm diameter to connect the cells provided slight flexibility between the two cells, enabling the same cell assembly to be used throughout the rest of this study. This added flexibility is necessary to prevent breaking of the connecting arms between the cells.

After the cells had been positioned in the infrared compartment in their final position by fastening the infrared windows, the upper sections of the inside side walls were covered with the same 1/2 inch thick Cotronix insulating blanket. This insulation must be placed carefully with special attention around the ends of the cylindrical sections of the cells and between the connecting loops and the lateral walls.

The top cover of the reactor tank, also insulated on its inside wall, was then positioned to close the infrared compartment. Two circular holes of adequate size had been drilled through the cover to permit the sliding of the lid over the entrance and exit vertical arms of the Pyrex assembly. On the lid , a small motor was mounted to drive a blade type stirrer which circulates the air inside the reaction oven. The stirrer was positioned in the space between the two cells by means of an extended shaft and a carbon bearing which can sustain the high temperatures used during the pretreatment of the catalyst.

The inlet and outlet Pyrex arms extended about an inch beyond the top of the aluminum cover. To close the recycle loop special adapters were constructed to connect the Pyrex tubes to the stainless steel sections of the reactor loop.

These adapters, with appropriate sealing Viton o-rings were slid over each arm of the cells before being tightened at the other end with Swagelock fittings to the valves S4 and S5 just outside the ~~pump~~ oven compartment (see Figure 4.3). To avoid breaking the glass while tightening the nuts, a 3 inch long section of flexible stainless steel tubing was inserted in the middle of the connecting lines of the adapters. Finally, the Pyrex ends were sealed by hand-tightening the adapters on top of the reaction compartment. This design provided a leak-free operation and enabled easy dismantling of the reactor assembly. Dismantling usually was necessitated by corrosive oxidation of the copper wires connecting the ports of the strap heaters at the bottom of the infrared compartment. Despite these drawbacks the reactor remained dependable and could be dismantled and reassembled in a few hours . A final layer of insulation (1/8 inch thick) covered all the external aluminum walls of the infrared compartment in order to reduce the heat losses to the surroundings and to prevent the direct contact of the hot metal surfaces with the sides of the analytical compartment of the spectrometer.

4.4 Catalyst Sample Holder

The catalyst sample holder shown in Figure 4.5 was fabricated of Pyrex and consisted of three separate pieces. The central piece was a 3/4 in. long 28 mm O.D. 23 mm I.D. Pyrex tube. At both ends, thicker glass walls were used to machine flanges that could fit exactly into the inside

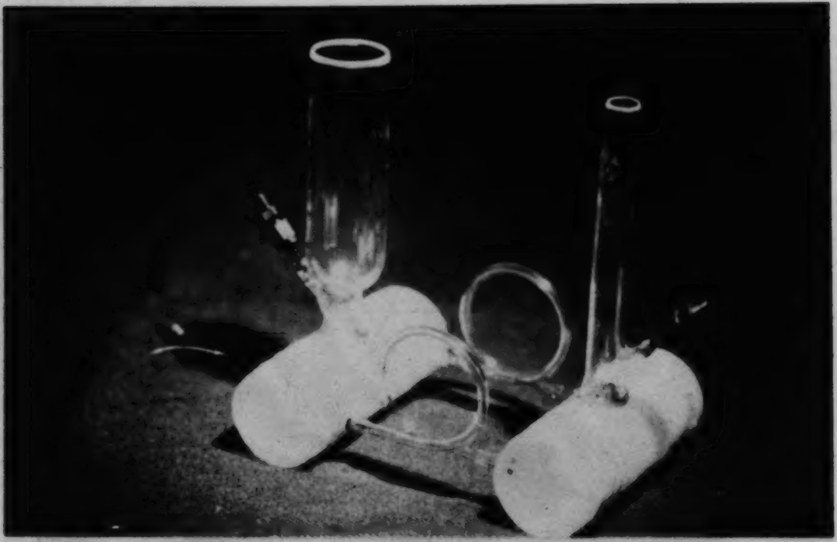

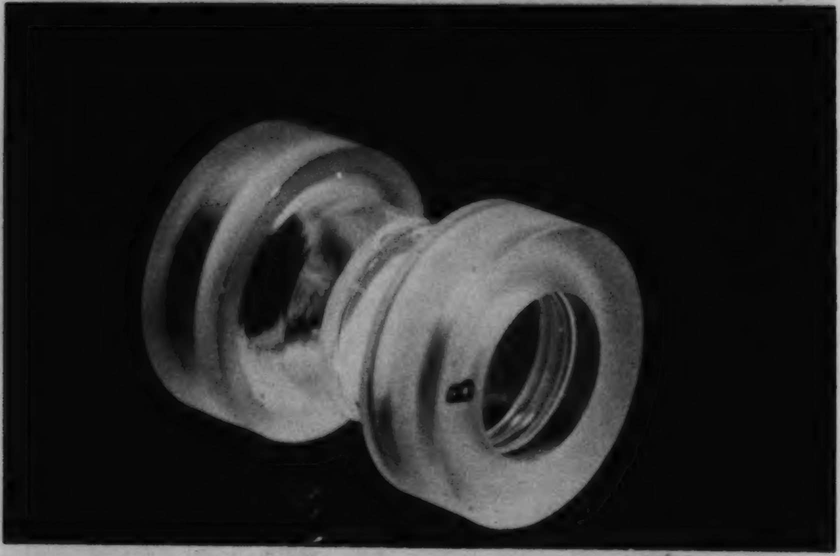

Figure 4.5 Photographs of Cell Assembly and Catalyst Sample Holder

cavities of the two identical external pieces. A slot, 1/16 in. wide was cut in the middle of the holder for insertion of the catalyst wafer. The wafer was supported in three places where the slot had not been cut . The thickness of the wafer was usually about 0.1 mm and the escape of the impinging gases occurred radially outwards through the remaining open space of the slot.

Two identical outer caps of geometry similar to the previous infrared caps were machined in the glass shop. The larger inside cavity (33 mm diameter) was dimensioned to accommodate exactly the flanges at each end of the central part of the sample holder. The smaller hole (23 mm diameter) on the front ends of the caps permitted the free flow of the gases to the catalyst as well as the passage of the infrared beams through the cells. The outer cylindrical surfaces of the caps were machined to fit as closely as possible the insides of the cells to minimize by-passing of the catalyst by the reacting gases.

Before an experimental run, a catalyst wafer was placed into the central slot of the sample holder. This was accomplished by picking the wafer up with a flat device such as a razor blade and inserting it horizontally into the slot of the sample holder. The entire sample holder unit could be inserted from either end of the reaction cell and positioned in its centre. Because of the minimal tolerances achieved in the construction of the sample holder, all the reacting gases were forced to impinge on the catalyst before being evacuated through the open parts of the slot at the periphery of the catalyst. When the pump was turned on, the pellet was exposed to the rapid flow fluctuations originating from the pump, and some deterioration of the wafer sometimes happened after a few hours. From experience with alumina, the use of pellets of less than 60 mg is not recommended. Above that weight, the mechanical strength of the wafer allowed trouble-free operation for many days.

5. EXPERIMENTAL PROCEDURES AND DATA EVALUATUION

5.1 Reagent And Catalyst

The high purity nitrogen (99.99%) used in the kinetics study was supplied in cylinders by Alberta Oxygen Ltd. Even though the oxygen impurity analyzed by gas chromatography on a typical sample was found to be negligible, a column filled a supported Cu-CuO catalyst was installed in the feed line of nitrogen. Moreover, traces of water and carbon dioxide vapours were also eliminated by passing the diluent nitrogen through a column filled with molecular sieve and ascarite before entering the reactor.

The reactant, 2-propanol was purchased from Fisher Scientific Co. and was of spectroscopic grade. No further purification was attempted since traces of impurity could not be detected by infrared and gas chromatography. In mixed feed experiments water was added. Nitrogen was the main impurity contained in the oxygen used for the pretreatment of the catalyst.

Only one type of catalyst was used in the present study.It is the γ-alumina supplied by the Cabot corporation, under the trade name of Alon.This alumina is no longer being manufactured by Cabot Corporation. The typical properties of the alumina, as specified by the manufacturer are listed in Table 5-1. Alon is a fumed alumina containing extremely small non-porous particles made by the hydrolysis of aluminum chloride in a flame process. The extremely small

Table 5.1 Typical Properties of Alon

Color and Form	=	White Powder
X-Ray Structure	=	90% Gamma Form
Alumina Content*	=	99% minimum
Ignition Loss	=	4.5% maximum
Metallic Oxides **	=	0.2% maximum
Avg. Particle Diameter	=	0.03 micron
Surface Area	=	100 m^2/g
pH (10% Aqueous Suspension)	=	4.4
Specific Gravity	=	3.6
Loose Density	=	1.8 - 2.0 lbs/cu. ft.
Bag Bulk Density	=	3.0 - 4.0 lbs/cu. ft.
Refractive Index	=	1.70

Note: *Excludes physically and chemically combined water

**Other than Al_2O_3

particles allow Alon to be pressed into wafers suitable for infrared spectroscopic studies. Thin infrared-transparent catalyst wafers were prepared by pressing the Alon in a die under high pressure (9.81×10^7 Pa). Forming much thinner wafers (8 mg/cm^2 compared to (16 mg/cm^2) was made possible by designing a new die and by using Teflon pads instead of stainless steel for squeezing the powder. Since the experience herein was limited to compacting Alon,other practical implications are therefore omitted. The use of very thin wafers diminishes scattering losses and lattice absorption by the solid and facilitates the interpretation of spectra, particularly in static studies. In this work, where the catalyst is used under dynamic conditions, the use of thinner wafers is in fact limited by the mechanical strength of the pellet (as seen in Chapter 3).

The typical surface area of the catalyst, 91 m^2/g,after pressing into wafers was determined previously by Chuang (75) and Liu (152) using the standard BET method of nitrogen adsorption. The adsorption isotherm was also measured and the associated pore size distribution calculated according to the procedure reported by Gregg and Singh (150).

5.2 Recording And Monitoring Of Process Temperatures

Five 1/8 o.d. type 316 stainless steel shielded iron-constantan thermocouples were introduced into the infrared reactor compartment before operation. These thermocouples were selected so that their readings,when calibrated in a bath of known temperature before installation,did not differ by more than 0.5°C from the true temperature in the range of reaction temperatures between 200 and 300°C.The length of each of these thermocouples permitted for making the required connections to the temperature recorder.

The thermocouple,T3,served as input to the Honeywell temperature controller (SCR trigger controller,Model R7161J) which controlled the temperature in the centre of the compartment,near to the fan. The output voltage from the controller was applied to two 400 watts strap heaters located in the bottom of the compartment. The other four thermocouples ,T1,T2,T4 were connected to a Speedomax type G temperature recorder (Leeds and Northrup Co.) and their specific role will be explained later.From time to time, a known voltage from a potentiometer was fed into the recorder or the contoller to check the voltage or correspondingly, the temperature indicated by the readings on both instruments. Throughout the study, no noticeable drift in temperature recording was experienced. This was confirmed by noticing that the same settings of the various Variacs always resulted in the same readings on the recorder.

The geometrical arrangement of the thermocouples inside the reactor tank is depicted in Figure 5-1. T5, one of the four thermocouples hooked to the Speedomax recorder, was positioned in the bottom corner of the tank just above the heaters. Another thermocouple T1 indicated the temperature

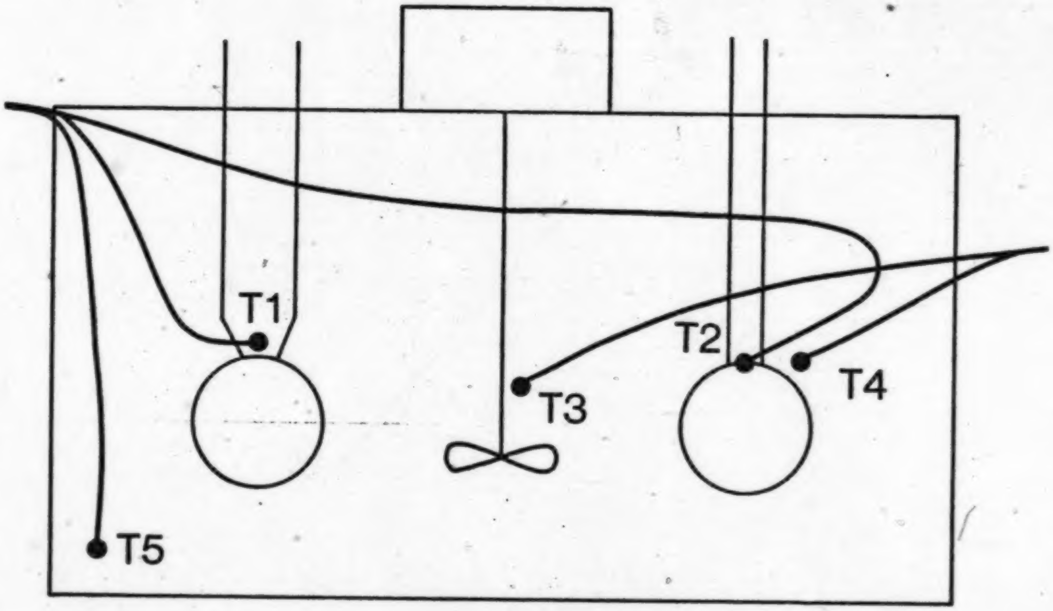
T1
T2
T3
T4
T5

Figure 5.1 Geometrical Arrangement of Thermocouples in the Reactor

of the recycling gases at the entrance of the reference cell below the preheater bed. The packed bed heater consisted of nichrome wire (4.28 ohm/ft) wound around the outside wall of the entrance tube of the cell assembly. Since it was designed to preheat the incoming reactive mixture, a 1/2 inch thick layer of insulation (Cotronix ceramic blanket) covered the heating wire to prevent the heat generated from diffusing appreciably into the compartment. This was subsequently checked during operation by changing the input voltage to the preheater while keeping the other heating devices unaffected. The high sensitivity of the thermocouple T1, to such a disturbance, compared to the absence of response of the other temperature readings suggests that most of the preheater load is transferred to the entering gases. To adjust the temperature, T1, accurately over a wide range of voltage inputs, the resistance of the preheater was set at 60 ohms. As mentioned in the previous chapters, this heating device was most helpful in performing the calibration tests enabling proper compensation for the gas phase absorbance.

The thermocouple T2 was the most important in the sense that its reading was taken to be the true temperature of the catalyst wafer. The end tip of T2 was inserted into the reaction cell just above the catalyst wafer. Both T1 and T2 were mounted on side arms of the cell assembly by means of Kovar joints. The tightening of the thermocouples to the Pyrex unit was done very carefully and permanently at the beginning of the study. No attempt was made to remove them, since the entire assembly can be removed from the top of the compartment even with attached thermocouples. The tip of T4 was placed in the oven just outside the reaction zone to indicate the difference in temperature between the inside and outside of the reaction cell. Finally the role and position of T3 have been specified above.

It was already mentioned at the end of Chapter 3 that substantial differences between the readings of T2, T3, T4 and T5 arose during the initial operation of the system. It was also discovered that the main cause of these differences was the significant heat loss through the infrared windows. This led to the incorporation of an additional heating device in these crucial areas. A single Nichrome wire heater was wound in series around each end of the Pyrex cells. Ten turns of 4.28 ohms/ft heating wire, covering a section of about 3 cm at each end of the cell, provided a heating resistance of 18 ohms in the vicinity of each window. The total resistance of the heater amounted to 80 ohms, which is appropriate for fine adjusting of the heating load with a Variac. In contrast to the preheater, no insulation was used to cover the sections of this heater, because it was found to be advantageous if some part of the generated heat was dissipated in the tank to give a more uniform distribution of temperatures throughout the compartment.

By adjusting the associated Variac (at settings usually between 80 and 100), several significant improvements were obtained. First, it was now possible to match within 2°C the temperatures T2, T3 and T4, which indicates that the radial gradients in the reaction zone on both sides of the Pyrex walls are practically non-existent. Before the incorporation of the heater, T2 and T3 could differ by as much as 50°C mainly because of the cooling of the gases while travelling past the windows. There were also differences of about 10°C between T3 and T4, indicating an insufficient circulation and mixing of the air enclosed within the oven compartment. All of these non-isothermal deficiencies have now been overcome.The new distribution of various heat sources inside the compartment helps to minimize the temperature inhomogeneities. Another advantage was already illustrated in Chapter 3; it was now possible to obtain good compensation of the gas phase absorbance between the two cells by simply adjusting T1 with the preheater Variac a few degrees (about 5°C) below the temperature of reaction T2. This suggests in turn that the axial temperatures gradients inside the two cells are very small, because of the reasonable balance between the heat supplied by the new heater and the heat lost via the windows. Of course, it remains likely that strong gradients are still present in a very thin layer in contact with the windows but these do not affect the crucial reaction zone.

In this final layout, the thermal behaviour of the reactor system was considered satisfactory to serve our purposes.

5.3 Infrared Spectrophotometer

All IR spectra were recorded on a Perkin-Elmer Model 621 infrared spectrophotometer. It is a double-beam, grating infrared spectrometer rated with a photometric accuracy of 0.4% of the transmittance over the entire 0 to 100% transmittance range. The spectrometer has a built-in presample chopper positioned in the IR source compartment to discriminate between the desired signal and thermal radiation from the sample. Heating or cooling of samples in the sample area can thus be carried out without introducing significant errors in the signal.

The slits of the spectrometer can be controlled automatically for constant reference beam energy, can be controlled manually, or in program mode, with or without automatic gain control. More details on the operation of the spectrometer can be found in the Perkin-Elmer Model 621 manuals. The spectrometer was purged with purified dry compressed air. The purging system consists of a series of filters and unheated adsorption columns to remove oil, water vapor and carbon dioxide from the air.

The model 621 is also equipped with an attenuator in the reference beam. This was used in cases where substantial scattering of the infrared beam is caused by the catalyst wafer (especially in the 3000-4000 cm^{-1} frequency range of the infrared beam). The slit opening which is directly proportional to the reciprocal of the original transmittance, can then be decreased to compensate for the loss in energy from scattering. On the other hand, decreases in slit opening reduce the total amount of light in the reference beam and also reduce the sensitivity of analysis.

By adjusting the slit opening, the transmittance indicated by the pen reading was normally set at 80% at 4000 cm^{-1}. For better results, the transmittance reading should lie between 10% and 90% throughout the entire range of infrared scan. This was achieved by stopping the scan and readjusting the beam attenuator as needed from time to time. Since the alumina has strong infrared absorption at frequencies below 1000 cm^{-1}, scans were terminated at 1000 cm^{-1}. For better accuracy, slow scanning speeds should be used. In spectral frequency ranges of no interest, the scanning speed was increased.

5.4 Gas Chromatographic Composition Analyses

5.4.1 Gas chromatograph operation

A Hewlett-Packard 5710A gas chromatograph was used to carry out the analysis. The following chromatograph column and operating conditions were used to separate nitrogen, water, propylene and isopropanol.

Column: The column was made of a 6 foot long, 1/8 inch diameter, 316 SS tubing and was packed with Poropak Q. An identical column was placed in the reference section.

Column temperature: The analysis was carried out with the column at 120°C ,i.e.isothermal G.C. oven temperature.

Carrier and reference gas supply pressure: Helium was used as the carrier gas. The upstream supply pressure was always regulated at 40 psig.

Carrier and reference gas flow rate: The flow rate through each of the columns was regulated at about 45 ml/min at ambient conditions.

Detector: The thermal conductivity detector was controlled at 200°C, and the bridge current sensitivity setting was set at 5 (about 200 milliamperes).

Gas sample valve: A 6 port Valco (LVSV-6-HP.) gas sample valve was used to inject vapour samples. The volume of the sample loop was 0.25 cc. The valve was located inside the pump compartment of the reactor where the temperature was maintained constant.

A typical chromatogram required a total elution time of about five minutes. The carrier gas flowrate was measured with a soap bubblemeter. Spot checks indicated that the carrier gas flow rate through the columns remained constant for the given constant regulated supply pressure. The same column was used throughout the study since it did not show any sign of degradation.

Short term (i.e. overnight) shutdowns of the G.C. system involved a reduction of the helium supply pressure to about 20 psig. The detector temperature controller remained set at 200°C with the sensitivity (bridge current) switch off and all other temperature controllers turned on. Initially, during the start-up period of the G.C. in preparation for a run, the detector output stabilized two hours after the bridge current was switched at 5. This time could be halved when the switch was first set at 6 for half an hour before being brought back to 5.

5.4.2 Calibration with gas samples

Some discussion of the difficulties attached to this routine operation are worthwhile. The basic principle involves that for a given injection of a multi-component mixture, the peak area of a particular compound will be proportional to the product of its characteristic thermal response by its molar fraction (see 5.1):

$$A_i = C_i x_i . R_i \qquad (5.01)$$

Generally, the value of R is not very sensitive to composition and can be assumed to remain constant over the range of concentration used in the kinetic studies. The response factors of the various compounds of interest are usually taken relative to a reference compound, which in the kinetics experiments was invariably chosen to be inert diluent, nitrogen in this work. The response factor of the diluent is arbitrarily fixed at 1 so that for each injection the response factor of compound i is given by (5.02):

$$R_i = (A_i/A_N).(x_N/x_i) \qquad (5.02)$$

It is then straightforward to obtain directly the corresponding relative response factors, by injecting binary mixtures of known composition of the reference compound and one of the other substances. This approach can be easily implemented in the case where all the compounds are liquids since synthetic mixtures of great accuracy are prepared by the weight method. When all the compounds are gases, gas synthetic mixtures can in principle be prepared Although with greater difficulty (152). In this study the presence of gaseous compounds (nitrogen, propylene) as well as liquids (isopropanol, water) renders the previous method more tedious because of the associated vaporization and condensation processes. Furthermore, as already reported (108), liquid phase response factors sometimes differ from the values obtained with vapour phase samples and consequently much danger exists in adopting calibration procedures (no matter how accurate they might be) which are not performed under conditions similar to the routine analyses gathered in the subsequent kinetic experiments. These common difficulties make the use of response factors tabulated in the literature somewhat arbitrary and it seemed preferable to determine their appropiate values when undertaking this study. A simple alternate approach to the calibration of response factors can be based on the assumption that at each injection the number of moles introduced in the gas chromatograph is always constant. Applying the ideal gas law, the total number of moles injected using a sample loop of volume V is almost constant.

During our analyses, repeated injections of samples of fixed composition had a repeatability better than 2% for all the integrated areas. Accordingly, the error introduced by assuming each of P, T and V (sample size) to be constant is less than 2%. This constitutes a minor source of error since frequently the response factors calculated by the more conventional synthetic mixture approach display fluctuations of 5% (108). The assumption that the number of moles introduced at each injection remains constant also means that the proportionality constant C in equation (5.1) remains the same between measurements. The response factors of water, alcohol and propylene relative to nitrogen can be obtained in a straightforward way which is illustrated for the case of propylene.

First, the system was maintained at steady temperature and pressure while a constant flow of nitrogen (using the Matheson flow controller) was passed through the system and analyzed by G.C. at the outlet of the system via the sampling loop. The result is summarized below:

$$A^o_N = C.x_N = C \qquad (5.03)$$

$$A^o_P = C.x_p.R_p = 0 \qquad (5.04)$$

Propylene was then added to the feed mixture at a constant flow rate. After a few minutes had elapsed, the composition at the system outlet was at steady state and the peak areas from successive injections were recorded. The results can be written:

$$A_N = A_N^o . x_N \qquad (5.05)$$

$$A_P = A_N^o . (1 - x_N) . R_P \qquad (5.06)$$

By eliminating the molar fraction x between the two equations we obtain an equation relating the peak areas of the two components:

$$A = A_N^o - (A_P / R_P) \qquad (5.07)$$

The procedure was repeated for a wide range of binary compositions. In fact, equation (5.6) should always remain valid, irrespective of whether the composition of the mixture was constant or not. This final equation enables rapid estimation of the relative response factors. This method relies on the unique assumption that the same molar quantity is introduced at each injection. We have seen above and verified that this constitutes a reasonable approximation since the sample volume, and the temperature and pressure of the sampling valve did not change

Plots of nitrogen peak areas versus peak areas of propylene, isopropanol and water, respectively, are shown in Figures 5-2 to 5-4. Tables 5-2 to 5-4 indicate the results

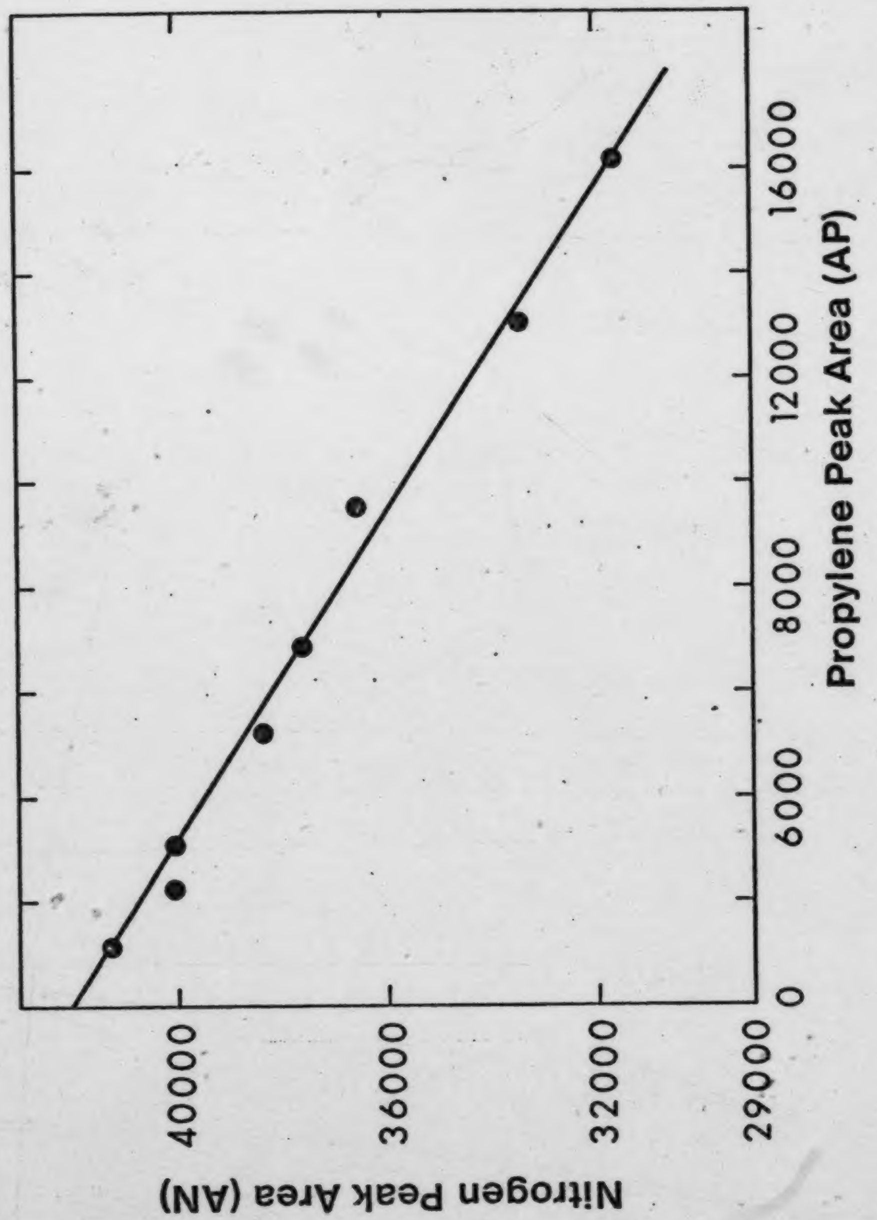

Figure 5.2 G.C. Calibration Plot of Propylene

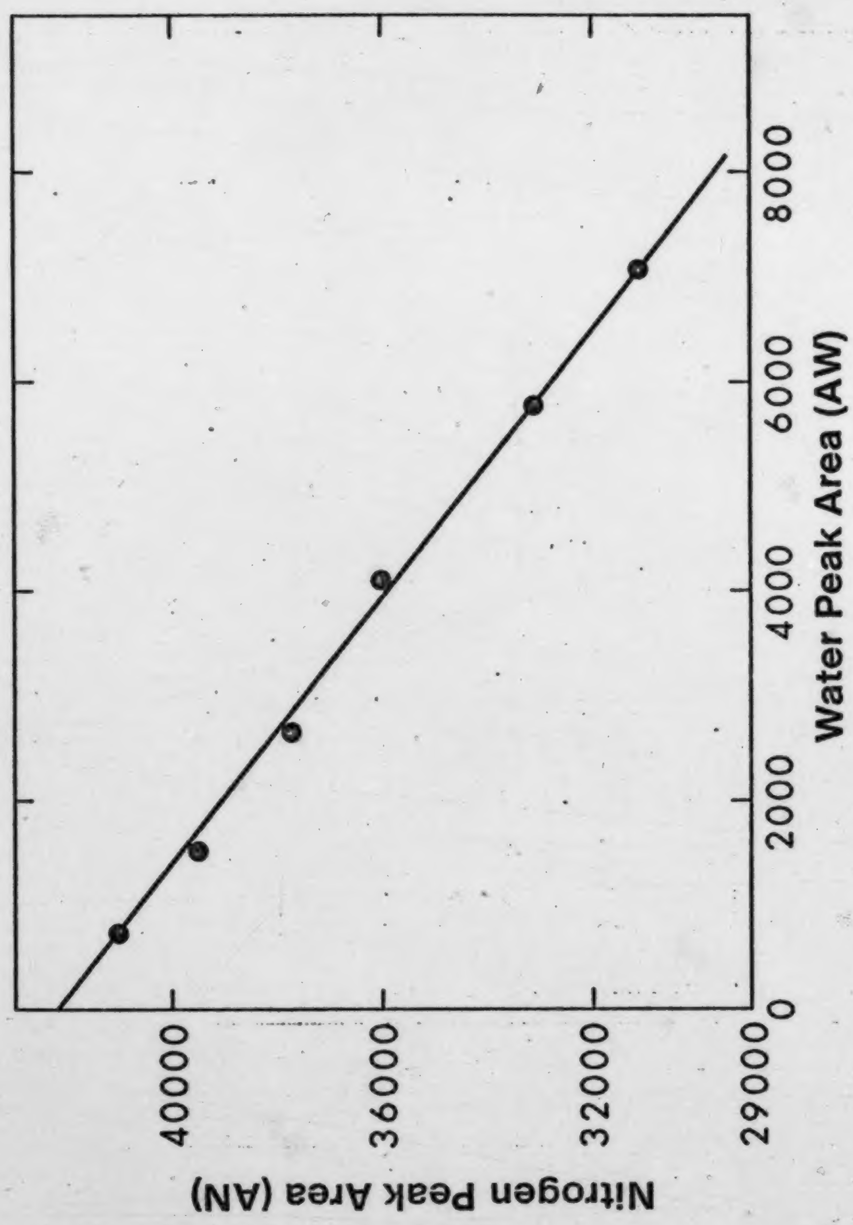

Figure 5.3 G.C. Calibration Plot of Water

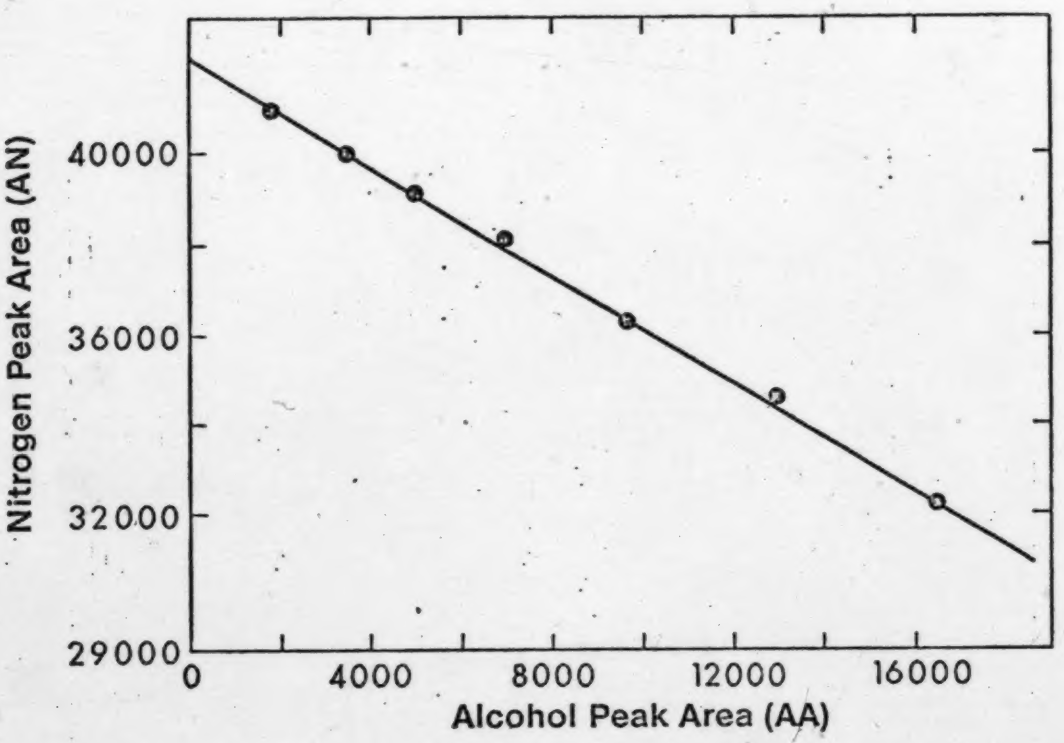

Figure 5-4. Relative Response Factor of Alcohol.

Figure 5.4 G.C. Calibration Plot of Isoproppanol

Table 5.2 Least Squares Fitting of G.C. Calibration Data for Isopropanol

Measured Alcohol Peak Area AA	Measured Nitrogen Peak Area AN	Calculated Nitrogen Peak Area
16520	32300	32402
13050	34610	34437
9650	36290	36430
7010	38110	37978
4970	39200	39174
3480	40040	40048
1855	40980	41000
1085	41440	41552
570	41750	41860

The coefficients of the straight line are

$a = 1.71 \pm 0.0385$

$b = 42088 \pm 110$

Relative Response Factor: 1.71 (2.0 in literature)

Table 5.3 Least Squares Fitting of G.C. Calibration Data for Propylene

Measured Propylene Peak Area AP	Measured Nitrogen Peak Area AN	Calculated Nitrogen Peak Area
16150	31600	31707
13080	33470	33687
9550	36650	35943
6900	37600	37644
5230	38400	38715
3100	40020	40082
2240	40050	40634
1160	41250	41328
680	41830	41636

The coefficients of the straight line are

a = 1.56 ± 0.09

b = 42072 ± 340

Relative Response Factor: 1.56 (1.55 in literature)

fitted by the least squares method for the same data. It is evident that at low concentrations of either propylene, alcohol or water, the relative variations of the peak areas of nitrogen became very small since then x remains practically constant. In order to overcome this problem at the lower concentrations, it was necessary to average as many as fifteen successive injections before obtaining a representative accurate value of the otherwise insensitive integrated area of nitrogen peak. Fairly good straight lines were obtained indicating that the response factors did not change appreciably over the range of concentrations investigated. On the other hand in Table 5-5 we observed significant deviations between the experimental values and the literature values of the response factors for the cases of water and isopropanol. These discrepancies point to the necessity of doing these calibrations to obtain reliable values for the one fixed mode of operation.

5.5 Data Evaluation

This section explains the procedure by which the reaction rates were derived from the experimental measurements. The infrared cell recirculation reactor was employed to generate experimental values of the reaction rate. In the recirculation loop, the recycled flow rate was between 20 and 25 l/mn when the pump was operated at 1725 rpm. The volume of the entire loop was estimated to be near to 600 cc and the total feed volumetric flow rate was always below 500

Table 5.4 Least Squares Fitting of G.C. Calibration Data for Water

Measured Water Peak Area AW	Measured Nitrogen Peak Area AN	Calculated Nitrogen Peak Area
7050	31125	31125
5760	33100	33154
4110	36020	35749
2670	37800	38013
1550	39550	39774
740	41030	41048

The coefficients of the straight line are

a = 0.636 ± 0.028

b = 42212 ± 276

Relative Response Factor: 0.64 (0.78 in literature)

cc/mn (at normal conditions of T and P). Consequently, the recycle ratio was always greater than 40 throughout the kinetic runs enabling low conversions per pass and treatment of the loop as being mathematically equivalent to a well-stirred flow reactor. The great advantage from use of this reactor model is the direct evaluation of the reaction rates from the material balance for the alcohol reactant (5.08):

$$r = F \ . X / W \qquad (5.08)$$

5.5.1 Determination of fractional conversions

Different alternatives are available for calculating the fractional conversion. The usual method consists of measuring the molar fractions of the reactant in the feed and exit streams and correcting these for the change in total molar flow rate due to the stochiometry of the reaction. The conversion X is then given by (5.09) where the subscripts represent the inlet and exit conditions:

$$X = (F \ .x \ \ -F \ .x \ \ )/ F \ .x \qquad (5.09)$$

This method was not adopted in our work because of the rapid fluctuations occurring in the feed composition. Much time and effort was spent to elucidate the nature and implications of this phenomenon. Initially the vaporization and reactant infusion systems were modified several times in order to improve this behaviour. In its final configuration (as described in the previous chapter) the composition fluctuations of the feed were decreased because of the short residence times of liquid alcohol in the heated lines (use of very thin needles) and in the vaporization chamber which was packed with glass wool and equipped with an independent heater. However even in that case, the relative magnitude of the deviations in alcohol composition in the feed stream at a constant setting of the syringe pump could still be as high as 30% as indicated on the chromatograms. At this stage it was difficult to decide whether these fluctuations originated from the imperfections in the syringe feeder or during the vaporization process of the alcohol. In any case, in practice one would have to take the average of numerous successive analyses of the feed stream before obtaining an accurate value of Xo in equation (5.8). This procedure was judged undesirable in consideration of the extensive repetitive labor involved and, more important, because of the possible longer-term systematic trends in the average feed composition, which may occur between the times of analysis of the feed and product streams.

These uncertainties led to the use of an alternate feeding technique incorporating the use of a thermostatted saturating device. The carefully metered nitrogen diluent bubbled through a series of two packed beds filled with isopropanol. Although the rapid feed fluctuations almost disappeared other impracticabilities became evident. First, the range of compositions attainable was limited by the high volatility of isopropanol. Secondly, the time required to reach a constant bath temperature (about one hour) was much longer that the instantaneous change of the dial setting of the syringe pump. Finally the saturating devices are not suited to the injection of various liquids in the same feed (i.e. mixed feed of water and alcohol). After consideration of these disadvantages, the decision was made to return to the use of the syringe pumps as initially planned.

To use the syringe pumps, another method to calculate the values of the fractional conversion had to be implemented. During a series of tests made without catalyst in the reactor, we noticed that the large fluctuations in alcohol composition in the feed stream were considerably dampened by the large volume of the reactor loop which acts as a noise filter towards the rapid erratic feed disturbances. On the other hand, accurate values of the relative response factors of the various compounds of interest have been established experimentally in the previous section. It is then possible from the chromatogram of the exit stream and from the stoichiometry of the dehydration reaction to derive the following expression:

$$A\,.R\,/A\,.R = x\,/x = X/(1 - X) \qquad (5.10)$$

The value of X can then be simply extracted from the known or measured quantities of AA, AP,RA and RP. To ascertain the accuracy and consistency of the fractional conversions thus obtained, we did some runs with the saturator. Since in this case the feed fluctuations were negligible, the values of the fractional conversions obtained by the two independent methods just outlined could be compared directly. The relative percentage deviations between the two values of X obtained for the same run were always within 2% and consequently in principle it does not matter which of the two methods is used by the experimenter provided their results are comparable. However we showed before that the first method could not be applied when using a syringe pump because of the induced fluctuations in the feed composition. In contrast, because of the dampening of the rapid feed fluctuations within the large volume of the reactor, the method corresponding to equation (5.10) becomes appropriate for the recycle reactor. In these conditions, the use of the syringe pumps can be maintained and this possibility may be one important practical advantage of using recycle reactors in general. A single-pass differential reactor would necessitate the use of a liquid saturator to maintain sufficiently stable compositions of the gas phase in the reaction zone since in that case the feed fluctuations would be fully transmitted to the reaction mixture.

5.5.2 Determination of reactant feed flow rate

In addition to the acquisition of the fractional conversions, the values of the reactant molar feed rates F in equation (5.7) were estimated before determining the specific rates of reaction. Again, this seemingly simple matter was not so straightforward as expected. We originally intended to follow a standard procedure used by other workers which consists of determining the calibration curves for the various pump feeders and syringe combinations employed. Distilled water was used as the calibration fluid and the procedure and results are described in more detail in Appendix B. The consistency of the calibration points could be checked in different ways. In principle, the ratios of the delivered flow rates for the same 50 cc syringe at the same settings of the two syringe pumps should be constant. This is shown in Table 5-6; the infusion rates differed by about 3.5 per cent with an error less than half a per cent. Similarly the delivered flow rate ratios were compared at the same settings of one syringe pump but for the 50 cc and 20 cc syringes, the results in Table 5-7 indicate that the flow rates differed by an average factor of 2.075 with deviations less than 3/4 per cent. These tests confirm that the evaporation losses of water was minimal during all the calibration points.

The results obtained for the calibration of the 20 cc syringe will be analysed in more detail. The duration of each calibration point was always between 80 and 120

Table 5.5 Comparison of the Two Syringe Pumps

Setting	30/1000	50/1000	70/1000	80/1000
Ratio	1.038	1.033	1.039	1.040

Table 5.6 Comparison of the 50 and 20 CC Syringes

Setting	Flow rate ratio 50cc/20cc
30/1000	2.08
40/1000	2.066
50/1000	2.061
60/1000	2.081
70/1000	2.088
80/1000	2.089
90/1000	2.064

minutes. Each piston speed was calibrated three times in such a way that the whole range of the piston travel (about 12 cm) was covered. The average value of the three independent runs at each speed was used for the final calibration values. On the lowest speed range (1/1000x), seven average data points were collected. The linearity of the dial settings could be checked by comparing the exact dial setting ratios with the delivered flow ratios at the seven different settings. The deviations from linearity in Table 5-8 are very small (less than 2 per cent) and could certainly be reduced to less than one per cent by fitting the data by the least squares method. These results are in agreement with the specifications of the manufacturer and the results obtained by other workers (108,152) who employed the same feeding technique. However, when one looks more closely at the individual calibration runs (Appendix B), it can be seen that the repeatability of the results at the same speed setting was not as good. More precisely, deviations of up to 5 percent between the individual runs were observed and which were not necessarily caused by the changing positions of the syringe piston. Recalling the fact that the value of each run corresponds to an average value over an experiment duration of 1.5 hours, it can be argued that if one could have recorded the continuous instantaneous flow rates during that time interval, substantially larger fluctuations would have appeared from time to time which were averaged out over the 1.5 hours duration of each run. Voltage fluctuations and

Table 5.7 Linearity of the Syringe Dial Settings

Setting	Dial Ratios	Flow Rate Ratios
30/1000	1	1
40/1000	1.333	1.33
50/1000	1.666	1.685
60/1000	2	2.011
70/1000	2.333	2.335
80/1000	2.666	2.695
90/1000	3.0	3.06

more likely some mechanical slipping in the gearing mechanism of the syringe pump might be the sources of these imperfections. They are difficult to check directly but several experimental observations in this study seem to favour this interpretation.

Before gathering accurate kinetic data, various series of experiments were performed to check the stability of the steady state in the reactor system, without catalyst in the reactor. The flow rate of diluent nitrogen was monitored at a constant level by means of the Matheson pneumatic flow controller described in the previous chapter and the dial setting of the alcohol syringe pump was fixed. In these conditions it was possible, by placing the reference cell in the sample beam of the infrared compartment and by monitoring the peak absorbance of an appropriate band of alcohol, to record continuously the trends in the composition of the mixture in the reactor loop. The transmittance at the maximum of the infrared peak was recorded on a paper chart at appropriate speeds for periods of up to one hour. From time to time, a G.C. analysis of the mixture exiting the reactor was obtained to verify whether at the same instant the trends in composition measured by the two independent methods were comparable. The trends patterns were found to be identical thereby proving that the composition of the gas leaving the system was identical to the one of the recirculated gases inside the reactor loop. The main advantage of the infrared analysis was to provide a continuous visual display of the changes occurring in the system.

Initially, when a straight 1/8 inch O.D. liquid feed line to the vaporization chamber was used, systematic sharp fluctuations of about 10% relative magnitude were repeatedly drawn by the pen of the infrared recorder. The time interval between two successive patterns was between 20 and 30 seconds and could be associated with the simultaneous pressure surges in the vaporization chamber. This parallelism suggested that the vaporization was irregular and submitted to sudden onsets in the liquid transfer lines. It is noteworthy that the G.C. analysis of the feed mixture before it entered the reactor were then completely unreliable. As already mentioned, the suppression of these strong disturbances was achieved by modifying the vaporization system configuration in such a way as to minimize the residence time of the liquids in the heated lines. The vaporization process was then sufficiently stabilized to permit an adequate dampening in the loop volume of the fluctuations still occurring to some extent in the feed stream. The drifts in the recorded alcohol concentrations were now very slow indicating that the reactor volume was in permanent quasi-steady-state. The relative magnitude of the long-term variations never exceeded 10% of the average composition value recorded over a period of one hour and the irregular pattern of the drift was ascribed to imperfections originating in the syringe pump as suggested before.

The practical implications of these direct observations are that a substantial source of error can be introduced in evaluating kinetic data when one is not careful enough and relies too much on the calibration points of the syringe feeder. The calibration procedure as already explained has a tendency to show the syringe pumps to be the better instruments which they really are. From our experience, the true values of the molar feed rate of reactant at a given time could differ by as much as ±10% from the average value obtained by converting the calibrated volume displacement into moles of alcohol. It is therefore important to realize that the syringe pump may deliver a reproducible volume over a period of one hour; this,however, does not guarantee that the instantaneous flow rate had remained unchanged during that period.

Returning to the initial discussion on the evaluation of rate data, it becomes obvious in view of equation (5.7) that even in presence of very accurate estimations of the fractional conversions, erratic values of the intrinsic rate data can still be obtained when using the commonly calibrated values of liquid feed rates. A different procedure was adopted for evaluating more reliably the true value of the alcohol feed rate corresponding to each data point.

During kinetic runs, the nitrogen carrier gas flow rate could be considered constant, since periodic checks of this process variable in the midst of experiments resulted in relative variations of less than one per cent. At steady state the G.C. analysis of the reacting mixture allows the determination of the nitrogen/alcohol molar ratio fed to the reactor. First, equation (5.10) states that the ratio of the nitrogen to alcohol peak areas corrected by their relative thermal response is equal to the molar ratio of the same two components in the injected sample.

$$A_{N} \cdot R_{A} / A_{A} = x_{N} / x_{A} \qquad (5.11)$$

The simple stoichiometry of the dehydration reaction can also be written as in equation (5.12) where the molar feed of reactant has been normalized.

$$\begin{array}{lccccc} & N_2 & A & \longrightarrow P & + & W \\ \text{inlet} & & 1 & - & & - \\ \text{exit} & & 1-X & X & & X \end{array} \qquad (5.12)$$

At the exit conditions, which are also the conditions prevailing in the recycle reactor, equation (5.11) is then rewritten:

$$A_{N} \cdot R_{A} / A = \alpha / (1-X) \qquad (5.13)$$

The only unknown remaining in this final form of the equation is " " ,whose value can now be extracted from the other known quantities. The molar feed rate of alcohol is then simply given by equation (5.14), where we know exactly

$$F_{Al} = F_{N} / \alpha \qquad (5.14)$$

the constant nitrogen flow rate,FN, which was kept constant for a whole series of runs. The intrinsic reaction rate data could then be directly evaluated using equation (5.7).

For the correlation of kinetic models additional calculations for the determination of the independent variables of the models (i.e. partial pressures of compounds) were also required. An example showing all the step- by-step calculations of the reaction rate and associated partial pressures is exhibited in Appendix C. For convenience, the total pressure in the reactor was kept constant throughout all the experimental runs. For more accuracy the average value of a series of three analyses taken over a period of ten minutes were used for the calculation of each kinetic run. This precaution ensured that, despite the slight changes in steady state due to the syringe pump imperfections, a good representation of the average steady state in the reactor during the period of analysis was selected for the final data.

Although it is felt that accurate kinetic data are possible by using this method of calculation and that rapid and simple acquisition of rate data are possible after the final procedure had been established, it is important to note its shortcomings. One may argue that this procedure has been based upon the perfect matching of the material balance around the reactor. To date no check on this assumption is available and additional comments are needed to justify this apparent weakness.

To check the material balance for the reactant isopropanol, it is possible to compare the calculated-nitrogen-to alcohol molar ratio fed to the reactor to the one that would be normally expected from the calibrations of the syringe feeder and from the accurately measured nitrogen flow rate. For instance, during the kinetic experiments sixteen runs were performed at the same setting of the alcohol syringe feeder (90/1000). These 16 data points have in fact been gathered at different temperatures, some with the 50 cc syringe others with the 20cc syringe, some in pure feed experiments, others in mixed feed experiments with water, and finally at various flow rates of the nitrogen diluent. For simplicity, the 16 calculated values of " " have been standardized for the conditions corresponding to the use of the 20 cc syringe and a constant flow rate of nitrogen of 1.065 gmol/h. The sixteen resulting values of " " can then be directly compared to the ideal value of " " obtained by taking the corresponding calibrated flow rate of the syringe at the same setting (see Appendix B) and at the same nitrogen flow rate. This ideal value of " " is 35.3, while the individual 16 experimental values vary as follows: 34.73, 32.94, 39.2, 35.6, 34.3, 35.9, 36.8, 35.6, 35.95, 34.83, 34.61, 33.48, 37.1, 33.85, 36.9, 36.7.Their average value being 35.5. The main conclusion is that there is a very good agreement between the expected value from the calibration of the syringe feeder and the corresponding sampled average value from the kinetic data. This contributes a rather severe test to support the internal consistency of our method of data evaluation considering that all possible sources of errors are included in the kinetic data. It is equally important to realize that important errors would have been incorporated in the kinetic data if the same calibrated value of the feed rate of alcohol had been used for the 16 individual runs. These significant experimental errors would of course render the model fitting and discrimination procedures used in Chapter 6 much more difficult to implement.

One could argue now that the good agreement obtained at the particular dial setting of the sixteen data was fortuitous. For that reason the same procedure was applied to other settings of the alcohol syringe feeder which were used for the acquisition of at least ten kinetic data points, so that a meaningful sampled average of " " be obtained in each case. The results, which prove the internal consistency of the material balance over a wide range of the kinetic data, are summarized in Table 5-8.
Once again, considering that the sampled values of " " incorporate all the possible sources of errors coming from the analysis and the calculation methods used in the evaluation of the kinetic data, the agreement is very good.

In conclusion, it is now agreed that syringe feeders can deliver a constant average flow rate over a sufficient length of time, but at any given time and for a period of a few minutes which are required for the gathering of kinetic data with our new reactor, the infusion rate may differ by

Table 5.8 Internal Consistency of the Alcohol Material Balance

Dial Setting of Syringe Feeder	30/100	15/100	90/1000	50/1000	30/1000
Number of Runs	10	16	16	13	15
Sampled Average of " "	10.95	23.62	35.5	65.0	114.3
Calibrated expected value of " "	10.83	23.07	35.3	64.55	110

±10% from its average rating. These variations become a major source of error in evaluating rate data and should be taken into account. Fortunately, because of the relatively slow response of our large reactor volume and of it resulting operation in permanent quasi-steady state , we could incorporate the syringe pump imperfections directly into our calculations and obtain much more accurate reaction rate data. The remarkable agreement obtained in Table 5-8 substantiates these findings.

5.6 Operation Of Equipment And Procedures During A Run

The method of preparation of the catalyst wafer was described in section 5.1. The weight of the catalyst was found by weighing the sample holder with and without the wafer. The wafer in its holder was then introduced in the middle of the reactor cell according to the method outlined in section 4.4. Two new Viton o-rings were usually employed for sealing the ends of the reaction cell while the same salt windows could usually be used again for further experiments after inspection of their infrared absorption spectrum.

5.6.1 Start-up and catalyst pretreatment

At startup, the nitrogen flow was turned on after setting the regulator pressure at either 30 or 60 psig. The needle valve on the flow controller was adjusted to give the desired reading on the upstream nitrogen feed rotameter. These conditions were maintained for a complete series of experiments. At this time, the possibility of leakage from all sections of the system was checked. The incorporation of various valves in key locations of the piping greatly facilitated the rapid determination of leakage areas, enabling by-passing of successively different sections of the reactor system. Since the flow delivered by the Matheson controller remained constant, independently of the downstream pressure, the flow rate measured with the soap-bubble meter had to remain identical when passing through different sections of the reactor. Because of the deterioration of the sealing surface of the infrared windows with time, these were usually the source of unexpected leaks and had then to be replaced.

In the present work, the following finalized pretreatment procedure was adopted. The fresh catalyst in position was heated at 400°C in a continuous stream of nitrogen. At that time one usually noticed the appearance of localized dark points on the pellet surface, probably due to the reduction to carbon of tiny pieces of paper which had adhered to the catalyst during the pelletizing process. The combustion of this carbon was carried out by switching off the nitrogen flow and replacing it with pure oxygen flow during overnight at 400°C. The pellet surface became spotless white after that treatment. The next morning the oxygen flow was again replaced by the nitrogen flow before cooling the reactor to the maximum reaction temperature of 274°C. The recirculation pump was then turned on at its normal operating speed of 1725 rpm. Before admission of the reactant, the baseline spectrum of the wafer was acquired to duplicate a baseline spectrum obtained in other studies, with its distinct characteristic OH stretching absorption bands. The presence of other infrared bands indicating the contamination of the catalyst by some remaining surface organic species was not detected in the spectrum. The alcohol feeder was turned on and the reactant started to pass through the vaporizer and into the reaction system. The system was maintained in these reaction conditions for the rest of the day, allowing the catalyst to stabilize to a constant activity level. The initial deactivation was accompanied by the formation of carboxylate species on the catalyst surface as evidenced by the simultaneous growth of absorption bands at 1570 and 1470 cm^{-1}. This surface process will be discussed more thoroughly in the next chapter. We are concerned here with the final pretreatment procedure that was selected for the obtention of reproducible kinetic data. Before the second overnight period, the alcohol feed was shut off so that the residual reactant and products could be flushed out of the system during the cooling of the infrared compartment down to about 100°C. Once the set point of the Honeywell controller had been lowered and the secondary heaters turned off the cooling required forty minutes and was slow enough to prevent the cracking of the NaCl infrared cell windows. The recirculation blower remained in operation until the reactor section was at 100°C before being stopped. This avoided unnecessary use of the pump and shortening of its life. The differential catalytic bed was maintained in a continuous stream of nitrogen overnight at 100°C. It should be mentioned that during all these procedures the pump oven temperature was kept constant since it required four hours to reach a steady state operation condition. The alumina pellet was then considered to be in a standard activated state and ready to be used for many days of operation without noticable degradation of its activity as long as the conditioning temperature of 280°C was not exceeded.

In the early stages of this study, it was found that leaving the catalyst during the overnight shutdown at a temperature close to operating conditions, caused some additional decrease in activity. A progressive build-up of carboxylate species on the surface of the wafer and also a darkening (probably some coke formation) of the pellet color were observed. It became impossible to obtain kinetic data at a constant activity level between dayto-day operations. This behaviour is difficult to explain since on the other hand during a normal daily operation at reaction conditions no noticable change in catalytic performance was observed. It can be postulated that traces of organic materials present in the system are responsible for the overnight degradation in activity but this seems to be contradicted by the fact that during kinetic runs at higher concentrations the deactivation process was no longer effective. Although not quite understandable the fact is that the catalyst in use was more stable than the catalyst at rest. In presence of traces of hydrocarbons, the deactivation process seems to be favoured at lower temperatures and consequently, we had to cool the catalyst overnight down to 100°C as mentioned before where the same process seems to be negligibly activated.

5.6.2 Steady state operation during kinetic runs

Each morning, the first step consisted of turning the pump on and checking that no leaks had developed in the system. At the same time, the bridge current of the G.C. thermal conductivity detector was switched on because it took about an hour before reaching a stable condition without drifting of the baseline. The strap heaters, connected to the Honeywell controller, were then used to heat the infrared compartment in successive steps of 30°C. This progressive increase in heat supply was intended to avoid the cracking of the infrared windows that could result from a too sudden thermal expansion. The recirculation fan was also in operation during this time. As soon as the controller had reached its final setting, the heating loads to the auxiliary heaters (packed bed preheater, window heaters) were adjusted with their respective variacs. After some stabilization period and fine adjusting of the heat supplies, the temperatures T2 and T3 matched the desired reaction temperature while the T1 reading was maintained about 5°C below as established in Chapter 3. About one-and-a-half hours had elapsed since the start. A baseline spectrum of the catalyst in pure nitrogen was recorded for comparison with the one of the previous day.

The reactant feed rate was then adjusted on the syringe pump control dials and because of the consecutive change in the thermal properties of the recirculating mixture, some minor tuning of the auxiliary Variacs was done, as required, to keep the same temperature readings inside the reactor. When taking kinetic data the reaction cell was removed from the infrared beam, for the reason that some internal heating of the catalyst resulted from absorption of energy from the radiating beam and this increased slightly the activity of the wafer. From the activation energy of the reaction, the change in the true temperature of the wafer was estimated to be of the order of 1 to 2°C and it is preferable to operate without that additional source of error. The total pressure in the reactor loop which was measured immediately downstream of the wafer was readjusted now and then to its permanent value particularly when the flow conditions to the reactor were modified.

To determine attainment of steady-state, a number of sequential gas chromatographic analyses were taken until the usual variations of the recorded peaks were minimal. The most sensitive peak between injections was always the one corresponding to isopropanol because of the syringe feeder imperfections mentioned in the previous section. In comparison, the propylene and water peaks were not affected by the reactant fluctuations because of the usually fractional or almost zero order of the reaction with alcohol concentration. The average of three successive injections where the relative variations of the alcohol peak areas had been less than five per cent was taken as representative of a stable steady-state in the system.

In the process of continuous kinetic runs, about 30 minutes should be allowed to elapse, starting from the time the reaction temperature was changed to where another new steady state condition was obtained. For feed- rate changes, up to 20 minutes were required, depending on the throughput in the system before a new data point was taken. Steady-state spectra of the catalyst in different working conditions could be recorded at any time.

At the end of the day, the system was returned into the standard overnight shutdown conditions described in the previous sub-section. The motors of the spectrometer were switched off and the source intensity of the Nernst glower reduced to a minimum to prevent its constant overheating. On the gas chromatograph, the carrier gas helium flow rate was reduced and the bridge current powered off.

5.6.3 Limitations of the technique

To complete this section, it is important from a practical point of view to assess the range of experimental conditions over which reliable surface spectra could be obtained during the dehydration of 2-propanol. It is unfortunate that the most intense infrared bands of adsorbed species (i.e., C-H stetching bands) are located in the same region of the infrared spectrum as the most intense bands of the associated gaseous 2-propanol molecules. Because of the considerations involved in the design of the cell, accurate control for the compensation of the gas phase absorbance was possible. However, when the gas phase concentration is sufficiently high to reduce the reference beam transmittance to roughly less than 3% of the incident energy, the lack of transmitted energy in both beams necessitates a widening of the slit opening, which in turn induces a drastic decrease in band resolution. It then becomes impossible to record accurately the difference in energy transmitted between the reference beam and the sample beam. In this study, the coverage of the catalyst as indicated by the C-H stretching absorption bands of the adsorbed alcohol could be recorded satisfactorily up to molar fractions of alcohol of about 8% in the gas mixture. The reactor loop was always maintained at a total pressure just above atmospheric pressure.

This limitation in band resolution will always be present to some degree in other applications of the technique utilized in this work, but its negative effects could be diminished in the following three ways:

1. *use of shorter cell lengths*; although feasible it is anticipated that substantial complications in the design would be encountered for preserving the good contacting between the gases and the catalyst as well as the good

isothermality in the reaction zone;

2. *use of a higher performance IR spectrophotometer*; what is recommended is an instrument with the highest capability to keep proper response throughout regions of high reference beam absorption. This would expand the range of concentrations where accurate surface spectra of an adsorbate-adsorbent system can be gathered;
3. *use of an appropriate adsorbate-adsorbent system*; it is obvious that reaction systems where adsorbed species display absorption bands in different regions from their gas-phase counterparts are most propitious to the implementation of the technique. This might surface when only very simple molecules are involved, but in general with organic molecules, the frequency shifts of the vibration modes between gaseous and adsorbed molecules are too small.

In addition to this problem at high substrate concentrations, one wishes to be able to analyze the gas composition of the mixture reacting with the catalyst. The use of gas chromatography with thermal conductivity detectors provide separations sensitive to molar fractions of 0.3% for most compounds. From this and the preceding discussion it could be expected that the combination of simultaneous IR spectra and kinetics would be limited to molar fractions of isopropanol in the range 0.3 to 8%. Indeed, within this range and at temperatures where the rates of reaction were measurable, the relative reactant coverages of the alumina, deduced from C-H stretching spectral bands, were sensitive to the alcohol composition (see Figure 6-1).

By varying the temperature of reaction in preliminary experiments, the range of applicability of the technique could be restricted to between 220°C and 280°C. Below 220°C, the rate of reaction is too slow and over the practical range of concentrations the catalyst remained saturated with adsorbed reactant. The coverage was strongly dependent on the catalyst temperature. Above 280°C, the coverages of the catalyst at reactant molar fractions not exceeding 8% was always very low, which limited considerably the information additional to the kinetics that could be gathered using infrared means. Subsequently, all kinetic data were taken in the range of temperatures between 220°C and 280°C.

6. RESULTS AND DISCUSSION

6.1 Infrared Spectra Of Alumina Under Reaction Conditions

6.1.1 General characteristics of surface spectra

The conditions for obtaining spectra representative of the baseline of the solid alumina plus absorption bands attributable to adsorbed species have been described in the previous chapters.Spectral scans , were recorded at steady-state reaction conditions during which all experimental parameters (T, P, flows) were held constant. Figure 6-1 summarizes the noteworthy regions of the IR spectrum in which spectral bands for the adsorbed species were interpreted. Discussion of those regions of the spectrum not of consequence in this work have been omitted.

The criterion initially employed for associating band character with available species likely involved in the dehydration reaction mechanism was to observe if changes in concentration of 2-propanol in the feed also influenced intensities of particular bands. Constancy of the band intensity when the reaction rate was so changed presumed independence from the surface reaction of interest. This criterion is not infallible, e.g. as will be seen, the 2-propanol adsorbs as a reactant and although the intensity of the 2970 cm^{-1} band changes appreciably, the reaction rate remains almost constant. However, both do change simultaneously at low surface coverages of 2-propanol. Spectral bands associated with spurious adsorbed species (using the above

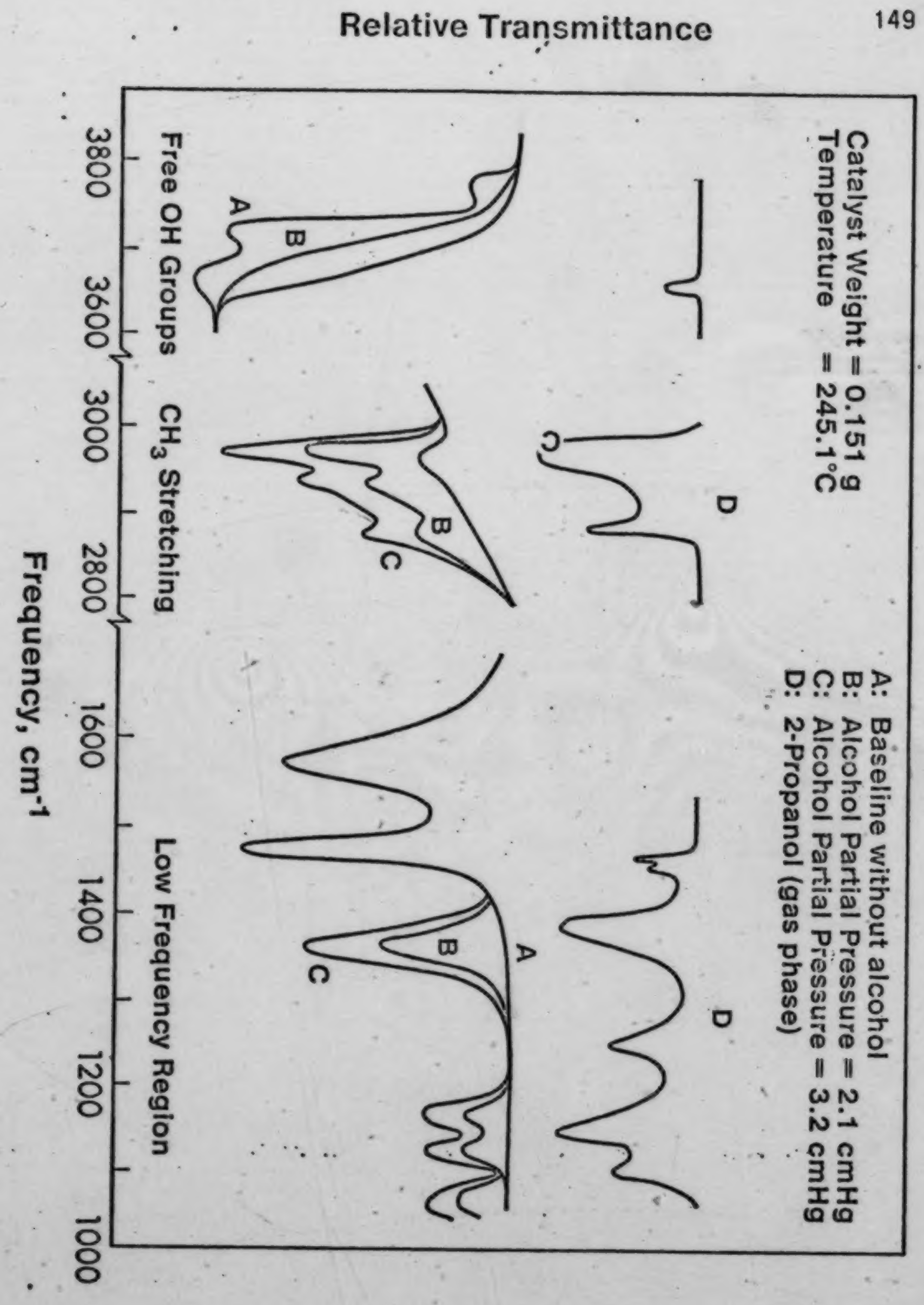

Figure 6.1 Infrared Spectra of Alumina Under Reaction Conditions

criterion) were examined to determine if they independently influenced the reaction rate.

Returning to Figure 6-1, one notes:

1. the surface hydroxyl groups (3600-3800 cm^{-1}) associated with the alumina surface progressively disappear with increasing 2-propanol concentration. This suggests that the hydroxyl site may indeed be a surface reaction site via some form of hydrogen bonding;
2. The stretching vibrations of the methyl groups in 2-propanol (2800-3000 CM^{-1}) change in band intensity directly with changes in 2-propanol concentration;
3. in the low-frequency region, the 1000-1200 cm^{-1} bands related to carbon skeletal vibrations also change;
4. and, also in the low frequency region, the 1380 cm^{-1} band related to C-H symmetrical deformation vibrations in the methyl groups increase with 2-propanol concentration. A comparison between the different C-H stretching bands of liquid 2-propanol (2970 cm^{-1} = CH antisymmetric (I); 2930 cm^{-1} = C-H stretching (II); 2870 cm^{-1} = CH symmetric stretching (III)) with the corresponding bands of the adsorbed alcohol may be relevant. In the liquid phase, the stretching bands (II) and (III) exhibit similar intensities. For the adsorbed state, band II is nearly double the intensity of band III, suggesting that the symmetric stretching mode had been somewhat hindered. This may be explained by assuming that the alcohol molecule adsorbs not only by

bonding of the OH group, but also via a bond with a -hydrogen atom. In effect, this eliminates half of the symmetric contributions from the two methyl groups, which is also approximately the magnitude of the reduction in the 2870 cm^{-1} band. This two-point mode of adsorption can also better explain the thermal stability of the reactant species at the temperature of reaction as opposed to single H-bonded species;

5. the two bands in the 1400-1600 cm^{-1} region do not change with 2-propanol concentration changes and it may be surmised that they are not involved in the reaction mechanism. These bands have previously been assigned (78) to irreversibly adsorbed carboxylate species.

On the basis of these observations, Figure 6-2 depicts plausible reaction mechanisms in accord with the above. Both surface configurations involve a direct interaction with surface OH groups as well as a two-point mode of adsorption. Nevertheless, the limitations of the present infrared technique to differentiate between two such species and to choose unequivocally the specific atomic configurations of bonding states have been discussed in section 2.2.

6.1.2 Carboxylate adsorbed species

The formation and nature of these oxidized species has been reviewed in Chapter 2. The method used to control their relative amount on the catalyst to maintain a reproducible

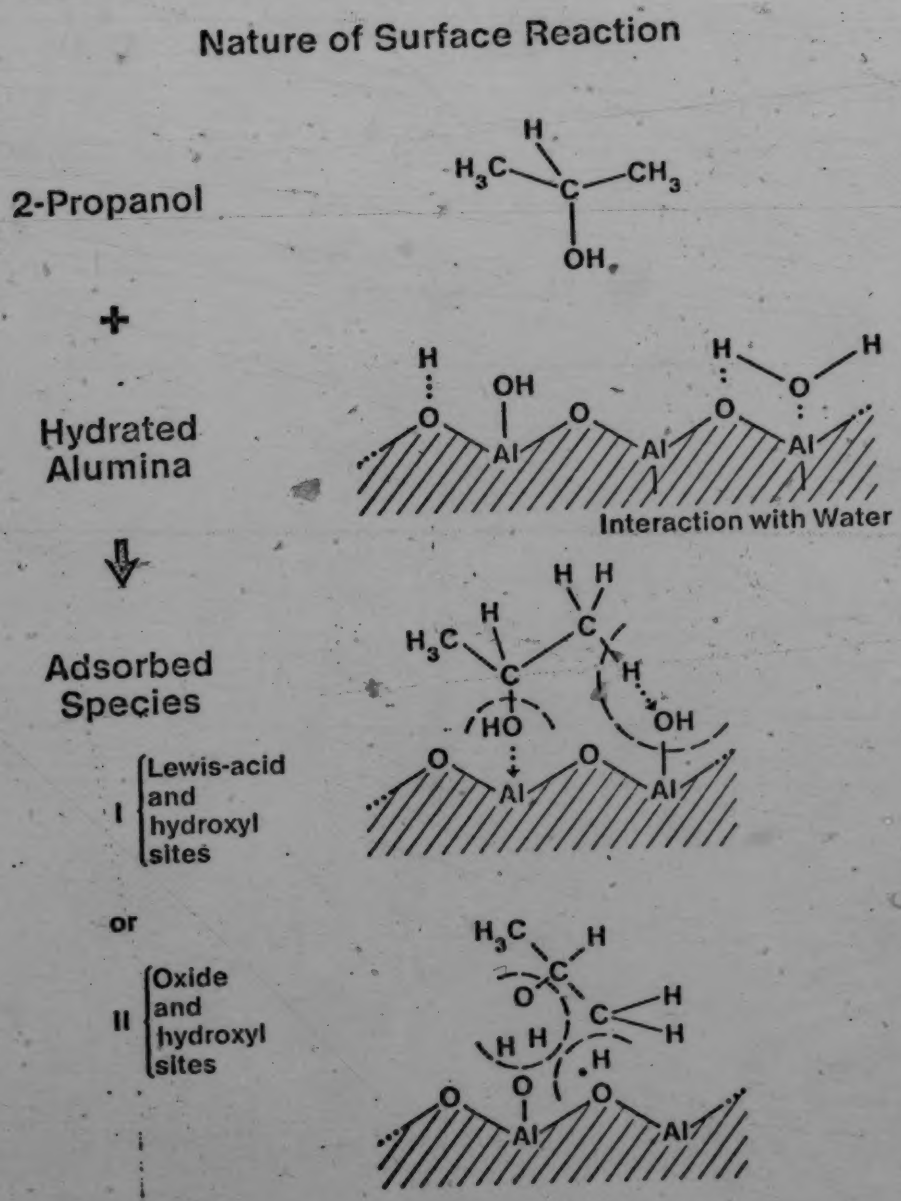
Nature of Surface Reaction
2-Propanol
H
H3C
C
CH3
OH
+
Hydrated Alumina
H
OH
O
Al
H
H
Interaction with Water
Adsorbed Species
I
Lewis-acid and hydroxyl sites
HO
OH
or
II
Oxide and hydroxyl sites
H3C
H
H

Figure 6.2 Mechanistic View of Surface Reaction

activity of the catalyst was established in detail in section 5.6. The results in the present section were obtained on a wafer which was not submitted to the standard pretreatment procedure followed during the kinetic runs. The population of the carboxylate species on the surface of this wafer had progressively increased and their influence on the reaction rates and surface spectra is now analyzed.

Figure 6-3 shows that the reaction rates obtained under similar conditions decline visibly when the absorbance of the 1570 cm^{-1} band of carboxylate species increased. The adsorption isotherm for 2-propanol, obtained by measuring the absorbance of the 2970 cm^{-1} band of 2-propanol, shows that all such absorbances are correlated by a single isotherm irrespective of the carboxylate species surface concentration (band at 1570 cm^{-1}). In all cases, the rate approached a limiting value upon attaining a saturation level of surface 2-propanol. This limiting value ,a measure of activity level, declined with increasing carboxylate concentration.

Since the carboxylate level did not influence the surface coverage of alcohol appreciably but affected the reaction rate adversely, this was interpreted to mean that the carboxylate and alcohol adsorbed on different sites. To account for the detrimental influence of carboxylate species, they are presumed to occupy sites which are essential for the reaction to occur. The formation of carboxylate appears to be a slow reversible activated process taking place on

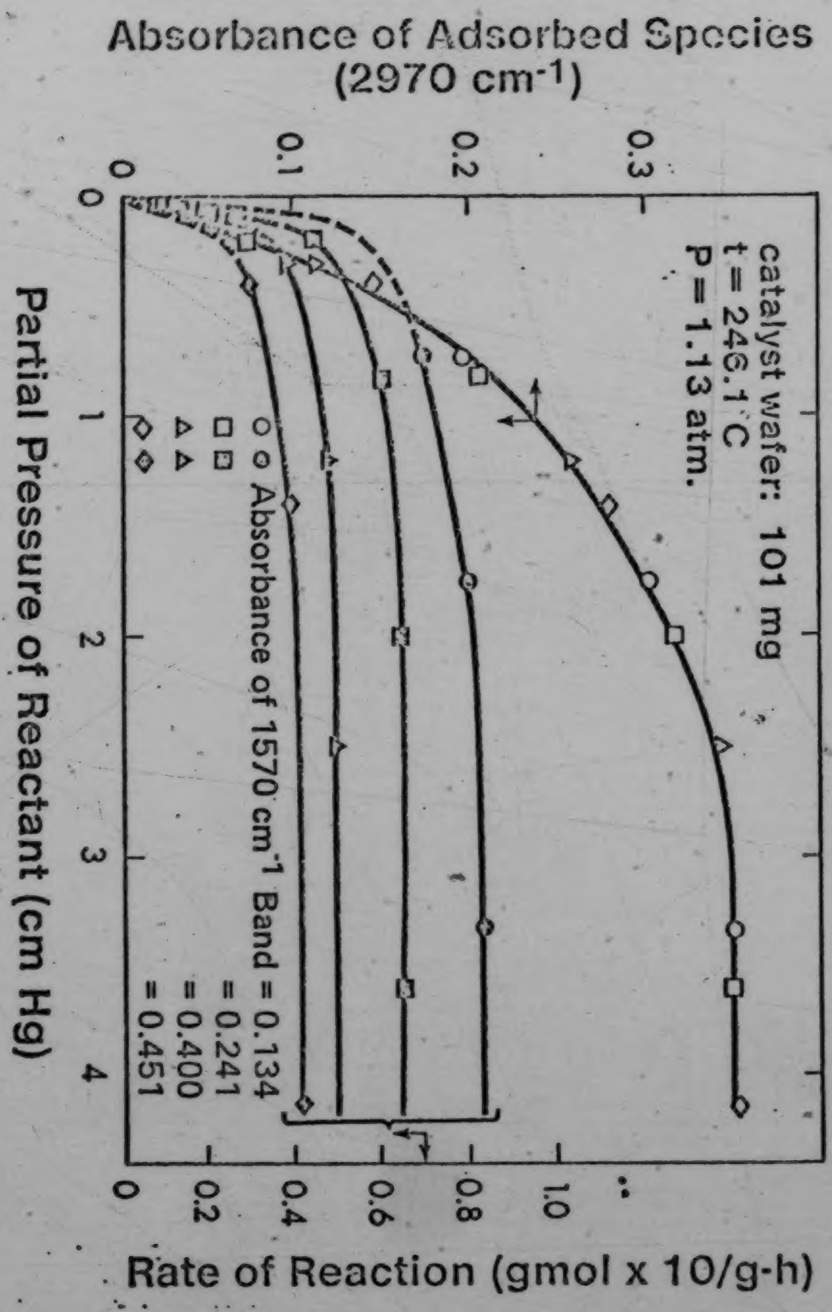

Figure 6.3 Influence of Carboxylate Species

sites of various energetic strengths. The formation of stable -pyridone, surface amides and surface carboxylates has been considered to occur on Lewis acid-base paired sites in a concerted way (39).

6.1.3 Influence of products

Although the dehydration reaction appeared to be irreversible, the influence of the presence of reaction products was also investigated. Addition of propylene to the feed produced no observable effect upon the reaction rate. The presence of adsorbed propylene on the surface of alumina at reaction conditions could not be detected by IR methods.

The addition of water to the feed generated the results shown in Figure 6-4. The adverse effect of increasing water content along with the unaffected adsorption isotherm of 2-propanol also suggests that adsorption of water occurs on sites of different nature than the alcohol adsorption sites.

Since both water and carboxylate retard reaction rates well before the adsorption sites for 2-propanol become saturated, it may be assumed that the total population of alcohol adsorption sites L , greatly exceeds the total population of active sites L (water adsorption sites). Removal of a few L -type sites by adsorption of water or formation of carboxylate suppresses the reaction rate disproportionately. The small number of water adsorption sites can also be indirectly inferred because of the inability to detect the presence of adsorbed water in measurable quantities on the

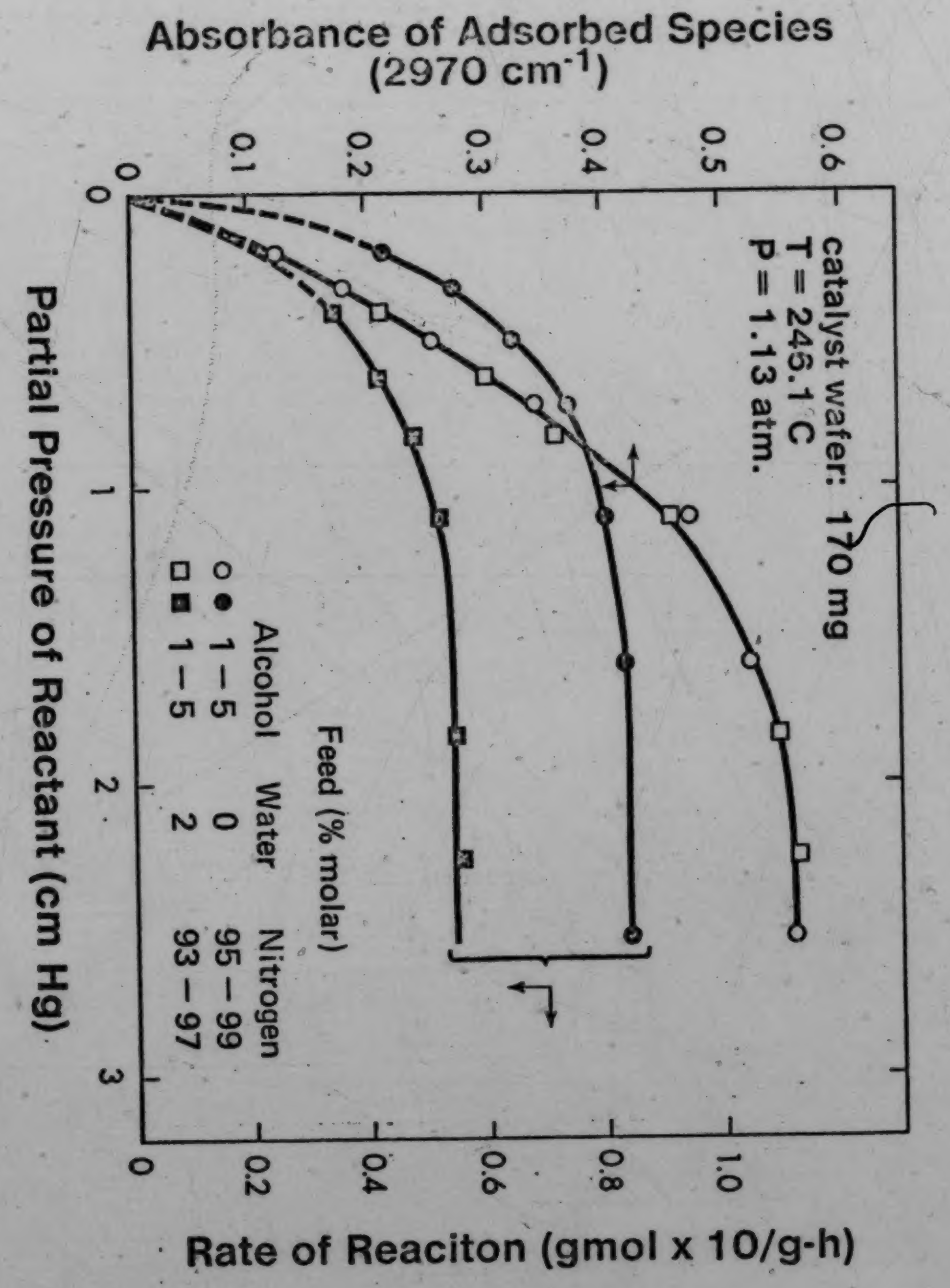

Figure 6.4 Influence of Water

reactive surface. When water was present in varying amounts in the gas mixture, the surface spectra remained unaffected despite the strong inhibiting effect of water. Consequently the formation of the observed adsorbed alcohol species is not considered to be a rate-determining step of the dehydration process and these species can be considered in thermodynamic equilibrium. It seems more likely that the adsorbed alcohol molecules are not direct activated intermediate complexes but only precursor species to the dehydration process (as will be seen later). The most important result from the infrared observations is that the non-competitive adsorption of water and alcohol occurs under reaction conditions.

6.1.4 Poisoning experiments with pyridine

Up to now little has been said on the nature of the true active sites involved during the dehydration process. In section 6.1.1 the adsorbed alcohol molecules were observed to interact stongly with the free OH groups of the alumina surface. From the pronounced inhibiting effects of water and/or carboxylates upon the rate of reaction at similar coverages, it was concluded that surfaces sites other than the alcohol adsorption sites were necessary for the completion of the dehydration process. It was observed in the literature survey that carboxylates and water molecules interact with acid-base pair sites. An important aspect of the stereochemistry of the dehydration reaction ,established by detailed isotopic studies,is the successful transition to the alkene which occurs when the -hydrogen is removed.This process takes place when the -hydrogen atom comes sufficiently close to a suitable basic centre on the surface. Little doubt then remains about the direct participation of basic sites during the rate-determining step of the reaction.Nonetheless,some controversy still remains about the involvement of Lewis-acid centres.

To clarify this point, series of experiments were performed where various amounts of pyridine were added to the feed mixture. The basic pyridine molecule is known to interact specifically in a coordinative mode of bonding with the exposed aluminium cations of the surface (Lewis-acid centres). The effects of pyridine were measured under reaction conditions and are summarized below:

1. The amount of adsorbed alcohol at steady state was not modified by changing the concentration of pyridine in the reacting mixture. The saturation level of alcohol stayed identical in all cases.
2. The appearance of a weak band at 1620cm^{-1} could be directly related to the relative amount of pyridine chemisorbed on the surface. The intensity of this band increased noticably with the concentration of pyridine in the gas mixture.
3. Finally a much more pronounced decrease in the rate of reaction was observed than was the case with water. This effect was reversible since the original activity was almost completely recovered when the addition of

pyridine to the feed was eliminated.

The influence of adsorbed pyridine upon the activity of the catalyst is shown in Figure 6-5 , where the amounts of propylene produced (plotted on a relative scale as G.C peak area) are related to the concentration of pyridine in the feed (plotted as intensity of the $1620 cm^{-1}$ IR peak of adsorbed pyridine). The typical small intensity of this band may have caused some scattering of the experimental data. The mole fraction of the reactant was maintained very close to 9% .

Although not linear, the curve in figure 6-5 clearly demonstrates that the amount of adsorbed pyridine is correlated with the activity of the catalyst and thus, the pyridine must occupy the true active sites on the surface. At sufficiently high concentrations the reaction tends to be completely suppressed. These results demonstrate the importance of the Lewis- acid sites in the reaction. In fact, these sites are probably similar to the ones occupied by water which were also found to influence the reaction adversely. In the case of water it was not possible to observe directly by infrared means the presence of adsorbed molecules of water. The initial steep curvature of the plot reflects the hetereogeneity of the alumina surface since the initial sites blocked by pyridine seem to affect the reaction comparably more than those sites occupied at higher coverage.

The experiments described above demonstrate how the new

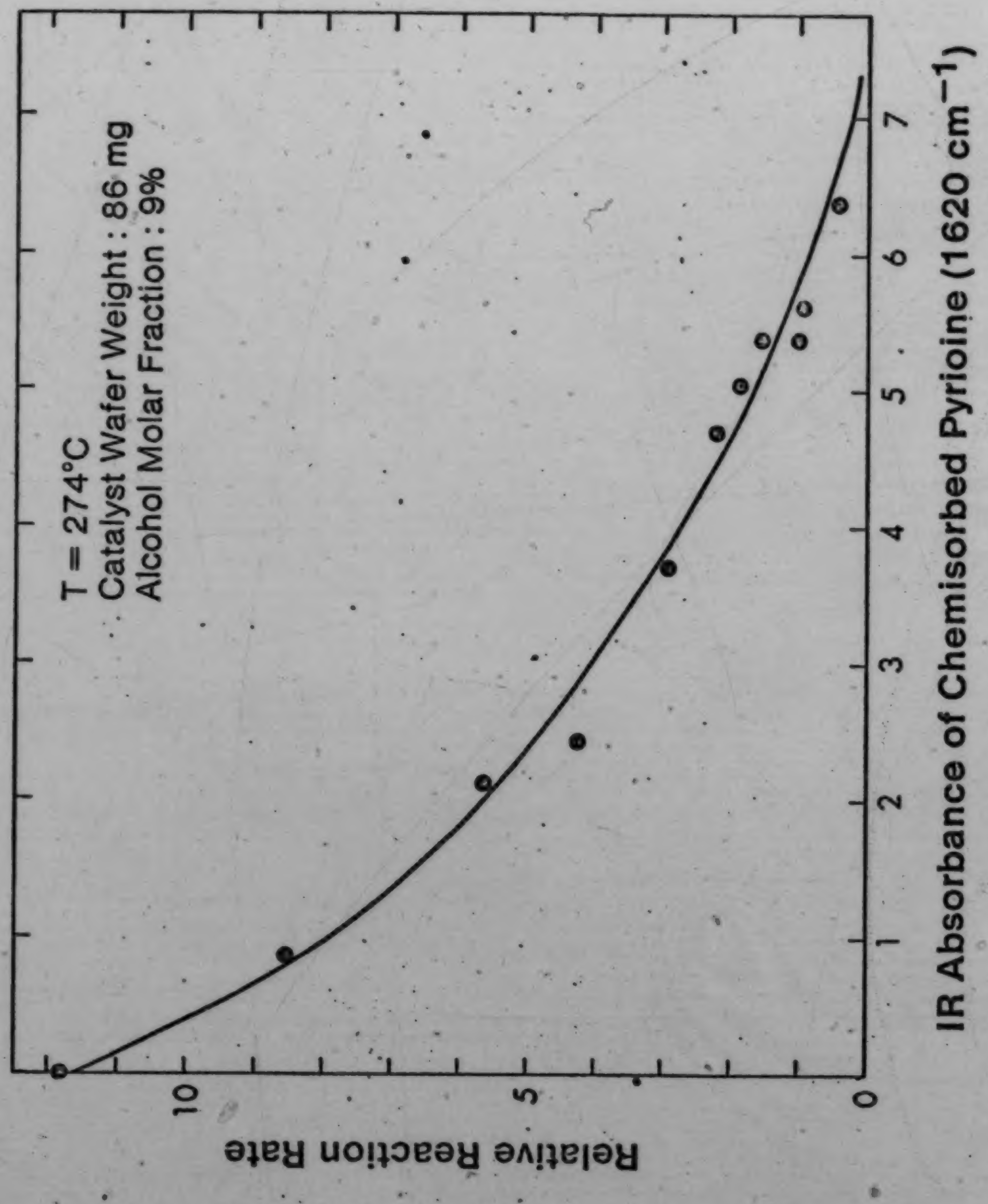

Figure 6.5 Poisoning Effect of Pyridine

reactor can be used advantageously in poisoning studies. Since both acidic and basic agents strongly poison the alcohol dehydration, one could interpret the existence of interdependent acid-base pairs of sites on the surface of aluminas and that these pairs provide the operative effect during the activation of the process.The precise atomic configuration of these active portions of the surface is certainly beyond the scope of this investigation. The interrelation between chemical and geometric factors on the surface remains an essential, somewhat mysterious, aspect of catalysis.

6.2 Kinetic Experiments

6.2.1 Preliminary kinetic experiments

Before commencing the interpretation of the kinetics results, a number of preliminary experiments were undertaken. In a "blank run" the possibilities of either homogeneous reaction or catalytic effect of the equipment walls were examined in the absence of catalyst in the reactor. No evidence of reaction could be detected even when the stainless steel vaporization chamber had been heated up to 300°C.

To understand the reaction mechanism and to develop the appropriate kinetic model, it is also necessary to establish wether the reverse reaction occurs within the range of reaction conditions adopted for the rate measurements. It is customary first to make a thermodynamic analysis of the system to determine the feasibilities of the forward and reverse reactions. This was done previously by Chuang (75) where he calculted the Gibbs energy change, G, for the reaction system and showed that the equilibrium fractional conversion, X, is essentially unity when the alcohol partial pressure is less than one atmosphere. Experiments were also carried out with the equipment mentioned in Chapter 5 to examine whether the reverse reaction was significant under the reaction conditions being studied. The absence of formation of alcohol when water and propylene diluted in nitrogen were fed to the reactor at the highest temperature employed agreed with the thermodynamic predictions. In addition, when the reactor was operated in the batch mode ,the conversion of alcohol became virtually unity after a sufficient time of reaction.

The investigation of catalytic reactions is often complicated by diffusion as well as chemical phenomena. These effects have been extensively reviewed by Satterfield (158) and Carberry (159) in consideration of both gas-film diffusion (external) and pore diffusion (internal). The external mass transfer performance of the new reactor has been explored in section 3.3. The simulation sublimation experiments could be interpreted relatively easily because of the well defined geometrical configuration of the catalyst wafer. Average superficial mass transfer coefficients of 20 cm/s were obtained, which indicates a very good contracting of the reacting gases with the catalyst, one of the main attributes of the reactor. Normally, gas-film diffusion control is more probable when the reaction rate is high and/or when the reactant pressure in the system is low. Consequently, the good contacting obtained in this case should facilitate the study of intrinsic kinetics at higher conversions without being mass transfer limited. In fact, during the kinetic runs the recycle flow was decreased from about 20 l/min to less than 10 l/min from time to time by manipulation of the throttling valve at the outlet of the bellows pump. Since, even for the highest conversion data, no noticable change was observed between the ensuing steady states, it is reasonable to assume that external mass transfer was probably negligible in all the kinetic runs in the present work.

6.2.2 Intraparticle diffusion

Intraparticle diffusion may occur by one or more of three mechanisms: ordinary bulk diffusion, Knudsen diffusion and surface diffusion. Ordinary gas diffusion occurs in large pores where gas-gas molcular collisions predominate. The effective diffusivity D may be used to relate the mass flux to the total cross section of the porous solid.

$$D \quad = D. / \qquad (6.01)$$

The range of values of the tortuosity factor, , is in most cases from 3 to 7.

If the gas density is low or if the pores are very narrow, the molecules collide with the pore wall much more frequently than with each other. This is known as "Knudsen diffusion", and in this case the gas flux is reduced by the wall "resistance" which causes a delay because of both the diffusion reflection and the finite time the molecule is adsorbed. Kinetic theory provides the following relation for Knudsen diffusion in gases in a straight round pore:

$$D = 9700.r .(T/M) \qquad (6.02)$$

where r is the pore radiux in cm, T the temperature in K and M the molecular weight. As the internal geometry of consolidated porous solids is poorly understood, it is also necessary to include a factor, Tm, allowing for both the tortuous path and the effect of varying cross sections of individual pores. The effective Knudsen diffusivity based on the total cross section of the porous solid is given by:

$$D = D . / \qquad (6.03)$$

The third mode of transport, surface diffusion, has generally not been considered in establishing the significance of intraparticle mass transfer resistances on the rate of chemical reactions. In consideration of what was said in section 2.5, it seems wise to consider the possibility of significant surface migration for our system. The effect of surface diffusion is to increase the effectiveness factor

(160), and when the effective diffusivity is back calculated from reaction rate data, it is substantially higher than would be expected, indicating that surface diffusion was probably significant. In the absence of surface diffusion, the effective intraphase diffusivity in the transition regime between molecular and Knudsen diffusion can be estimated by equation (6.4) as derived by Satterfield (158).

$$1/D \quad = 1/D \quad + 1/D \qquad (6.04)$$

From a practical aspect, when reaction is occurring in a porous structure, some concentration gradient will always exist, and the effectiveness factor for an isothermal reaction will never equal unity, except as a mathematically limiting case. A general criterion to indicate the absence of significant diffusion effects can be taken as the conditions for which exceeds about 0.95.However, the accuracy with which the effectiveness factor can be expressed in terms of the Thiele modulus depends largely upon one's degree of knowledge concerning the intrinsic kinetics, the accuracy with which the effective diffusivity can be estimated, and the degree to which the catalyst is isothermal.

It is therefore imperative that the effect of pore diffusion be determined experimentally by measuring the reaction rates for various particle sizes of catalyst under otherwise identical conditions (161). If the reaction conversion remains constant when the pellet thickness is varied, while keeping the space velocity as well as other reaction conditions constant, then pore diffusion is probably not significant. In this study using wafer-shaped catalyst pellets, the critical dimension for diffusion path is the wafer thickness .Consequently, five different catalyst weights and correspondingly, five different wafer thicknesses were investigated. The experimental conditions and results from these runs are displayed in Figure 6-6, The graph clearly indicates that pore diffusion is probably negligible as long as the catalyst weight is kept below 150mg during rate experiments.

One of the best methods of estimating the effectiveness factor is reported in detail by Satterfield (158). The definitions of the terms and examples demonstrating the calculation method can be found in Appendix B . The data chosen for these calculations were the ones corresponding to the onset of significant pore diffusion for the 187.5 mg and the 292 mg wafers. For these two data points the estimated values of the Thiele modulus are respectively, 1.045 and 1.48. It is interesting to compare these values from Figure 4-2 in Satterfield's book. On his plot, pore diffusion is predicted to become significant at values of of 0.5 and 2 for the cases of first order and zero order reactions, respectively. Since the experimental order of reaction for the dehydration reaction will be demonstrated subsequently to exhibit behaviour equivalent to a fractional order, the

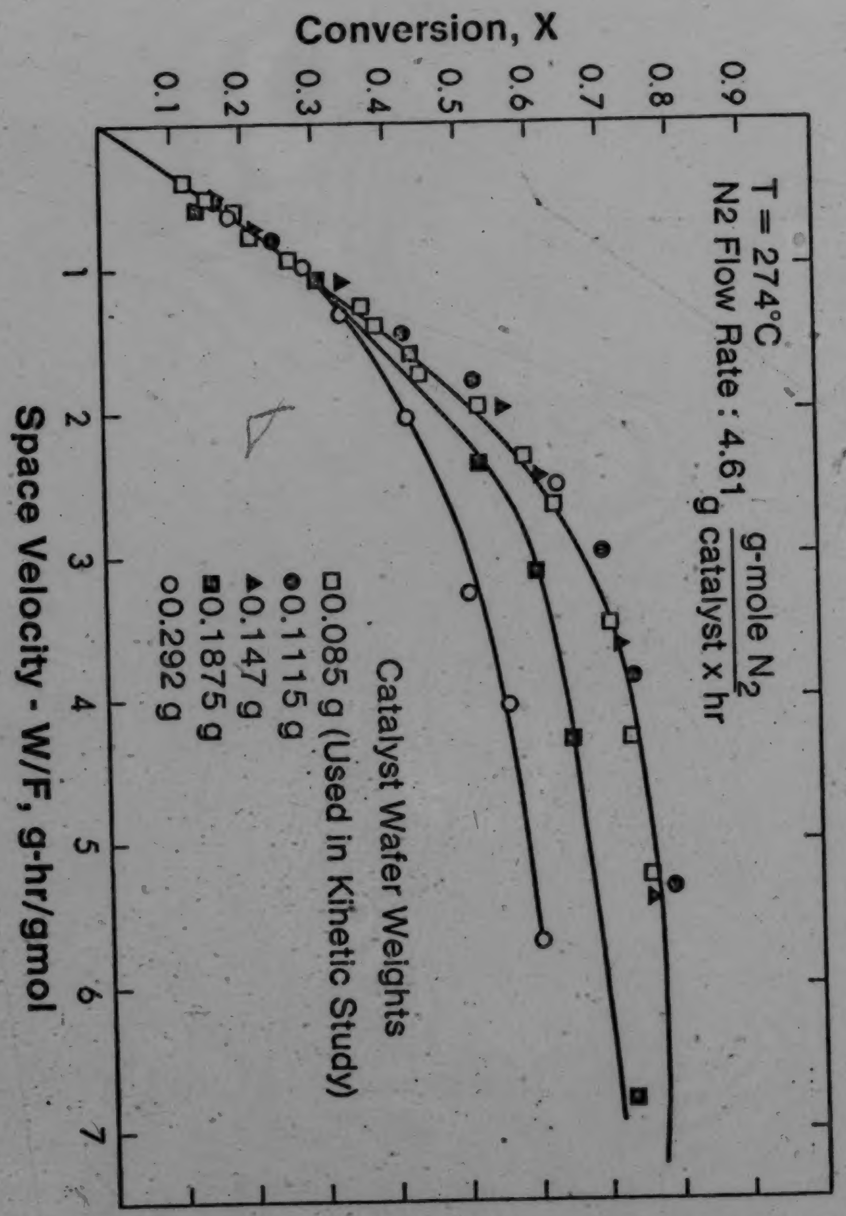

Figure 6.6 Evaluation of Pore Diffusion

corresponding values of the Thiele modulus, 1.045 and 1.48, could be interpreted to provide agreement between these results and Satterfield's method of predicting effectivness factors. It is therefore reasonable to assume that pore diffusion limitations were also negligible in our work even at the relatively high conversions obtained because the wafer weights as employed were always less than 0.15g. However, a few additional comments should be made.

First, the low value of the tortuosity factor 0.85 used in the estimation of the effective diffusion coefficient was based on experimental data by Smith et al (162) which were obtained by diffusion measurements through plugs compressed from alumina powder. The mean pore radius of their catalyst was 9.6 nm which compares well with the 8.4 nm for the catalyst used herein. Nevertheless, a value of tortuosity less than 1 has no physical interpretation unless it accounts for a significant contribution of surface diffusion to the global transfer inside the solid.

Secondly, Satterfield points out (158) that: "At rates above about 10^{-5} gmol/s.cm^3 of pellet, severe mass and heat transfer problems will usually be encountered with pellets of typical size". In this study, dehydration reaction rates of 10^{-4} gmol/s x cm^3 of catalyst were obtained at the highest temperature without apparent mass transfer limitations. These contradictory remarks can be reconciled when one considers that the thickness of a 100 mg wafer is only about 0.1 mm (200 mesh). The characteristic length of the diffusion path becomes then very small so that in principle much higher intrinsic reaction rates per unit volume of catalyst can be secured than in industrial pellets; the Thiele modulus having a square dependency upon the characteristic length of the pellet.

6.2.3 Summary of kinetic runs

A total of 186 data points were collected from the kinetic measurements covering four reaction temperatures,231°,246.5°,260.3° and274°C. The data sets and the partial pressure range of the compounds in the reactor under each of the four temperatures are summarized in table 6-1. More detailed information on the 186 runs are te be found in Appendix E. In the folowing sections, a plausible reaction mechanism, one which is in agreement with the overall chemistry (IR observations) and the main characteristics of the kinetics behaviour (rate surface response) will be proposed. Criteria for evaluation of model adequacy will then be discussed. Using statistical model discrimination, the superiority of the new rate expression over other alternate mechanisms will be demonstrated.

6.3 Development of a New Kinetic Model

6.3.1 Development of mechanism consistent with experimental evidence

Infrared spectroscopy can provide considerable insight into the identity of chemisorbed species which may be

Table 6.1 Summary of Kinetic Data

T (c)	Data Set	No. of points	Partial Pressure Range (atmx100) PA	 PW
231.2	T1A	11	0.23-10	0.308-0.494
	T1B	12	0.16-9.95	1.75-1.91
	T1C	4	2.86-8.62	0.734-0.777
246.5	T2A	9	0.219-12.4	0.76-1.67
	T2B	4	3.57-4.16	1.62-5.89
	T2C	13	0.171-8.24	0.316-0.85
	T2D	12	0.284-8.4	2.86-3.21
260.2	T3A	12	0.336-8.88	0.498-1.41
	T3B	10	0.326-6.85	1.72-2.54
	T3C	11	0.334-20.8	1.15-2.99
	T3D	11	0.380-8.64	5.79-6.35
	T3E	9	0.286-8.72	0.49-1.66
	T3F	15	0.177-9.42	0.332-3.74
	T3G	13	0.196-9.33	0.339-1.58
274.0	T4A	13	0.63-10.11	1.01-6.36
	T4B	13	0.709-9.68	2.51-9.15
	T4C	14	0.855-26.0	2.47-5.12

intermediates in catalytic reactions. This information obtained at the molecular rather than the macroscopic level, should serve as a good basis for screening models because the mechanism proposed according to infrared evidence would incorporate more detailed knowledge of the mechanism taking place on the catalyst surface.

In section 6.1, the combination of some rate data with the detailed infrared observation of the adsorbed species during reaction, led to the development of a reaction mechanism. It was also clearly established that the alcohol and water occupy different sites on the surface and that the inhibition effect of water and pyridine on the rate of reaction makes the indirect participation of Lewis acid sites essential for the reaction to proceed.

By analogy to our reaction system, it is useful to consider more generally the process of an irreversible monomolecular decomposition of ~~a~~ reactant involving the participation of two different sites,as suggested by the infrared studies. If the reactant and one of the products occupy two dissimilar sites, the reaction steps may be written,

$$\begin{array}{llll} (1) & R + 1 & R1 & \\ (2) & R1 + 1 & P1 + 1 & \\ (3) & P1 & P + 1 & \end{array} \qquad (6.05)$$

with: R(reactant); P(product); 1 ,1 (different sites).
The usual Langmuir-Hinshelwood treatment of such a mechanism for step (2) rate-controlling results in equation 6.06,

$$r = k.L\ .L\ \frac{K\ P}{} \qquad (6.06)$$

$$(1+K\ P\ ).(1+K\ P\ )$$

This dual dissimilar-sites rate expression was used previously by Chuang (75) to correlate one set of isothermal data at 251.2°c for the dehydration of isopropanol on alumina. However, it will be shown later that this rate equation does not fit the rate data obtained here, even if the associated mechanism is consistent with most of the infrared observations. These apparent discrepancies were interpreted as follows to derive a new kinetic model.

6.3.2 Influence of coverage upon reactivity of reactant adsorbate

First it is implicitly assumed in equation 6.06 that any species R1 may have access to any available empty sites 1 . This accessibility is only true in the unlikely event that high surface diffusion of the adsorbed reactant prevails. On the other hand, assume the active surface to contain a random distribution of adjacent pairs of sites, 1 1 , without the presence of significant surface diffusion. This would be equivalent to postulating that for each adsorbed reactant species, the only way to decompose into the products is by interaction with the adjacent empty site, 1 ,to the exclusion of any other 1 site available on the surface. In this latter case, it is actually more accurate to write the reaction sequence as follows,

$$\begin{aligned} &(1)\quad R + 1 - 1 \qquad\qquad R1 - 1 \\ &(2)\quad R1 - 1 \qquad\qquad P1 - 1 \end{aligned} \qquad (6.07)$$

$$(3)\quad P1 - 1 \qquad\qquad P + 1 - 1$$

and to approximate the surface as one comprising homogeneous sites of the type, 1 1 . The corresponding rate equation assuming the surface reaction to be rate-controlling and that P adsorbs as well is,

$$r = k.L\ .K\ P\ /(1 + K\ P\ + K\ P\ ) \qquad (6.08)$$

similar to the single-site mechanism rate equation . It is apparent that a reaction involving the participation of two distinct chemical sites, on a surface (i.e. Al cations and OH groups or other combinations of sites) could lead to an equation equivalent to the single site mechanism rate equation. This illustrates the contradictions that may seemingly occur between observations made at the microscopic level (infrared studies, poisoning effects, isotopic effects etc.) and at the macroscopic level (rates of reaction) for a reaction system.

So far two limiting cases have described, where the surface diffusion was either significant (mobile adsorption layer) or absent (fixed adsorbed molecules). During a real catalytic process, intermediate conditions may often prevail. This discussion emphasizes the approximations involved in the derivation of such standard kinetic models. It may also be argued that on the alumina, the populations of the different atoms exposed on the surface differ greatly. For instance, the strong retarding effect of water upon the reaction rate, even though the coverage by the reactant was not affected (section 6.1 and Figure 6.4), suggests that L >>L on the surface. Each surface site 1 will then be surrounded on the average by a number of adsorption sites 1 (>1). This means also that at high relative coverage more than one adsorbed reactant molecule could in principle migrate to the same active site 1 in order to complete the reaction. Since at a given time only one R1 species can interact with a neighbouring 1 , it is plausible that the average reactivity of each species R1 will decrease as its population increases on the catalyst. This phenomenon was indeed observed directly under the conditions of reaction and was not incorporated in the previous arguments. It was also noticed that although the coverage of the catalyst by isopropanol increased steadily with its partial pressure (as indicated by infrared), the rate of reaction went through a maximum (see Figure 6-6). An explanation of this retarding influence of the reactant is now attempted in light of the limitations just discussed. Considering the likelihood of an adsorbed species, R1 , being able to react with an adjacent 1 site, in terms of relative coverage by R1 species, a distribution of reactivities could be proposed, such as that shown in Figure 6-7. In this postulated distribution, the ordinate, I, is defined as the average reactivity of the R1 species at any coverage relative to their reactivity at zero coverage. A limiting value, I=d, where d>>0, is associated at full coverage by the reactant. The decline in I with coverage is

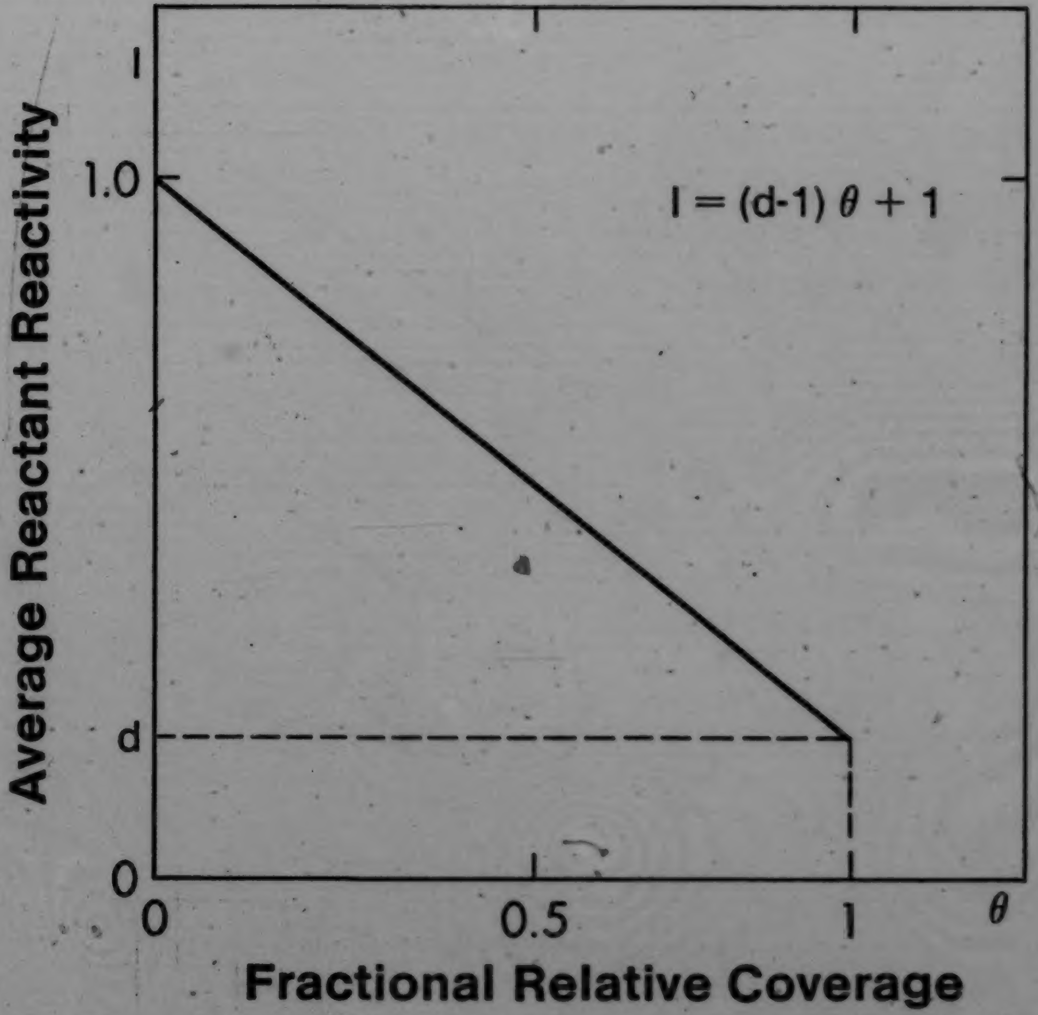

Figure 6.7 Interaction of Adsorbed Reactant Molecules as Function of Their Relative Coverage

```
     180      14      386.4                          r = K.I.<LSB>R1<RSB>.<LSB>1 <RSB>
Line width exceeded in ASIS or PREFORMATTED mode.
in column                  72 "6.10)"
```

attributed to the steric and/or inductive effects of adsorbed alcohol molecules adjacent to a common 1 site. In simpler terms, this is a way of accounting for the possible interaction of adsorbed reactant molecules on the surface. Equation 6.09 defines I in terms of coverage,

$$I = (d - 1). \; + 1 \qquad (6.09)$$

using I as a weighting factor, i.e. to define the relative reactivity of R1 species for a given , the surface reaction step in equation 6.5 is given by equation 6.10,

$$r \quad = \quad k.I.[R1].[1 \quad]$$

(6.10)

In the absence of the influence of the products, the overall reactivity, C, of the catalyst surface is then expressed as in equation ,6.11,

$$C(\;) = I. \; . = (d-1). \; ^2 + \qquad (6.11)$$

The dependence of C with coverage has been plotted on Figure 6-8 for different values of the parameter d. The straight line for d=1 represents the usual ideal case when all reactant intermediate species retain the same reactivity indpendently of the surface coverage (Langmuir-Hinshelwood model). Between 0.5 and 1, the rate of reaction increases

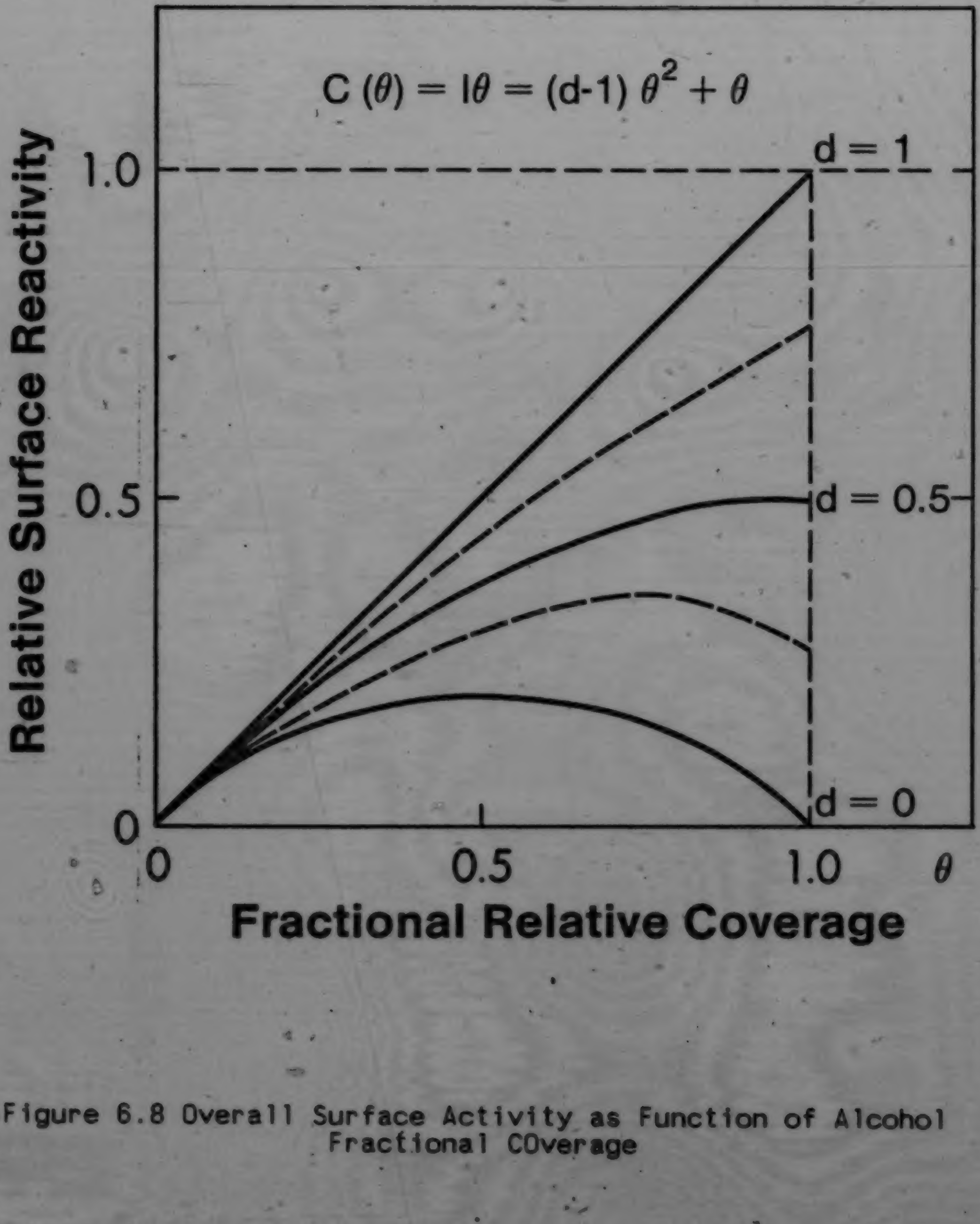

Figure 6.8 Overall Surface Activity as Function of Alcohol Fractional COverage

continuously with the reactant coverage, but in a slower manner than in the ideal case when the direct mass action law applies. For d<0.5, the rate of reaction is predicted to exhibit a maximum at some intermediate value greater than half coverage. Finally in the particular case of d equals to zero, the reaction will be completely autoinhibited at full relative coverage as in the case of a dual similar sites mechanism.

From the different curves on Figure 6-8, it is apparent that substantial deviations from the ideal behaviour can be predicted by the model. This only requires the incorporation of the steric factor d, whose values are limited between zero and one. The addition of this parameter,to account for the change of the surface reactivity with fractional coverage, should greatly improve the predictive behaviour of the standard Langmuir-Hinshelwood type kinetic models. More generally,two limiting basic assumptions in the derivation of standard kinetic model may be taken as underlying the physical reality of the new parameter.

At first it has been often reported that a real catalytic surface is non ideal (heterogeneity),thereby affecting the quantitative validity of the Langmuir theory. This problem has been reviewed recently by Boudart (176), where he showed that rate equations are not drastically distorted by non-uniformity but that "ultimately rate parameters extracted from rate equations valid for ideal sufaces must be considered as averaged out parameters and not rate parameters for specific events on specific sites". In the proposed model, for 0.5<d<1, it can be seen from Figure 6-8, that the intermediate species become progressively less reactive as the coverage increases. In the limit for d=0.5, the last sites occupied have practically no influence upon the global activity of the surface. Accordingly, by adding the parameter d, we may take into account the dynamic behaviour of the catalyst without having to modify the form of the rate equation corresponding to the basic reaction mechanism and thereby distorting the values of the relevant parameters.

At last, apart from surface heterogeneities, the assumption of no interaction between adsorbed species is usually made in deriving kinetic models. This assumption means that the excess energy and/or accessibility of reaction sites is not affected by the presence or absence of adsorbed molecules on neighbouring sites and consequently, the reaction models fail to predict any autoinhibition effect by the reactant when it occurs. Some mode of interaction between surface species can be accounted for in our model, especially when the value of the parameter d is less than 0.5. In this condition, a maximum of the rate of reaction is predicted at some intermediate coverage where the tendency to enhance the reaction by additonal intermediate reactant adsorbed species is exactly balanced by the competition of the same species to react further with the vacant reaction sites.

6.3.3 Derivation of new rate expression

The derivation of the rate equation corresponding to the presently modified Langmuir-Hinshelwood model is described in Table 6-2. As mentioned earlier, any influence due to propylene has been omitted and the surface reaction is rate-controlling. The participation of two dissimilar sites stems from the direct independent infrared observations in section 6.1. A simple linear dependence between the average reactivity of intermediate adsorbed alcohol and its fractional coverage is built in the model. This last assumption is somewhat arbitrary and empirical and other forms of the dependency will be considered later. In conclusion we rewrite now the derived rate expression in terms of the only four parameters that can be estimated from the analysis of kinetic data.

$$r = \frac{a.b.P\ .(1+b.d.P\ )}{(1+c.P\ ).(1+b.P\ )^2} \qquad (6.12)$$

This model will be referred as model M7 in the subsequent sections .

6.4 Testing Of Model Adequacy

6.4.1 Fitting adequacy

For the new kinetic equation M7 to be acceptable, agreement with the experimental data must be demonstrated. Information on the non-linear estimation of the model parameters can be found in section 6.5. The listing of the computer programs are shown in Appendix C. The purpose of

Table 6.2 Derivation of New Rate Expression

DERIVATION OF MODIFIED DUAL-DISSIMILAR SITES MECHANISM
FOR DEHYDRATION OF 2-PROPANOL, A P + W

A=2-PROPANOL; P=PROPYLENE; W=WATER;

$$A + 1 \qquad A1 \qquad (1)$$

$$A1 + 1 \qquad P + W + 1 + 1 \qquad (2)$$

$$W + 1 \qquad W1 \qquad (3)$$

Rate controlling step expression:

$$r = k \times I \times (A1) \times (1)$$

with

$$I = (d-1) \quad + 1$$

$$I = (d-1)\frac{K.PA}{1 + K.PA} + 1 = \frac{1 + d.K.PA}{1 + K.PA}$$

Final rate experession:

$$r = \frac{K .K.L\ L\ PA.(1 + d.K.PA)}{(1 + K.PA)^2 (1 + K\ .PW)}$$

Expressions for limit cases:

$$d=0 \qquad = \frac{k\ .K.L\ L\ .PA}{(1 + K.PA)^2 (1 + K\ .PW)}$$

$$d=1 \qquad = \frac{k\ .K.L\ L\ .PA}{(1 + K.PA)\ (1 + K\ .PW)}$$

Parameter d represents the average normalized reactivity of intermediate species at full coverage.

Figures 6-9 to 6-12 is to illustrate visually how the four subsets of isothermal data are conform to the model predictions. At each temperature,three or four series of experiments at constant flow rates of nitrogen and water and variable feed rate of the reactant isopropanol were carried out. At a given temperature, the change in the setting of the diluent gas flow rate allows to simulate different residence times in the reactor loop in order to modify the conversion levels. The inhibiting influence of water upon reaction rate was studied by altering the water feed rate between series of experiments (mixed feed experiments). Because of the systematic operating conditions, the deviations in the trends between the model and the data in function of the independent variables (the partial pressures of isopropanol and water in this case) can be inferred from the graphs. By visual inspection of the curves in Figures 6-9 to 6-12, one may obtain simultaneously a direct feeling of the overall goodness of fit as well as of the systematic trends in the residuals. This feature is often absent in other kinetic studies where the space of the independent variables is covered randomly (as in statistical design of experiments). In such a case, the detection of systematic sources of errors originating either from the model and/or the data may not be so apparent.

From these results, the graphs show that model M7 depicts the major trends of the data. The overall fit is satisfactory since at each temperature the calculated average

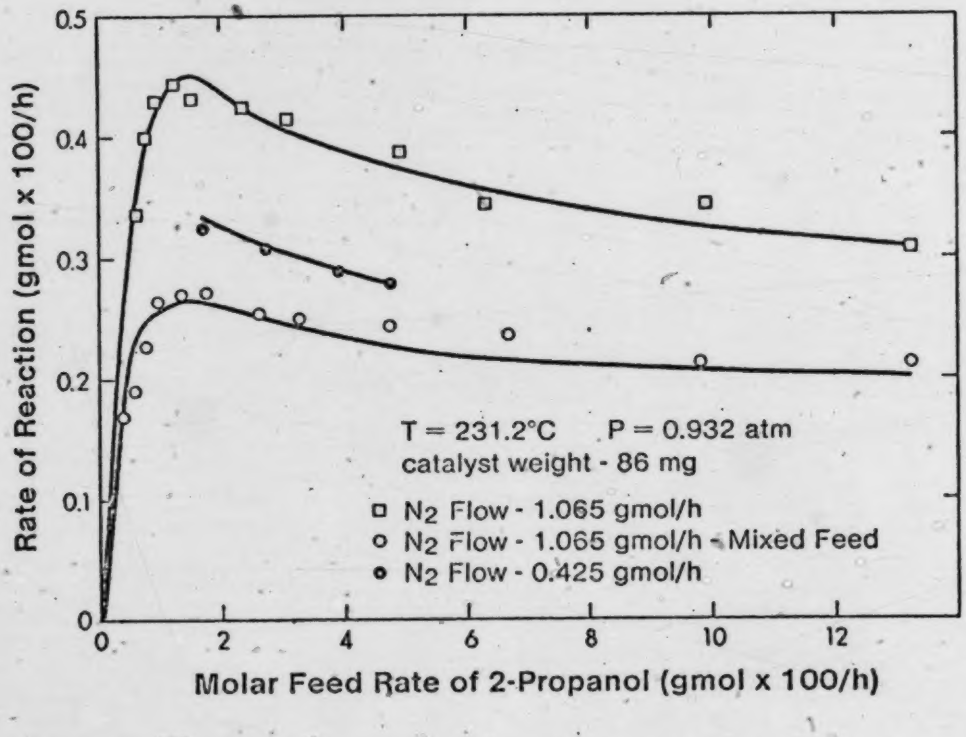

Figure 6.9 Comparison Between Experimental and Predicted Reaction Rates at 231.2°C

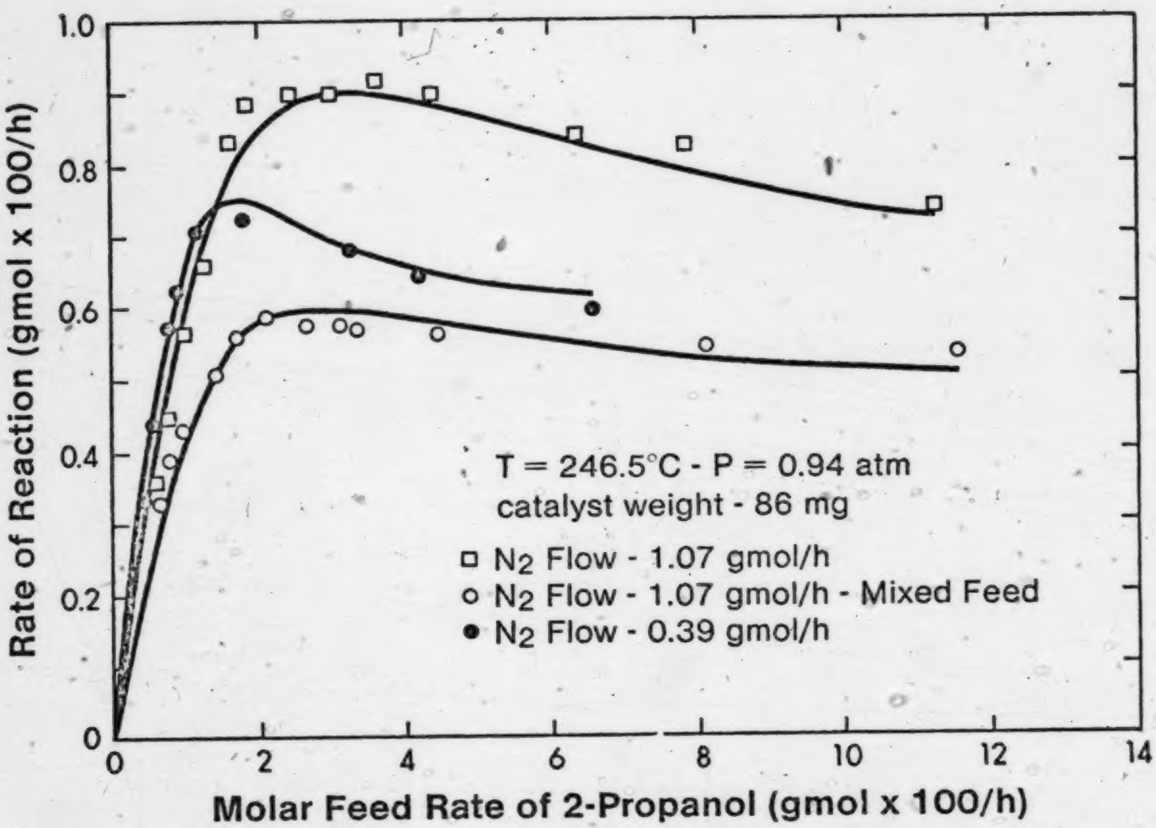

Figure 6.10 Comparison Between Experimental and Predicted Reaction Rates at 246.5°C

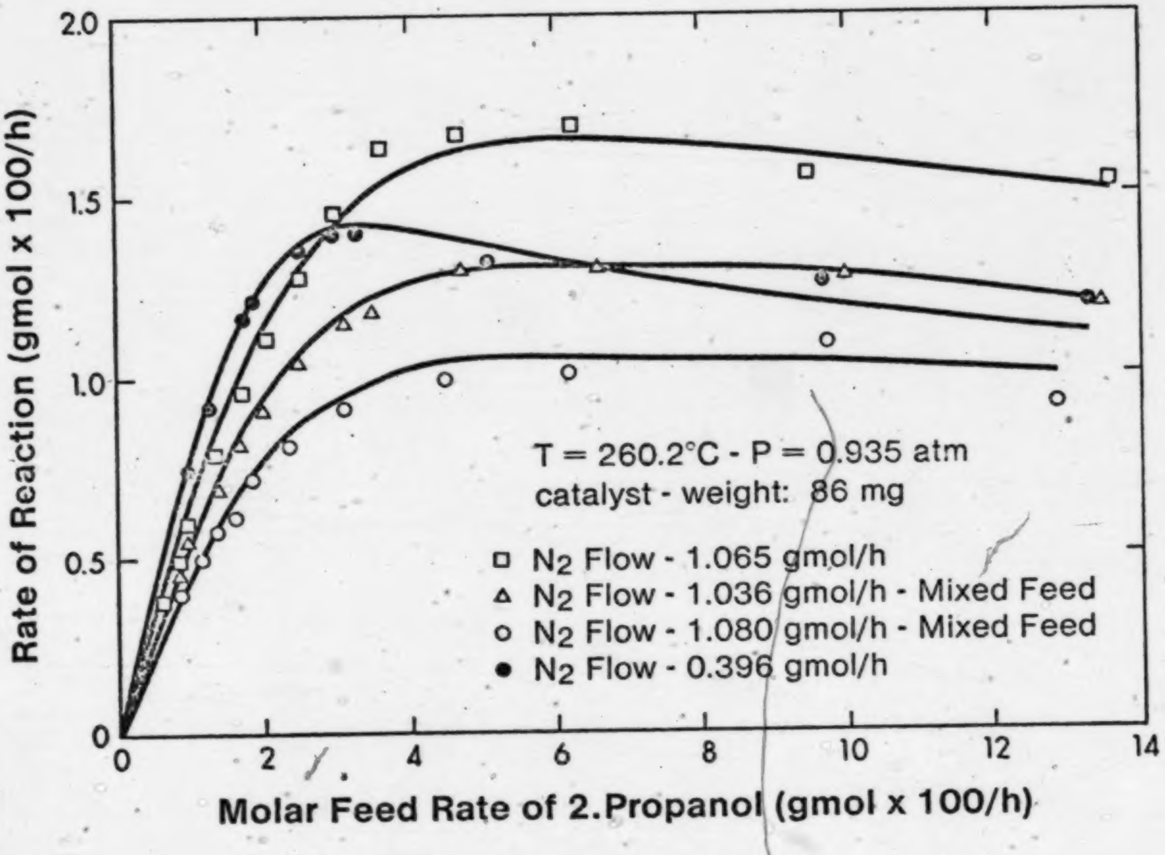

Figure 6.11 Comparison Between Experimental and Predicted Reaction Rates at 260.3°C

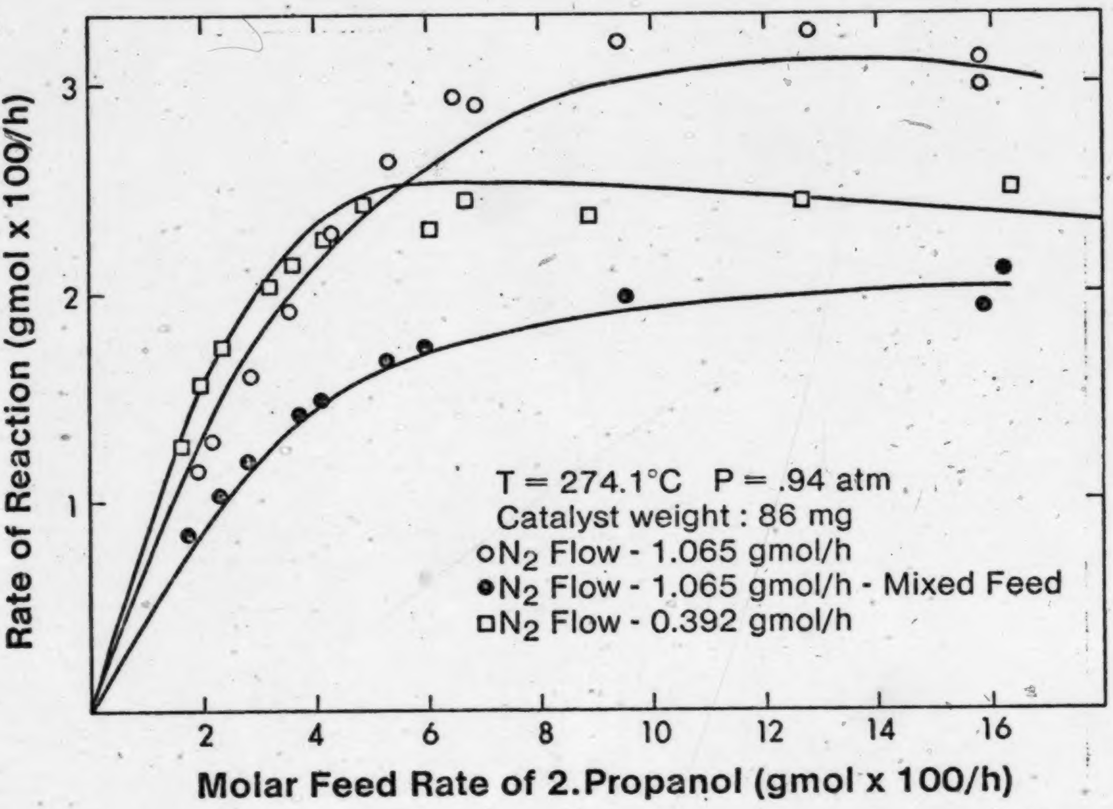

Figure 6.12 Comparison Between Experimental and Predicted Reaction Rates at 274.0°C

relative value of the residuals is between four and five per cent of the absolute value of the ordinate corresponding to the experimental data. These deviations may be explained by some minute change in activity of the catalyst and by errors in the analytical method. The latter influence not only the dependent variable (rate of reaction) but also, the two independent variables, P and P . It is known that one can generally expect some degree of nonrandom behaviour in the residuals(as suggested by Bard (175)). This behaviour is clearly exposed on the graphs 6-9 to 6-12 and is attributed to minor imperfections in the model.

6.4.2 Temperature dependency of the parameters

Another criterion of model adequacy is peculiar to the field of chemical reactions and deals with the physical reasonableness of the parameter values:

1. estimated adsorption and rate constants should be positive;
2. a plot of the logarithm of a rate constant with reciprocal absolute temperature should be linear with a negative slope;
3. a plot of the logarithm of an adsorption constant versus reciprocal temperature should be linear with a positive slope (exothermic adsorption).

For consistency, it is therefore desirable to check the dependency of the individual parameters with temperature. The physical meaning of the four independent parameters is recalled in Table 6-3. According to Arrhenius theory, the three parameters a, b, c should obey the following expressions:

$$a = a \exp(-E /RT)$$
$$b = b \exp(H /RT) \qquad (6.13)$$
$$c = c \exp(H /RT)$$

where E , H and H represent,respectively, the activation energy of the surface reaction and the exothermic heats of adsorption of alcohol and water. A semi-logarithmic plot of a, b,c,and d versus reciprocal catalyst temperature is given on Figure 6-13. as expected, the values of a, b and c lie on straight lines and from the respective slopes we are able to estimate the values,

E = 102.4 KJ/mol-K
H =-112.4 KJ/mol-K
H = 83.6 KJ/mol-K

Unlike these 3 parameters, the value of the autoinhibition coverage factor d does not change appreciably in the range of temperatures studied. This behaviour may be expected if the proposed mechanism for the reaction remains valid over the entire range of temperatures. The parameter ,d,reflects the autoinhibiting influence of alcohol with respect to its fractional coverage.Consequently, at similar fractional coverages this effect should be comparable at all temperatures. The constancy of d,therefore, gives additional support to the intrinsic validity of the new kinetic model,

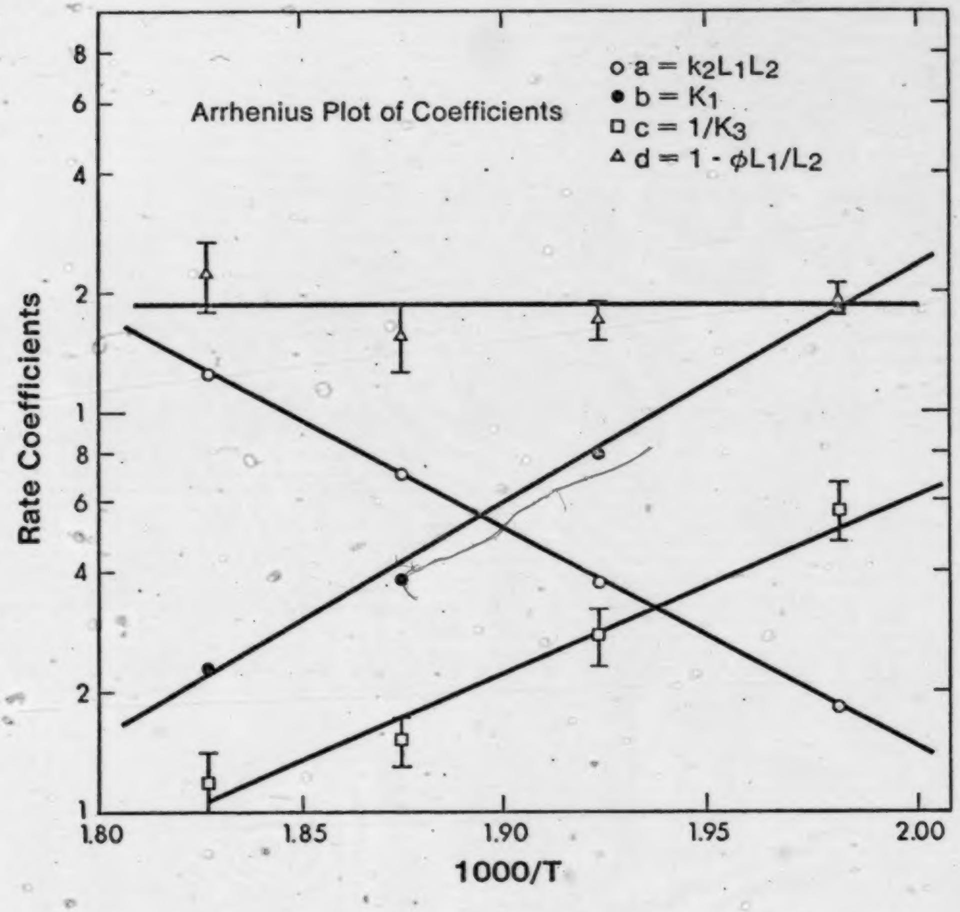

Figure 6.13 Arrhenius Dependency of Model Parameters

Table 6.3 Model Parameters

PHYSICAL MEANING OF INDIVIDUAL PARAMETERS FOR MODEL M7

Rate expression:

$$r = \frac{a.b.PA\ (1 + b.d.PA)}{(1 + b.PA)^2\ (1 + c.PW)}$$

Physical meaning:

a: Rate constant of surface reaction

b: Adsorption constant of Isopropanol

c: Adsorption constant of Water

d: Autoinhibition coverage factor

M7.

In addition to simpler computations, there was some fundamental reasoning in choosing to correlate the data independently at each reaction temperature, rather than simultaneously at all four temperatures. Because of the apparent activation energy of the dehydration reaction, the absolute deviations between the experimental points and the predictions of the model differ greatly at various levels of the reaction temperature. Consequently, the incorporation of appropiate weighting factors, which are difficult to ascribe judiciously, would be required in the regression analysis. In kinetic modelling, one usually designs a sequence of experiments at each temperature until the model parameters are defined with sufficient accuracy.

6.4.3 Agreement between coverages observed by infrared and coverages predicted by the model

The qualitative infrared observations described in section 6.1 provided the basis for the development of the new kinetic model. Reciprocally, it would be a more powerful check of the internal consistency of the model to find some quantitative agreement between the measurement by infrared of a kinetic parameter and the value of the same parameter as predicted by the kinetic model. The only parameter suitable for this sort of analysis is the adsorption constant of isopropanol which can be obtained independently by both the infrared and kinetic methods. As mentioned before, at the lower temperatures (231.2°C, 246.5°C), the relative amounts of adsorbed alcohol could be measured reasonably well during reaction by infrared transmittance spectroscopy. This enabled direct measurements of the fractional coverages of the surface by isopropanol as a function of its partial pressure in the gas mixture. The Langmuir isotherm, was assumed to apply to the adsorption of alcohol in the development of the rate equation.

$$= K.P/(1 + K\,P) \qquad (6.14)$$

The values of K (b in equation M7) that resulted from the regression analysis of the data at 231.2°C and 246.5°C were found to be 191.2 atm^{-1} and 78.6 atm^{-1}. To check the reliability of these values obtained by regression analysis, they were used in the Langmuir isotherm, equation (6.14), to predict the fractional coverages of alcohol at various partial pressures of alcohol. Figure 6-14 shows this comparison to be very favourable (which should be expected since equation 6.14 is embodied in the development of equation M7 and re-emphasizes the consistency in this approach to kinetic modeling. It is more difficult to question the appropriateness of the model equation M7, since it simultaneously predicts rather well both the reaction rates and the relative coverages of the surface by the reactant. Now, one cannot argue that the reactant species which were present on the surface in sufficient quantities to be measured by infrared,

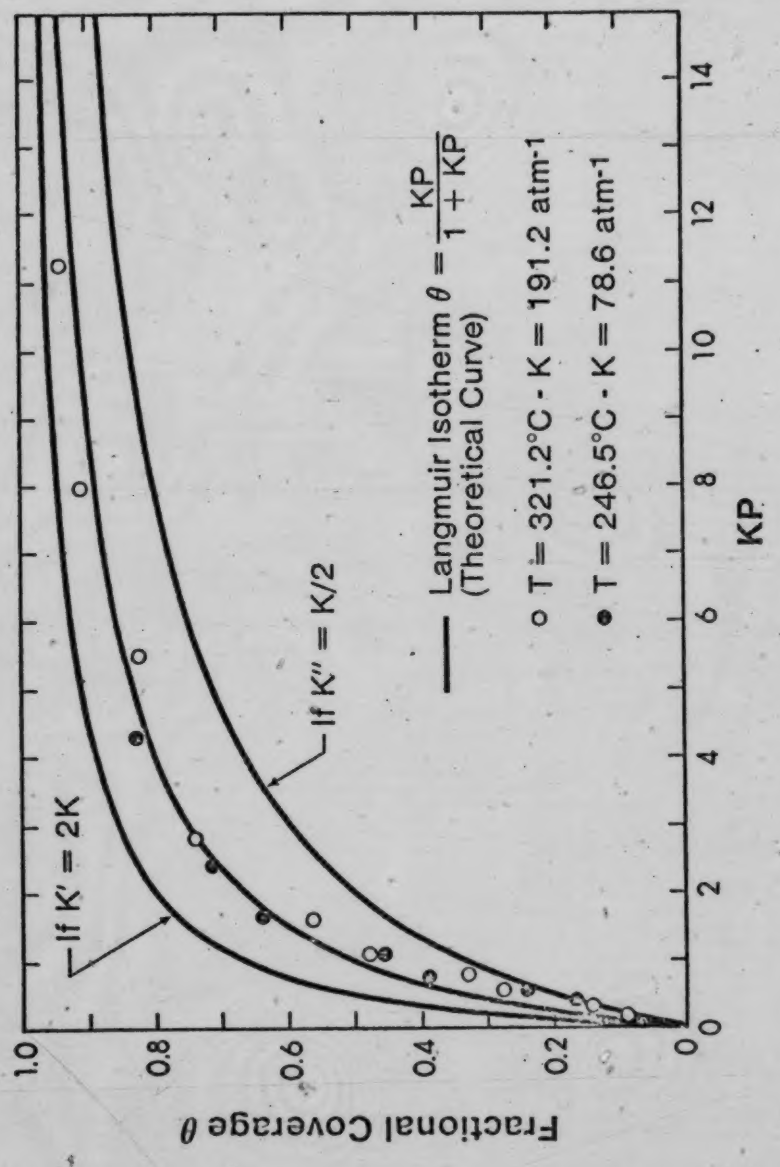

Figure 6.14 Comparison Between Measured and Predicted Fractional Coverages of the Surface

may well have been irrelevant to the reaction mechanism. More exactly, it has been suggested that only a small fraction of these entities act as active intermediates in the reaction mechanism. In this work, it is impossible to prove or disprove this criticism because no direct proportionality was observed between the rate of reaction and the concentration of adsorbed alcohol. However, if the adsorbed alcohol species observed by infrared are not involved in the reaction mechanism and only act as "passive species", their adsorptive properties are less likely to be consistent with the kinetic model,because the latter is then an incorrect model. In contradiction Figure 6-14 shows clearly that the adsorption constant of the "reactive alcohol species" (from regression analysis) and of the "observed alcohol species" (from infrared absorbance) are almost identical. This agreement strongly favours the direct involvment of the observed reactant surface species in the course of the reaction despite the complicated dependence of the reaction rate upon their relative concentration. One satisfactory explanation is to postulate that the adsorbed isopropanol molecules are only the precursors to the true activated complex giving propylene and water. These precursors formed on "less active 1 sites can either desorb or migrate on the surface towards the much smaller number of "true active sites" (1) where the adsorbed molecule is further activated before decomposing into the products of the reaction. This interpretation on the timing of the reaction mechanism seems realistic since conclusive evidence upon the mobility of the alcohol molecules on the alumina surface has been provided in section 2.5.

6.4.4 Measurement Of Batch Conversions

The recycle loop was designed to switch from open to closed (or vice-versa) operating modes instantaneously. Starting from a steady-state operation, IR data were recorded continuously at a fixed chart speed. The 1140 cm^{-1} band of gas-phase isopropanol was calibrated to obtain its extinction coefficient within 5% accuracy. To monitor this band, the reference side of the cell-reactor was positioned in the sample side of the infrared spectrophotometer. Monitoring this band using single beam attenuation by the gas phase provided the concentration of 2-propanol.

By eliminating sampling, the mass of the gases in the loop remained constant during the batch operation. Because the two ovens in the loop operated at different temperatures, the constant volume loop is not at a uniform temperature. This temperature gradient within the loop complicates the determination of the circulating number of moles at any instant. The resolution of this problem required some additional experiments.

To provide the value of Mt, number of moles in batch system at time, t, the procedure requires knowledge of the flow rate of N entering an open loop (through which only N and water are passed), and the mole fraction of water in the feed at the outset of the experiment. The reactor was operated at the same temperature and pressure anticipated in subsequent kinetic runs, but with a continuous nonreactive N -H O feed mixture. At t=0, the water was switched off but N flow maintained. The transient decay of the contained water in the loop was determined by G.C. sampling and analysis at intervals of 70 seconds.

At time, t, the mass balance for H O in the reactor is,

$$M.(0-x\ ) = M\ \frac{dx}{dt}$$

in which M is the constant molar flow of N through the loop. Integrating between t=0 and t=t, x=x and x=x , obtain

$$M = -M.(\ t)/\mathrm{Log}(x\ \ /x\ \ )$$

Applying this equation to any transient period, t, should give the same value, Mt. The values, Mt, so obtained were averaged to give a value for the initial number of moles,Mo,in the loop at the start of a batch run.

To develop the integral equation for the batch reactor, consider the following stoichiometric calculations for the dehydration reaction, A--- P+W, in which the desired mole fraction, x , is to be expressed in terms of Mo, the original number of moles in the loop at the start of the batch reactor operation, and Mt, the corresponding number of moles at a time, t, later. Defining,

$$X = (x \quad -x \;)/x \quad .(1+x \;) \tag{6.15}$$

and introducing this into the isothermal differential material balance equation for a batch reactor,

$$M_t.\frac{dx_A}{dt} = W.\frac{aP_A.(1+bdP_A)}{(1+bP_A)^2.(1+cP_W)} \tag{6.16}$$

and after substituting to eliminate Mt and PA and PW, obtain

$$dt = \frac{M_o.(1+b^1x_A)^2.(c^1+c^2x_A)}{W.a^1.x_A.(1+x_A)^2.(1+d^1x_A)}.dt \tag{6.17}$$

where,

$a^1 = a.P$
$b^1 = 1 + bP \;.(1+x \quad)$
$c^1 = 1 + cx \quad + cx \quad P$
$c^2 = 1 - c + cx \quad P$
$d^1 = 1 + dP \;.(1+x \quad)$

Now, knowing the initial conditions for a batch run and the parameters a, b, c, d in the rate expression, the five constants a^1, b^1, c^1, c^{11}, d^1 may be evaluated. Mo was obtained from the N -H transient experiment for the same recycle loop pressure and temperature distribution.

A batch experiment has been plotted in the form, x vs t, in Figure 6-15. The experimental points show very good agreement with the predicted curve obtained by integrating equation (6.18) numerically. Two valuable points can be made from this integral treatment of experimental kinetics data. First, the good predictions obtained in the run of Figure

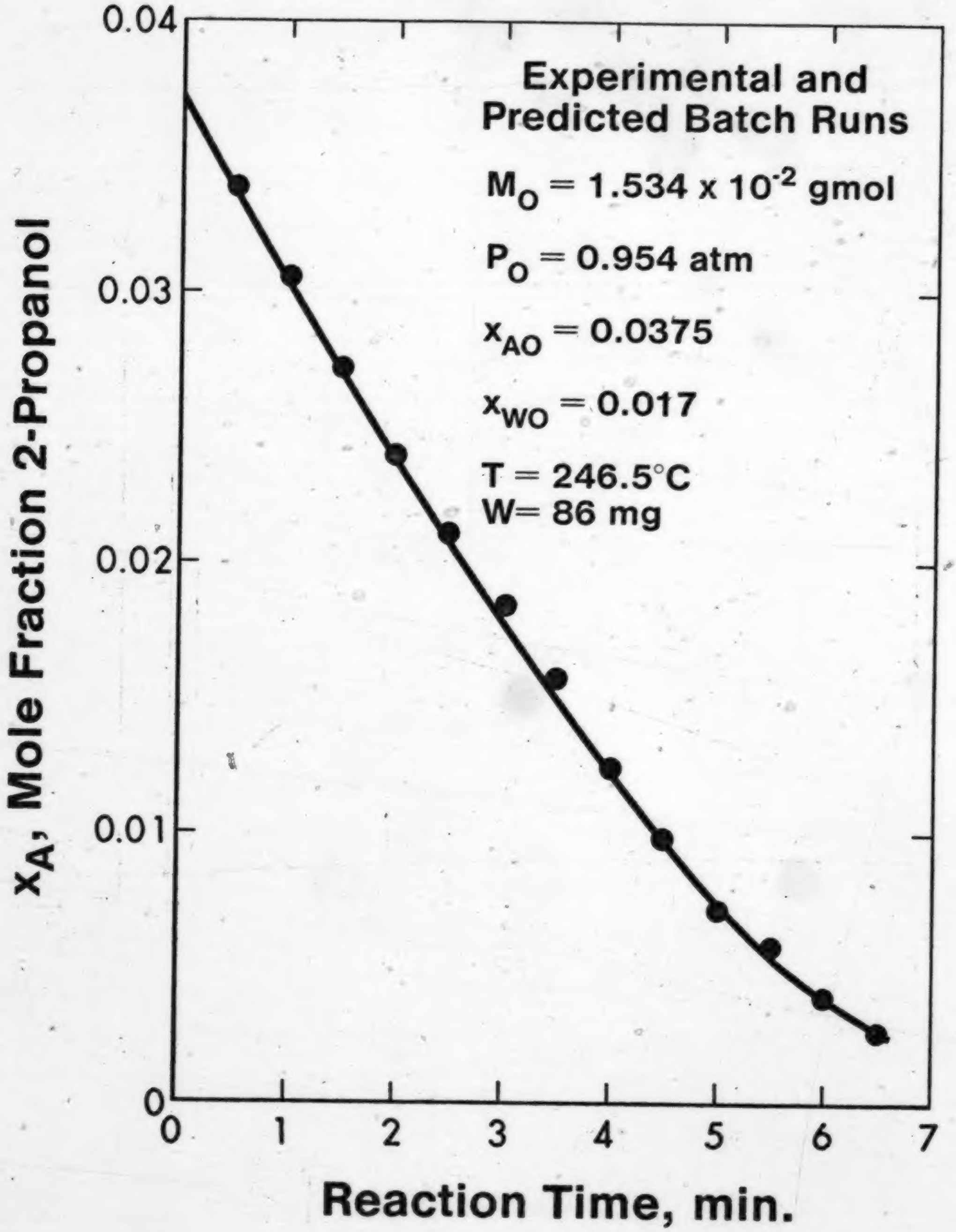

Figure 6.15 Correlation of Batch Experiment

6-15 confirm first the adequacy of the new kinetic model and associated parameters which were obtained from differential kinetic data. Secondly, the assumption of permanent quasi-steady-state in the reactor system seems reasonable, since otherwise substantial deviations from the predicted decay in reactant concentration should result from the inadequacy of mixing of the recycling gases with the working catalyst. The slightly changing steady-states mentioned in chapter 5 should not be significant any more since at any moment the G.C. analysis can be associated closely to an instantaneous steady-state in the reactor.

6.5 Statistical Discrimination Between Alternative Models

6.5.1 Kinetic modelling in heterogeneous catalysis

A rigorous theory of heterogeneous kinetics is unfortunately not available, because the surface of a catalyst is not uniform, geometrically or energetically and,as a result the adsorbate molecules may interact to give adsorption energies that depend on surface coverage. To complicate further, in homogeneous kinetics one can measure directly the concentrations of the reactive species, but in heterogeneous kinetics ,the surface concentrations of adsorbate are generally not measurable. In favourable circumstances however,as in this work,the measurement of the IR absorption of adsorbed species may provide an indirect estimate of surface concentrations. On top of these difficulties, the investigator always assumes that the simple mass action law applies to elementary surface reactions, which may not be true if the adsorbed species interact.

Despite some of these limitations, the Hinshelwood kinetic models based upon the Langmuir theory of adsorption has provided a popular pragmatic approach to the correlation of experimental data for heterogeneous catalytic reactions. Hougen and Watson (163) pioneered the application of this approach to a variety of general reactions and showed the significant features of this method. When applied to a particular reaction system, the global kinetic behaviour can be consistent with one or more plausible models. If there is only one such model, the investigator might accept this as the correct model. More often than not,on an "a priori" basis, several models are adequate. This may result from a poor experimental design in which the response surface for the reaction rate has been insufficiently explored. Another reason may also be that the rate equations for different chemically meaningful mechanistic models are mathematically too similar, so that a discrimination between them is not possible within the normal range of experimental error. This latter point is well illustrated in a paper by Knozinger (164) on the kinetics of ether formation from alcohols on alumina. Kinetic analysis was concluded not to be a useful tool for the elucidation of the mechanism of this reaction. Finally, cases where no single Langmuir-Hinshelwood model describes the kinetic behaviour satisfactorily may occur. Changes required by heterogeneity or interaction must be incorporated in the final rate law to account for the discrepancies. The difficulty in such cases is that a priori considerations do not reveal which model characteristics are quantitatively justified. Finally, it is doubtful wether a unique truth concerning the way in which a reaction actually occurs will result from kinetic studies alone. Nevertheless, there are generally two methods for developing and testing kinetic models. Empirical models may be postulated, for example, by fitting arbitrary power-function models to the rate data. For instance, the rate equation for the dehydration of isopropanol may be written,

$$r = k.P\ .P \qquad (6.18)$$

When applicable, such a simple model has some advantages. The powers represent the apparent orders of reaction of reactants and products. Also, the dependence of k with temperature provides means for estimating the apparent activation energy of the reaction. Another practical point (165) is that a power rate law seems to give a satisfactory fit to experimental data with a minimum number of adjustable parameters.

Unfortunately, many cases arise where the data simply cannot be fitted adequately by an equation of this form, for instance, when the rate of reaction exhibits a maximum with reactant concentration. This reversal at some intermediate concentration is not compatible with the use of a power law term for a reactant. Other disadvantages are that it does not provide any insight into the nature of the elementary processes involved during the reaction , and that it is not safe to extrapolate the range of application beyond the range of experimental data.

In another so called "mechanistic approach", the rate data are correlated by using models based upon plausible reaction mechanisms. To do this, it is common to treat surface reactions in terms of the fundamental concepts advanced by Langmuir and Hinshelwood in which the molecules may react while adsorbed, at surface coverages not exceeding a monolayer. Once a mechanism and individual steps have been postulated, its associated rate equations may be derivated. The main advantage of using mechanistic rate equations is to provide some understanding on the nature of the reaction. Some cautious extrapolation beyond the experimental range can in principle be performed. The reason for caution is that outside the range where the independent variables (compositions, temperature) are varied, the rate-controlling step might change, thereby modifying the form of the rate equation. However, modeling should be related as closely as possible to the underlying physico-chemical phenomena and not deviate into empirical fitting because only then, can we expect to progress towards better understanding of catalysis (166).

When all possible reaction models are listed within the assumptions of the Hougen-Watson scheme, a relatively large number of models may be generated for a particular reaction system. For example, 84 models have been postulated for methane oxidation (167) and 47 models for ethanol dehydration (168). A prohibitive amount of computer time is required to establish the best model. Besides, once the differences between the model estimates become smaller than the experimental error, no further statistical model discrimination is justifiable. In a recent paper by Cropley (169), the point is made that modern statistical methods are virtually limited to non-linear models of fewer than four or five parameters. As the number of parameters is increased to describe more complex chemistry more adequately, the ranges of the reaction conditions required for the estimation of unique parameter values correspondingly widen. It may happen that the required range is unrealistic because the ratelimiting mechanisms change before such a range can be reached. One other danger of the "mechanistic approach" is that the most appropriate model may not be contained in the original set.

In view of all these interrelated problems, it was hoped in this work, that all the information accumulated by infrared spectroscopic technique at the molecular rather than the macroscopic level, should serve as a good screening method because the mechanisms proposed according to infrared data would incorporate more detailed knowledge of the processes taking place on the catalyst surface. In the following sections , the superiority of the new kinetic expression,M7, developed previously will be established in comparison to rival kinetic models as derived more conventionally.

6.5.2 Correlation of kinetic data with other published models for dehydration of alcohols

It has been established in the literature that the surface reaction is the rate-controlling step in the dehydration of alcohols on alumina (171). Therefore, in the following derivations of rate equations, the cases where the adsorption of the reactant or the desorption of products would be rate-controlling were not considered. Since the infrared techniquee did not detect the presence of propylene over the surface of the catalyst and since the addition of propylene in the reaching mixture did not influence the rate of reaction, all plausible mechanisms excluded the steps associated with the adsorption of propylene. When the feed consisted of propylene and water only, no isopropanol product was detected. Accordingly one of the reaction steps must be irreversible and since adsorption and desorption of gaseous reactants and products are inherently reversible steps, the surface reaction is the most likely irreversible step. These experimental observations reduce considerably the number of possible rate equations and parameters associated with a single mechanism.

When reviewing some kinetic studies on various systems that have appeared in the literature (152,164,172,173) it is remarkable that the best proposed rate equation obtained by the authors in their final analysis, always imply the active participation of a maximum of two sites, which may be identical or dissimilar. In all cases, more complicated mechanisms with three or more sites have failed to show any improvement on the overall fit of the experimental data and indeed such mechanisms are unlikely to occur. It seems wasteful to start a model discrimination by postulating complicated multi-parameter models. On the contrary, as suggested by Weller (174), the common approach should be to start with simple models that can progressively be adapted to meet the requirements of the general kinetic behaviour satisfactorily.

Following these considerations,this search for an adequate kinetic model was started by proposing five simple mechanisms for the dehydration reaction on alumina (M1,M2,M3,M4,M5). The mechanisms are listed in detail in Table 6-4 with their associated rate expression, whose derivation follows directly the procedure given by Hougen and Watson (163). In the case of M4 and M5, the step-by-step derivation can be found in Appendix E. It is sufficient to mention here that adequate assumptions provided rate expressions with only three adjustable parameters. The three parameters a, b, and c in Table 6-1 correspond respectively to the rate constant of the surface reaction, and the equilibrium adsorption constants of isopropanol and water. It is important to realize that this subset of five models was not

Table 6.4 Published Simple 3-Parameter Kinetic Models for Dehydration of Alcohols

A=2-Propanol; P=Propylene; W=Water;

(a) Single-site mechanism M1

$$A + l_1 \rightleftharpoons Al_1$$

$$* \quad Al \longrightarrow P + Wl_1$$

$$Wl \rightleftharpoons W + l$$

$$r = \frac{a.b.PA}{1 + b.PA + c.PW}$$

(b) Dual similar sites mechanism M2

$$A + l_1 \rightleftharpoons Al$$

$$* \quad Al + l \longrightarrow P + Wl$$

$$Wl_1 \rightleftharpoons W + l_1$$

$$r = \frac{a.b.PA}{(1 + b.PA + c.PW)^2}$$

(c) Dual dissimilar sites mechanism M3

$$A + l_1 \rightleftharpoons Al_1$$

$$* \quad Al_1 + l_2 \longrightarrow P + Wl_2$$

$$Wl_2 \rightleftharpoons W + l_2$$

$$r = \frac{a.b.PA}{(1 + b.PA)(1 + c.PW)}$$

(d) Dual similar sites mechanism with dissociative adsorption of alcohol M4

$$A + l_1 + l_1 \qquad A_1l_1 + A_2l_1$$

$$* \quad A_1l_1 + l_1 \xrightarrow{\text{slow}} P + Rl_1$$

$$Rl_1 + A_2l_1 \xrightarrow{\text{fast}} Wl_1 + l_1$$

$$Wl_1 \rightleftharpoons W + l_1$$

$$r = \frac{a\sqrt{b.PA}}{(1 + c.PW + 2\sqrt{b.PA})^2}$$

* indicates the rate determining step of each mechanism

TABLE 6-4 (Continued)

(e) Dual dissimilar sites mechanism with dissociative adsorption of alcohol M5

$$A + l_1 + l_2 \rightleftharpoons A_1 l_1 + A_2 l_2$$

$$* \; A_1 l_1 + l_2 \longrightarrow P + R l_1 + l_2 \qquad r = \frac{a\sqrt{b.PA\,(1+c.PW)}}{(1 + c.PW + \sqrt{b.PA\,(1+c.PW)})^2}$$

$$A_2 l + R l_1 \xrightarrow{\text{fast}} W l_2 + l_1$$

$$W l_2 \rightleftharpoons W + l$$

chosen arbitrarily, but contained models proposed previously by various authors in the literature (see section 2.5); and on this basis it appeared judicious to confront these models with the experimental data obtained herein. In fact, from the infrared evidence obtained in section 6.1, which clearly established the noncompetitive adsorption nature of water and isopropanol, one should tend to favour M3 as the best of the five alternatives since it is the only model to possess this feature. However, the appearance of a maximum in the rate of reaction with increasing reactant partial pressure (see Figure 6-9) under certain conditions can not be predicted by the form of equation M3. This apparent contradiction between the infrared and kinetic evidence exemplifies a frequent situation encountered in catalytic studies, in which the overall aspects of a given process are only partially revealed by each individual method. The kinetic runs tabulated previously were correlated separately at each of the four temperatures studied with the present five competitive models. The reasons for using isothermal data have been exposed in section 6.4.2.

The results are unsummarized in Tables 6-5 to 6-8, each of which corresponds to one temperature of reaction. Each table displays the values of the 3 parameters together with 95% confidence limits and average standard deviation between predicted and observed rates of reaction.

Model M1 is decidedly inappropriate since it correlates most poorly at all temperatures and even fails to converge

Table 6.5 Correlation of Some Published Kinetic Models with Rate Data At 231.2°C

Kinetic Models*	a	b	c	Standard Deviation
M1		does not converge to final values		
M2	0.0244 ±0.00353	109.17 ±22.48	51.97 ±24.37	5.72×10^{-4}
M3	0.00474 ±0.000665	13172 ±67988	58.26 ±23.80	4.45×10^{-4}
M4	0.0405 ±0.00315	45.44 ±13.63	51.29 ±12.58	2.83×10^{-4}
M5	0.0207 ±0.00152	134.12 ±30.36	56.16 ±26.01	2.57×10^{-4}

*Models defined in Table 6-1

Table 6.6 Correlation of Some Published Kinetic Models with Rate Data At 246.5°C

Kinetic Models*	a	b	c	Standard Deviation
M1	0.00784 ±0.000670	1551.37 ±2067.63	194.85 ±358.29	1.31×10^{-3}
M2	0.0480 ±0.00400	59.11 ±6.72	27.67 ±8.17	9.59×10^{-4}
M3	0.001 ±0.00104	532.58 ±176.72	20.85 ±8.25	9.66×10^{-4}
M4	0.0728 ±0.00548	8.52 ±2.75	15.32 ±5.43	9.70×10^{-4}
M5	0.0374 ±0.00325	30.70 ±9.12	18.47 ±14.70	9.45×10^{-4}

*Models defined in Table 6-1

Table 6.7 Correlation of Some Published Kinetic Models with Rate Data At 260.3°C

Kinetic Models*	a	b	c	Standard Deviation
M1	0.0167 ±0.00101	316.08 ±118.53	41.37 ±29.33	1.84×10^{-3}
M2	0.0807 ±0.00336	33.04 ±2.00	10.98 ±2.06	1.06×10^{-3}
M3	0.0217 ±0.00189	176.44 ±30.02	13.67 ±4.16	1.44×10^{-3}
M4	0.144 ±0.0130	2.41 ±0.83	6.72 ±2.63	1.90×10^{-3}
M5	0.0747 ±0.00816	8.76 ±2.93	8.76 ±8.50	1.88×10^{-3}

*Models defined in Table 6-1

Table 6.8 Correlation of Some Published Kinetic Models with Rate Data At 274.0ºC

Kinetic Models*	a	b	c	Standard Deviation
M1	0.02994 ±0.0023	275.68 ±241.48	56.45 ±67.55	3.16×10^{-3}
M2	0.0153 ±0.0112	18.80 ±1.96	8.44 ±2.21	2.17×10^{-3}
M3	0.0440 ±0.00507	91.20 ±19.35	11.37 ±3.43	2.10×10^{-3}
M4	0.279 ±0.0304	1.463 ±0.635	5.59 ±2.00	2.77×10^{-3}
M5	0.147 ±0.0201	-5.01 ±2.06	7.23 ±6.51	2.70×10^{-3}

*Models defined in Table 6-1

at 231.2°C. At 246.5°C the four other models fit the data equally well, but the superiority of M2 is indicated by the comparatively narrower confidence limits of its estimated parameter values. The same preference is yet more pronounced at 260.3°C where the average standard deviation of the data for M2 is almost half that of the other models. At the highest temperature, the negative estimated value for the adsorption constant of alcohol for M5 is unrealistic, and according to Kittrell (173), model M5 should be rejected. Overall, the dual-similar sites mechanism M2 displays the best behaviour on the grounds of prediction accuracy and parameter determination. This does not signify however, that model M2 is fitting the data adequately.

Ideally a kinetic model is considered to provide a good fit when its residuals can be explained as errors in the observations. Reciprocally, large residuals of a nonrandom nature indicate immediately the poorness of fit of a model. Nevertheless, the kineticist should be conscious that rate equations are at best quasimechanistic, because of the numerous underlying approximations required in their derivation. In practical terms a slight nonrandom nature in the residuals may be anticipated. This point is well discussed by Bard (175) where he stated: "In cases where data are very accurate, neglected minor effects (in the model) outweigh random errors in measurement. Consequently, nonrandomness of residuals is the rule, rather than the exception, when models are fitted to good data". Careful judgment by the experimenter is therefore required in accepting or rejecting models, even more so, since the statistical methods he may intend to use in his analysis are invariably only approximate methods.

The predictions of a few selected subsets (T1A,T4A and T4B) of the kinetic data obtained in this thesis by the models M2, M3, and M4 are displayed in Figure 6-16 and 6-17. Both at the lower and the higher temperatures, the large systematic trends in the residuals indicate that the modeling error far exceeds the experimental error. Up to this point,from examining Figures 6-16 and 6-17 the models tested must be either rejected or at least modified to include those effects observed in their residuals.

These poor correlations are surprising, considering that each of these models had been selected by previous workers studying the dehydration of alcohols on alumina! Most astonishing are the discrepancies between these results and the ones obtained by Chuang under exactly the same conditions. At the time, model M3 was found to correlate the dehydration rates of isopropanol on alumina almost perfectly at 252°C. In this study, model M3 is not adequate at any temperature but also, could be rejected in favour of M2.

In the previous 3-parameter models, the predicted rates had only 3 degrees of freedom and this might have caused the major shortcomings of the models. Following Kittrell's principle of "parsimonious parametization", one can hope to obtain a model just sufficiently complex to appropriately fit

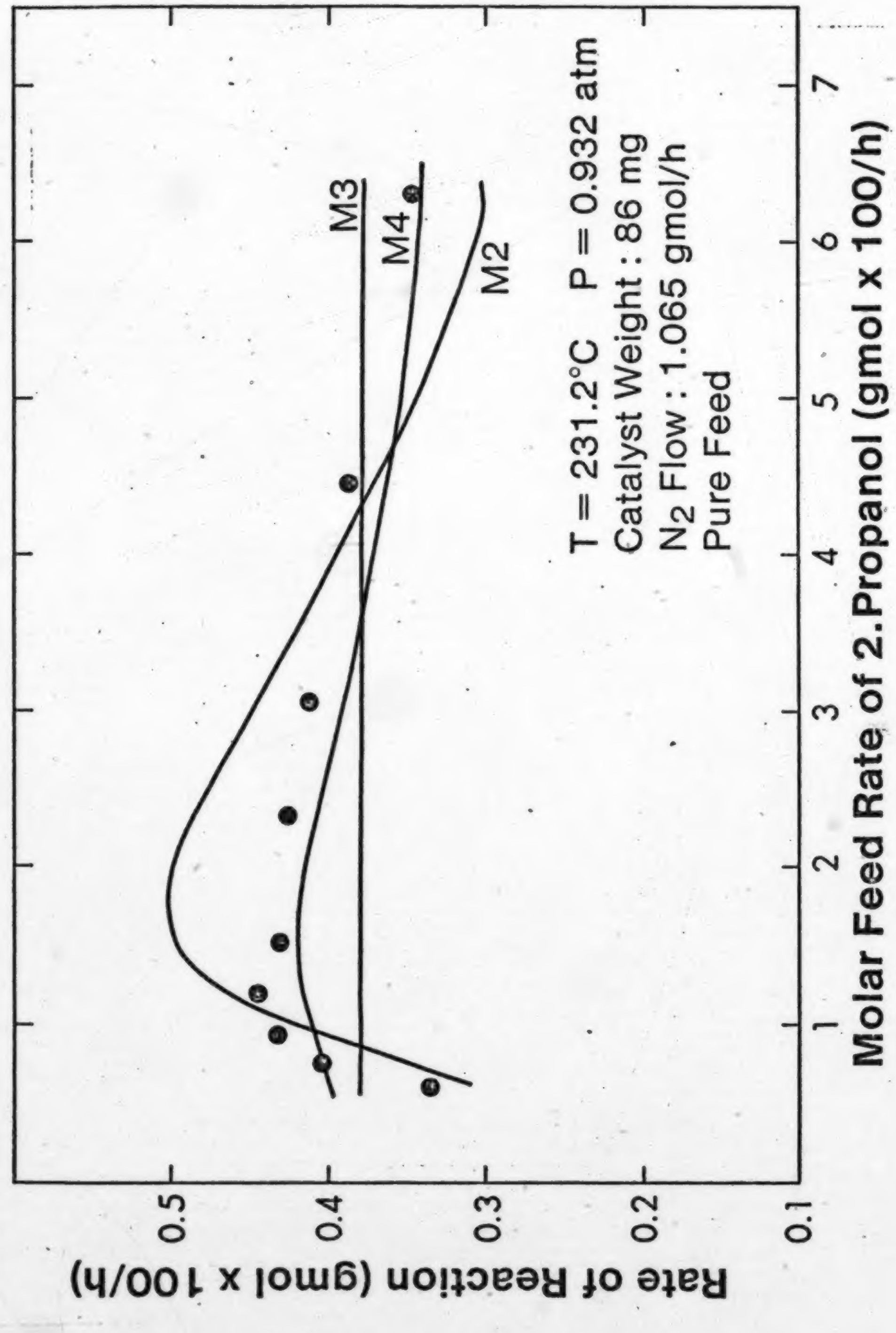

Figure 6.16 Misfit of Published Models at 231.2°C

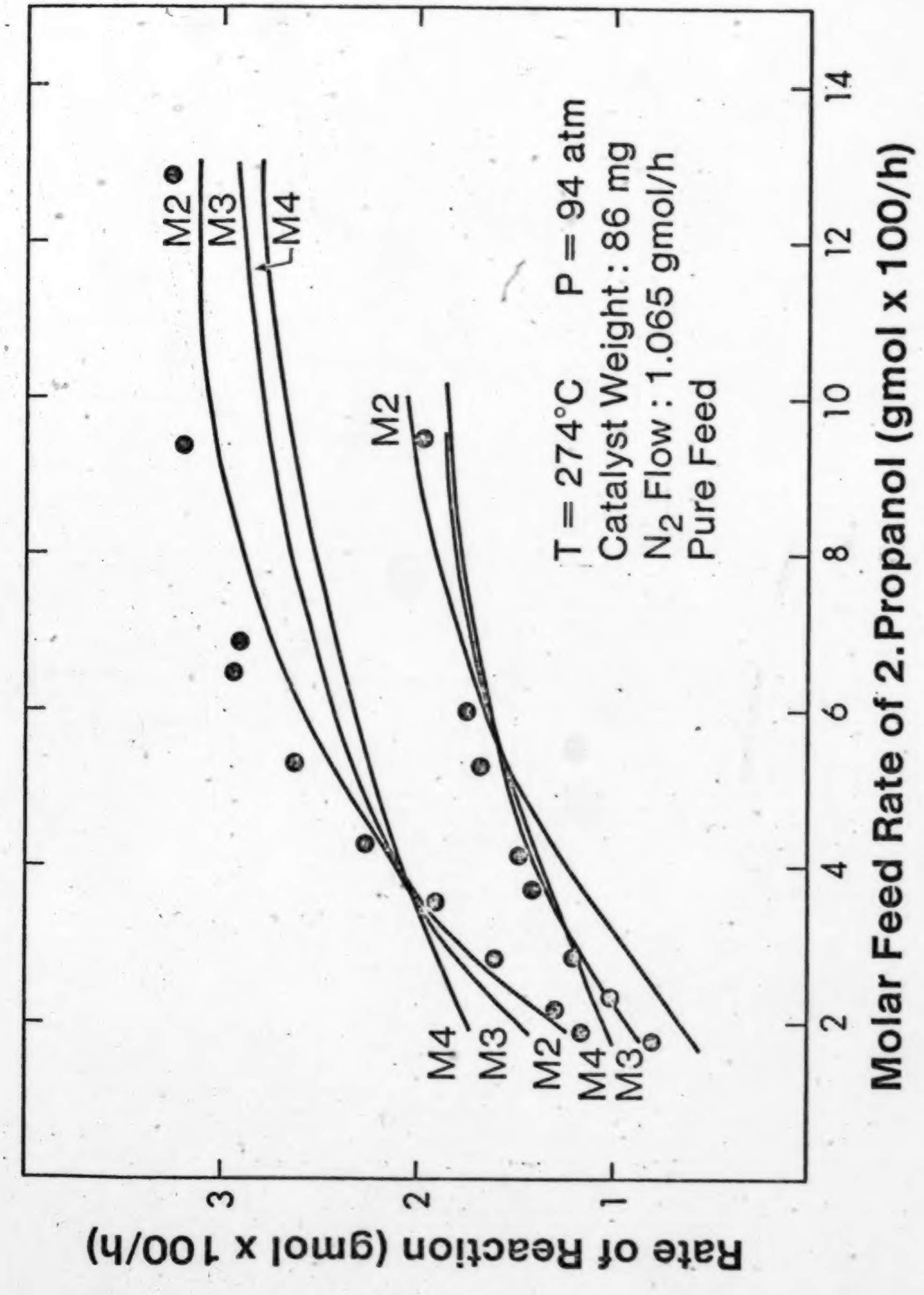

Figure 6.17 Misfit of Published Models at 260.3°C

the data. However, useful observations may be extracted from the behaviour of the individual models tested thus far. The participation of two sites in the reaction process can be inferred from the somewhat better behaviour of the associated rate equations M2 and M3. On the other hand, the concept of a dissociative adsorption of alcohol on the surface had a rather detrimental effect on the predictions of M4 and M5 as compared to M2 and M3 and will be discarded. In conclusion, models M2 and M3 provide crude basic mechanisms which may possibly be improved by increasing their complexity judiciously.

6.5.3 Correlation of improved published models

The concept developed in section 6.3 and accounting for the possible increasing interaction of adsorbed reactant molecules with increasing coverage is not restricted to a dual dissimilar sites mechanism. It can be readily incorporated in the case of a single-site and dual similar-sites mechanisms. The derivation of the associated rate equations M8 and M9 is straightforward and given in Appendix E. Model M10 in Table 6-9 differs from M7 by the introduction of an additional parameter reflecting the unlikely competitive adsorption of water on the alcohol adsorption sites. The purpose of incorporating this model was to check whether the information generated by infrared spectroscopy was consistent with the kinetic results. A good agreement between the two independent methods may be inferred if the additional

Table 6.9 Modified Langmuir-Hinshelwood Models

(a) Modified dual-dissimilar sites mechanism: M7

$$= \frac{a.b.PA\ (1 + b.d.PA)}{(1 + b.PA)^2\ (1 + c.PW)}$$

(b) Modified dual-similar sites mechanism: M8

$$= \frac{a.b.PA\ (1 + c.PW + b.d.PA)}{(1 + b.PA + c.PW)^3}$$

(c) Modified single site mechanism: M9

$$= \frac{a.b.PA\ (1 + c.PW + b.d.PA)}{(1 + b.PA + c.PW)^2}$$

(d) Modified dual dissimilar sites mechanism with additional competitive adsorption of water: M10

$$= \frac{a.b.PA\ (1 + c.PW + b.d.PA)}{(1 + b.PA + c.PW)^2\ (1 + c.PW)}$$

(e) Dual-dissimilar sites mechanism with alcohol adsorbed on both sites: M11

$$= \frac{a.b.PA}{(1 + b.PA)\ (1 + c.PW + d.PA)}$$

parameter will not differ significantly from zero after correlating the data. The last model M11 listed in Table 6-7 conforms more strictly to the normal Langmuir-Hinshelwood approach. Since by infrared we were not able to measure with sufficient accuracy the adsorption of water during reaction, it remains plausible that some of the alcohol displaces the water from its adsorption sites, e.g., by forming alkoxide species on the Lewis-acid sites of the surface. The corresponding equation M11 also contains four adjustable parameters and can be incorporated as a plausible model in the discrimination procedure. Each of the five models of Table 6-7 was used to fit the experimental isothermal data tabulated in Appendix E. The results of the correlation are summarized in Tables 6-8 to 6-11 which are analogous to Tables 6-2 to 6-5 of section 6.4.1.

The examination of the tables reveals a clear superiority of M7 over the rival equations M8 and M9. At all temperatures investigated, the average standard deviation of the residuals is about twice smaller for M7 and, the difference would be still much more significant if the maximum deviations between measured and predicted rates had been considered. By looking more closely at the tables, and comparing M8 and M9 with the previous equations M1 and M2, one may conclude that the introduction of the concept developed in this thesis does not bring much improvement on the predictive behaviour of the single-site and dual-similar sites models. On the other hand, when the results of the

Table 6.10 Correlation of Modified Kinetic Models with Rate Data At 231.2°C

Kinetic Models*	a	b	c	d		Standard Deviation
M7	0.0179 ±0.00166	191.2 ±38.8	56.62 ±10.56	0.191 ±0.035		2.07×10^{-4}
M8	0.0244 ±37.0	109.14 ±165409	51.97 ±24.91	0.999 ±3029		5.84×10^{-4}
M9	0.00966 ±0.00405	1189.6 ±7127	485.95 ±3164.6	0.291 ±0.204		7.48×10^{-4}
M10	0.0178 ±0.00153	223.73 ±57.84	54.75 ±9.55	0.188 ±0.032	24.75 ±27.03	1.90×10^{-4}
M11	0.00662 ±0.00099	983.27 ±512.70	67.63 ±17.16	10.86 ±4.70		2.57×10^{-4}

*Models defined in Table 6-7

Table 6.11 Correlation of Modified Kinetic Models with Rate Data At 246.5°C

Kinetic Models*	a	b	c	d		Standard Deviation
M7	0.0368 ±0.00305	78.60 ±9.82	27.67 ±4.48	0.170 ±0.035		4.22×10^{-4}
M8	0.048 ±17.28	49.14 ±21309	27.66 ±8.62	1.000 ±721		9.69×10^{-4}
M9	0.0187 ±0.0065	294.62 ±275.47	104.01 ±136.11	0.368 ±0.197		1.30×10^{-3}
M10	0.0369 ±0.00283	72.65 ±9.28	28.18 ±4.27	0.172 ±0.0325	24.75 ±4.77	3.98×10^{-4}
M11	0.0158 ±0.00263	229.12 ±61.45	33.84 ±9.05	9.17 ±3.70		6.03×10^{-4}

*Models defined in Table 6-7

Table 6.12 Correlation of Modified Kinetic Models with Rate Data At 260.3°C

Kinetic Models*	a	b	c	d		Standard Deviation
M7	0.0697	38.18	15.17	0.156		7.30x10^{-4}
	±0.00550	±4.25	±2.23	±0.0448		
M8	0.0808	33.03	10.97	1.00		1.07x10^{-3}
	±29.87	±12215.9	±2.10	±739		
M9	0.0492	68.8	33.93	0.197		1.53x10^{-3}
	±0.00769	±21.92	±17.18	±0.103		
M10	0.0701	37.66	15.59	0.157	-0.820	7.34x10^{-4}
	±0.0057	±4.78	±2.92	±0.045	±3.37	
M11	0.0377	77.65	18.67	10.17		9.00x10^{-4}
	±0.00695	±18.16	±4.04	±3.82		

*Models defined in Table 6-7

Table 6.13 Correlation of Modified Kinetic Models with Rate Data At 274.0°C

Kinetic Models*	a	b	c	d	Standard Deviation
M7	0.125 ±0.0179	22.90 ±4.74	11.80 ±2.35	0.225 ±0.0866	1.42×10^{-3}
M8	0.152 ±120	18.79 ±14862	8.44 ±2.27	1.000 ±1580	2.20×10^{-3}
M9	0.0703 ±0.0272	70.67 ±59.74	39.38 ±37.55	0.343 ±0.260	3.11×10^{-3}
M11	0.0632 ±0.0142	51.74 ±15.84	13.70 ±3.62	3.75 ±2.34	1.60×10^{-4}

*Models defined in Table 6-7

regression analysis are compared between M3 and M7, it appears that in addition to a much tighter fit, the three analogous parameters of the two models are better defined in the case of the four parameter equation. This is more pronounced at the lowest temperatures. The proposal of a dual-dissimilar sites mechanism as suggested by the infrared observations seems now corroborated by the kinetic data. This was by no means apparent when we only considered the simple published Langmuir-Hinshelwood models of section 6.5.1. The important point to see at this stage of the discrimination procedure, is that the agreement on the participation of two different sites could only be unveiled by the introduction of the so called "steric factor" of section 6.3.Without it, the statistical analysis, no matter how sophisticated, would have led us to incomplete and erroneous conclusions, which illustrates the danger of omitting adequate models at the start of a model discrimination. In fact, all statistical discrimination techniques are developed on the basic assumption that one adequate model must be contained among the rival models to be discriminated. It is noteworthy that after the regression analysis is completed for M10, no substantial improvement on the residuals appears and the estimated value of the adsorption constant of water on the alcohol sites does not differ significantly from zero. Indeed slightly negative values are obtained, which is unrealistic according to the Hougen-Watson scheme, while the values of the other parameters remain practically the same. We conclude that the infrared evidence of section 6.1 is "statistically" verified by the kinetic data. Finally, both models M7 and M11 are related to a dual dissimilar sites mechanism, but the nature of the autoinhibiting effect of alcohol is different as stated before. Model M11 is the best classical Langmuir-Hinshelwood model proposed so far, and could be selected as the most adequate model in a conventional analysis. Nevertheless, the new type of rate equation M7 derived in this thesis fits the data closely at all temperatures. The superiority of M7 is further stressed by the narrower relative confidence intervals of the estimated parameters. This latter argument is of paramount importance in model selection since it is linked directly to the volume of the confidence region in parameter space (173). The smaller this confidence region, the more knowledge is contained in the model. This constitutes a direct measure of the information attached to a particular model (175). In effect, the ability of a model to generate information is one of its most important tests of adequacy. Intuitively, it is always conceivable to use an empirical model with enough parameters that will fit a set of experimental data. The problem then is that by adding parameters we will invariably expand the volume of the confidence region and lose information on the individual adjustable parameters. This discussion renders the superiority of M7 over all its rival candidates more evident. In the next section, we will comment upon the linear dependence between the average reactivity of the adsorbed molecules of alcohol and their fractional coverage. Up to now, this has been postulated arbitrarily for convenience and a sensitivity analysis of the form of this dependence should be done for completeness.

6.5.4 Final model selection and considerations on the form of the autoinhibiting dependence

A priori there was no fundamental reason for choosing a linear negative dependence between the average reactivity of alcohol in the adsorbed phase and its relative coverage. One method to test for its validity consists of trying other forms of the dependence and comparing their behaviour. Figure 6-18 is a plot for a variety of dependencies between I and O. On this plot the values of I have been fixed at 1 and 0.2 at zero coverage and saturation since these are close to the regression results of the previous section. According to what was discussed in section 6.3, the additional steric parameter d is therefore fixed at 0.2. The appropriate steric equations and associated rate expressions are summarized in Table 6-14. The results of the parameter estimation are tabulated in Appendix E for each of the five models of Table 6-14. Unfortunately,it is impossible from the analysis of the data to determine which steric dependency is more appropriate. The residuals remain of comparable values for the five regression equations considered here. Similarly, the confidence regions of the individual parameters are of similar relative magnitude for each model. It may act as a

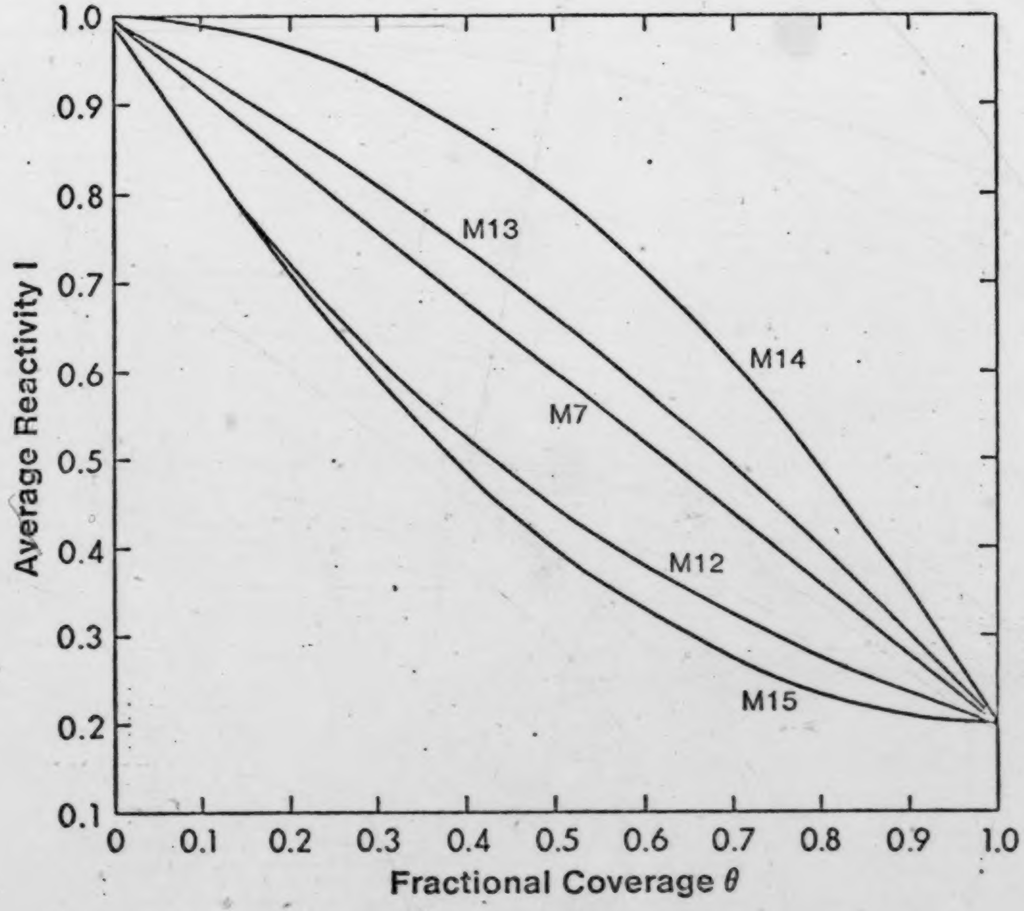

Figure 6.18 Other Dependencies of Reactivity of Adsorbed Alcohol with Fractional Coverage

Table 6.14 Kinetic Models For Various Forms of the Autoinhibition Dependency

TABLE 6-12

KINETIC MODELS FOR VARIOUS FORMS OF THE AUTOINHIBITION DEPENDENCE*

Kinetic Models	Steric Equation	Rate Equation
M7	$I=(d-1)+1$	$\frac{a.b.PA\ (1+b.d.PA)}{(1+b.PA)^2\ (1+c.PW)}$
M12	$I=d$	$\frac{a.b.PA\ d\ \frac{b.PA}{1+b.PA}}{(1+b.PA)\ (1+c.PW)}$
M13	$I=2-(2-d)$	$\frac{a.b.PA\ 2-(2-d)\ \frac{b.PA}{1+b.PA}}{(1+b.PA)\ (1+c.PW)}$
M14	$I=(d-1)^2+1$	$\frac{a.b.PA\ (1+2bPA+db^2PA^2)}{(1+b.PA)^3\ (1+c.PW)}$
M15	$I=(1-d)^2-2(1-d)+1$	$\frac{abPA(1+2bdPA+b^2dPA^2)}{(1+bPA)^3\ (1+cPW)}$

*See plot in Figure 6-18

surprise that the important deviations displayed on Figure 6-10 between the different dependencies are not reflected in the nonlinear regression analysis. Some deeper considerations will help to explain this apparent anomaly.

It is well known that both the experimental as well as the modelling errors are reflected in the uncertainty of the values obtained for the different model parameters. In direct connection to our discussion, the parameter d (I at full coverage) is not single valued (deterministic variable) but can only be defined within a margin of error (stochastic variable). This uncertainty in turn tends to hide or to narrow the theoretical deviations observed between the different curves of Figure 6-10, corresponding to a known fixed value of d (0.2). Also, it can be seen in Appendix E that there is always a rather strong correlation coefficient between the parameters b and d due to the nature of their confidence regions. This problem has been pointed out by Kittrell et al. (177) where the characteristically elongated shape of the hyperellipsoids associated with the parameters of hyperbolic type models has been substantiated. The inherent functional form of the Hougen-Watson models under investigation was the source of this behaviour. In our case, the relative coverage depends directly on the value of b according to the Langmuir-type isotherm ($=bP/(1+bP)$). When we defined the value of d as in this thesis, we inevitably create a strong correlation between b and d. Practically, this means that by making suitable compensating changes in the values of the two parameters, different values of b and d are obtained that agree almost as well with the data. The important deviations illustrated on Figure 6-18 become much less predominant when the values of b and d can be independently adjusted. Combined with the different sources of error, this correlation effect constitutes the main reason why it is impossible to discriminate between the different forms of the coverage hindrance dependence in this work. In fact a detailed simulation study would probably show that experimental data of unrealistic accuracy and reproducibility would be required to resolve this discrimination problem. Besides, it is certain that in any real kinetic study, the models proposed are at best approximate and there is no point in further trying to discover the exact continuous dependency between the average reactivity of adsorbed reactant at all coverages. The overall sensitivity of the data (rate surface response) is satisfactorily reflected by incorporating the additional coverage hindrance factor d as in the form of model M7. This latter model is now selected as the best plausible model for the dehydration of isopropanol on alumina.

7. CONCLUSIONS AND RECOMMENDATIONS

7.1 Conclusions

1.An improved infrared-cell recycle flow reactor has been designed which enables simultaneous measurement of the reaction rates as well as infrared spectra of adsorbed species under reaction conditions. Although the technique is not novel, the improvements in the technique enable considerably better quality experimental data to be measured. The apparatus distinguishes by substantially improved gas-solid contact, considerable reduction in temperature gradients in the infrared reaction cell for better isothermal conditions in the ractin zone, and by the elimination of undesired effect of absorbance of infrared radiation by gaseoue compunds.

2.The merit of the improved cell-recycle rector was demonstrated by a study of the mechanism and kinetics of isopropanol on alumina. An additional important advantage of this approach is thah it enables the direct observation of the relative coverages of the catalyst by the alcohl during the dehydration reaction. The adsorbed molecules are sufficient in number to enable quantitative detection by the infrared detector at temperatures where the rates of reaction can also be measured conveniently in the laboratory. By contrast, in normal kinetic studies inferences concerning the physico-chemical processes taking place on the catalyst are only obtained by indirect means.

3.On the basis of surface spectra obtained during reaction conditions,the dehydration of 2-propanol appear to involve the participation of two different types of sites; one for the alcohol adsorption sites and the other for water adsorption. The water adsorption sites (Lewis acid-base pairs) are involved during the rate-determining step of the process. On the other hand, no linear dependency was observed between the adsorbed alcohol molecules and the rates of reaction except at low coverages.

4.The use of the simultaneous IR spectra-kinetics technique also enables the role of specific sites to be assessed by blocking them under reaction conditions. For example, the role of Lewis-acid sites was studied by adding pyridine to the reactor feedstream -pyridine is known to block Lewis-acid surface sites and would thus be expected to inhibit the reaction rate if Lewis-acid sites are involved in the reaction mechanism.

5.Similarly, stable carboxylate species formed on the surface strongly deactivate the catalyst. Because these species are formed on Lewis acid-base pairs of sites on the surface, it may be deduced that Lewis acid-base pairs of sites constitute the active portions of the alumina surface towards alcohol dehydration.

6.On the other hand, the population of adsorbed alcohol molecules was not significantly influenced by the presence of water or pyridine, or by surface carboxylate species. Therefore the initial interaction of isopropanol molecules with the surface does not seem to involve Lewis acid-base pairs. It was also established by infrared that these alcohol molecules interact with the surface OH groups.

7.The derivation of kinetic models according to Langmuir-Hinshelwood theory fgailed to generate rate expressions which could correlate the experimental reaction rates adequately. In addition infrared-based evidence showed a maximum in the rate of dehydration at intermediate alcohol concentrations. Accordingly, one basic assumption in the Langmuir-Hinshelwood approach, namely no interaction between adsorbed molecules, was concluded to be inappropiate for this rection system. By assuming a simple coverage-interaction dependency between the adsosbed alcohol molecules, it was possible to derive new rate equations for different mechanisms. Among these modified models, only the one corresponding to a dual-dissimilar sites mechanism was found to correlate the kinetic data adequately.

8.The origin of the autoinhibition effect by the adsorbed reactant species could be explained on steric grounds. The accessibility to the second type of sites involved in the proposed reaction mechanism may be sterically hindered when such sites are surrounded by an increasing population of neighbouring adsorbed alcohol molecules. As expected, the autoinhibition parameter was found to be a function only of coverage since it did not vary significantly with temperature. The mechanism of the process thus appears to be complicated, but the predictive behaviour of standard kinetic models was improved considerably by the incorporation of the autoinhibiting factor.

$$r=ab.P\ .(1+bd.P\ )/(1+c.P\ ).(1+b.P\ )^2$$

9.The use of very thin catalyst wafers exposed to flowing recycled gases on both faces enabled measurement of reaction rate free of both inter and intra-particle diffusion effects. Operation at relatively high conversion and space velocities makes the apparatus a very effective tool for kinetic studies in the laboratory.

10.Provided the rates of reaction are not too fast, the apparatus could be advantageously used in batch operation. Infrared analysis through the reference cell enables constant monitoring of the recycled gases.

7.2 Recommendations

1.In future work, the difficulties encounterd in this work in using the same syringe pumps to feed liquids to a rection system should be reconsidered. Very accurate data are attainable if the G.C. response factors of the relevant compounds have been carefully calibrated. However, it was also demonstrated that although the flowrates delivered by the syringe feeder show good reproducibility over periods of a few hours, the feed rates may fluctuate from time to time due to the slipping of the gears driving the syringe pump.

2. Although a reliable method for eliminating the gas-phase absorbance has been developed, the range of application of the technique for measuring adsorption during reaction conditions could be greatly enlarged by using a higher performance IR spectrophotometer.

3. In order to be able to use the infrared results quantatively, like inferring a number for the molecules adsorbed on the catalyst, it is neceesary to estimate the value of the extinction coefficient of at least one of the surface absorption bands. This could be done by performing independent gravimetric studies with a microbalance. The number of alcohol molecules present on the surface could thus be estimated. In similar conditions, the infrared spectra of the catalyst could be recorded allowing to correlate the number of adsorbed species with their infrared absorbance.

4. Another potential refinement would be to slightly modify the existing cells to permit the attainment of higher pretreatment temperatures. This could be achieved by adding another heater around the middle section of the reaction cell where the wafer is located. Pretreatment temperatures as high as 550-600 c may be very beneficial to regenerate catalysts such as alumina which can be poisoned with very stable species such as carboxylates on their surface.

REFERENCES

(1) Thomas, C.L., "Catalytic Processes and Proven Catalysts", Academic Press, New York, 1970.

(2) Lippens, B.C., Ph.D. Thesis, Delft University of Technology, The Netherlands, 1961.

(3) Lippens, B.C., and Steggerda, J.J., "Physical and chemical aspects of adsorbents and catalysts", Academic Press, New York, 1970.

(4) Verwey, E., Krist, Z., *91*, 65, (1935).

(5) Lippens, B.C., and de Boer, J., Acta Crystallogr., *17*, 1312, (1964).

(6) Golasso, F.S., "Structure and Properties of Inorganic Solids", Chapter 8, Pergamon Press, 1970.

(7) Schuit, G.C., and Gates, B.C., A.I. Ch.E. Journal, *19*, 417, (1973).

(8) Leonard, A.J., and Fripiat, J.J., Proc. Br. Ceram. Soc., p. 103, 1969.

(9) Moliere, K., Rathje, W., and Strauski, I., Disc: Farad. Soc., *5*, 21, (1949).

(10) Bhasin, M.M., Curran, C., and John, G.C., J. Phys. Chem., *74*, 3973, (1970).

(11) Peri, J.B., and Hannan, R.B., J. Phys. Chem., *64*, 1526, (1960).

(12) Peri, J.B., J. Phys. Chem., *69*, 220, (1965).

(13) Peri, J.B., J. Phys. Chem., *69*, 211, (1965).

(14) Carter, J.L., Lucchesi, P.J., Corneil, P., Yates, D.J., and Sinfelt, J.H., J. Phys. Chem., *69*, 3070, (1965).

(15) Dunken, H., and Fink, P., Z. Chem.; *6*, 194, (1966).

(16) Bremer, H., and al., Z. Chem., *10*, 161, (1970).

(17) Bell, J.H.,et al. Anal. Chem., *25*, 1720, (1953).

(18) Knozinger, H., Ratnasamy, P., Catal. Rev. Sci. Eng., *17*, 31-70, (1978).

(19) Zecchina, A., Disc. Faraday Soc., *52*, 89, (1971).

(20) Borello, E., Ghiolti, G., and Zecchina, A., *Ibid.*, *52*, 149, (1971).

(21) Morterra C., Ghiolti, G., Garrone, E., and Boccuzzi, F., J. Chem. Soc., Faraday Trans. I, *72*, 2722 (1976).

(22) Pauling, L., "The nature of the chemical bond", third edition, Cornell University Press, Ithaca, New York, 1960, p. 548.

(23) Jones, L.H., J. Chem. Phys., *22*, 217, (1954).

(24) Parkyns, N.D., J. Phys. Chem., *75*, 526, (1971).

(25) Fink, P., Z. Chem., *7*, 324, (1967).

(26) Amenomiya, Y., Morikawa, Y., and Pleizier, G., J. Catal., *46*, 431, (1977).

(27) Knozinger, H., Krietenbrink, H., Muller, H.D., and Schulz, W., Proc. VIth Int. Congr. Catalysis, (The Chemical Study, London, 1977), Vol. *1*, p. 183.

(28) Morterra, C., Ghiorino, A., Ghiolti, G., Garrone, E., J.C.S. Faraday I, *75*, 257, (1979).

(29) Chukin, G.D., Zh. Struk. Khim., *17*, 122-128, (1976).

(30) Maciver, D.S., and Barth, R.T., J. Catal., *2*, 485, (1963).

(31) Hendiksen, B.A., Pearce, D.R., and Rudham R., J. Catal., *24*, 82, (1972).

(32) Morinoto, T., Shiomi, K., and Tanaka, H., Bell. Chem. Soc. Jpn., *37*, 392, (1964).

(33) Holdeman, R.G., and Eurmelt, P.H., J. Am. Chem. Soc., *78*, 2917, (1956).

(34) Hindin, S.G., and Weller, S.W., Adv. Catal., *9*, 70, (1957).

(35) Stablin, W., and Knozinger, H., unpublished results.

(36) Arai, H., and al., J. Catal., *9*, 146, (1967).

(37) Boreskov, G.K., and al., Dokl. Akad. Nauk., SSSR, *156*, 901, (1964).

(38) Hertl, W., Cuenca, A.M., J. Phys. Chem., *77*, 1120 (1973).

(39) Knozinger, H., Adv. Catal., *27*, 179, (1976).

(40) Rosynek, M.P., and Hightower, J.W., Int. Congr. Catal. 5th, Miami, Florida, 851, (1973).

(41) Peri, J.B., J. Phys. Chem., *70*, 3168, (1966).

(42) Larson, J.G., and Hall, W.K., J. Phys. Chem., *69*, 3080, (1965).

(43) Burwell, R.L., and al., Adv. Catal. Relat. Subj., *20*, 1, (1969).

(44) Tanabe, K., "Solid Acids and Bases - Their catalytic properties", Academic Press, New York, 1970.

(45) Benesi, H.A., Winquist, B.H., Adv. in Catalysis, *27*, 97, (1977).

(46) Iquatieva, L.A., Khalikova, R.K., Zh. Prikl. Spekt., *5*, 642-647, (1966).

(47) Bourne, K.H., Cannings, F.R., J. Phys. Chem., *74*, 2197, (1970).

(48) Balliuet, D., Barthomeuf, D., and Pichat, P., J. Phys. Chem., *74*, 2197, (1970).

(49) Parry, E.P., J. Catal., *2*, 371, (1963).

(50) Knozinger, H., and Kaarlein, C., J. Catal., *25*, 436, (1972).

(51) Pines, H., and Haag, W.O., J. Am. Chem. Soc., *82*, 2471, (1960).

(52) Pines, H., and Haag, W.O., J. Am. Chem. Soc., *82*, 2488, (1960).

(53) Greenler, R.G., J. Chem. Phys., *37*, 2094, (1962).

(54) Ono, Y., Keii, T., J. Phys. Chem., *72*, 2851, (1968).

(55) Basset, J., Mathieu, M.V., and Prettre, M., J. Chem. Phys., *66*, 1264, (1969).

(56) Parkyns, N.D., Chem. Comm., 530, (1965).

(57) Flockhart, B.D., Scott, J.A., and Pink, R.C., Trans. Faraday Soc., *62*, 730, (1966).

(58) Kiselev, A.V., and Uvarov, A.V., Surface Sci., *6*, 399, (1967).

(59) Flockhart, B.D., Leith, I.R., Pink, R.C., J. Catal., *9*, 45, (1967).

(60) Naccache, C., Kodratoff, Y., Pink, R.C., Imelik, B., J. Chim. Phys., *63*, 341, (1966).

(61) Flockhart, B.D., Leith, I.R., Pink, R.C., Trans. Faraday Society, *65*, 542, (1969).

(62) Kagel, R.O., J. Phys. Chem., *71*, 844, (1967).

(63) Deo, A.V., Dalla Lana, I.G., J. Phys. Chem., *73*, 716, (1969).

(64) Knozinger, H., Ress, H., Buhl, H., Naturwissenschaften, *54*, 516, (1967).

(65) Knozinger, H., Buhl, H., and Ress, H., J. Catal., *12*, 121, (1968).

(66) Treibmann, D., Simon, A., Ber. Buns. Phys. Chem., *70*, 562, (1966).

(67) Schwab, G.M., and Kral, H., Proc. 3rd Intern. Congr. Catal., Vol. 1, p. 433, North Holland Publ. Comp., Amsterdam, 1965.

(68) Flockhart, B.D., and Pink, R.C., J. Catal., *8*, 293 (1967).

(69) Ghorbel, A., Hoong Van, C., Teichner, S.J., J. Catal., *33*, 123, (1974).

(70) Figueras, R., and al., C.R. Acad. Sc., Paris, *266*, 1123, (1968).

(71) Marczewski, M., Malinowski, S., Bull. Acad. Polen. Sci., Ser. Chim., *24*, 187, (1976).

(72) Fink, P., Rev. Roun. Chim., *14*, 811, (1969).

(73) Knozinger H., Angew. Chem. Intern. Edit., *7*, 791, (1968).

(74) Geschke, D., and Pfeifer, H., Z. Physik. Chem. (Frankfurt), *232*, 127, (1966).

(75) Chuang, T.T., Ph.D. Thesis, University of Alberta, Edmonton, Canada, 1971.

(76) Bradkey, D.C., Progr. Inorg. Chem., Vol. 2, 303, (1960).

(77) Schekochikin, Y., Davydov, A.A., Adsorb i Adsorbenty, Vol. 4, pp. 75-80, (1976).

(78) Deo, A.V., Chuang, T.T., and Dalla Lana, I.G., J. Phys. Chem., *75*, 234, (1971).

(79) Corso, V., Compt. Rend., *259*, 1413, (1964).

(80) Knozinger, H., and Bihl, H., Z. Naturforsch., *246*, 290, (1969).

(81) Knozinger, H., in "Recent Progress in Hydrogen bonds" (P. Schuster, G. Zundel and C. Sanderly, editors), North Holland Publish., Amsterdam, 1976.

(82) Spanheimer, H., Knozinger, H., Ber. Buns. Phys. Chem., *70*, 570, (1966).

(83) Hall, W.K., in "Catalysis Progress in Research", (F. Basolo, and R.L. Burwell, editors), Plenun Press, New York, 1973.

(84) Pines, H., and Manassen, J., Adv. Catal., *16*, 49, (1966).

(85) Solomon, H.J., Bliss, H., and Butt, J.B., Ind. Eng.

Chem., Fundamentals, *6*, 325, (1967).

(86) Isagulyants, G.V., Balandin, A.A., Zh. Fiz. Khim., *38*, 20, (1964).

(87) De Mourgues, L., Trambouze, Y., and Prettre, M., J. Catalysis, *7*, 117, (1967).

(88) Balandin, A.A., Esam, I., and Rudenko, A., Kinet. Kat., *9*, 1101, (1968).

(89) Pines, H., and Haag, W.O., J. Am. Chem. Soc., *83*, 2867, (1961).

(90) Deo A.V., and Dalla Lana, I.G., J. Phys. Chem., *73*, 716, (1969).

(91) Vasserberg, V.E., Davydova, J.R., and Georgieskaya, T.V., Kinet. i Kat., *2*, 773, (1961).

(92) Schwab, G.M., and Lassak, L., Kolloid-Z., *206*, 37, (1965).

(93) Schwab, G.M., and Jenkner, O., Z. Elektr. Ber. Buns. Phys. Chem., *63*, 461, (1969).

(94) Eucken, A., and Wicke, E., Z. Naterforsch., *2a*, 163, (1967).

(95) Krylov, O.V., Zh. Fiz. Khin., *39*, 2956, (1965).

(96) Jain, J.R., Pillai, C.N., J. Catal., *9*, 322, (1967).

(97) Beranek, K., Kraus, M., Koechloefl, K., Actes Congr. Int. Catal., 2nd, Paris, 1960, *1*, 749.

(98) Topchieva, K.V., Yun-Pin, K., Adv. Catal., *9*, 797, (1957).

(99) Miseno, M., Saito, Y., and Yoneda, Y., Proc. Inst.

Congr. Catalysis, Elsevier, Amsterdam, p. 408, (1964).

(100) Tamatu, K., Soma, Y., and Onishi, T., Trans. Faraday Society, *65*, 2215, (1969).

(101) Knozinger, H., Scheglila, A., and Watson, A.M., J. Phys. Chem., *72*, 2770, (1968).

(102) Knozinger H., Koechloefl, K., Proc. Vth Int. Congr. Catal., 1159, (1972).

(103) Knozinger, H., Scheglila, A., J. Catalysis, *17*, 252, (1970).

(104) Pines, H., and Blanc, E.J., J. Org. Chem., *33*, 2035, (1968).

(105) Yarnoguchi, T., Tanabe, K., J. Chem. Soc., Japan, 240, (1973).

(106) Hall, W.K., Kilby, C.L., J. Am. Chem. Soc., *94*, 214, (1972).

(107) Harris, J., Wamser, C., "Fundamentals of Organic Reaction Mechanisms", John Wiley and Sons, 1976.

(108) Scheck, R.L., M.Sc.Thesis, University of Alberta, Edmonton, Alberta, 1977.

(109) Pines, H., and Herling, J., J. Org. Chem., *31*, 4088, (1966).

(110) Knozinger, H., Behl, H., Z. Physik. Chem. (Frankfurt), *63*, 199, (1969).

(111) Knozinger, H., and al., J. Catal., *24*, 57, (1972).

(112) Banthorpe, D.V., "Elimination reactions", Elsevier, Amsterdam, p. 11, 1963.

(113) Notari, B., Chim. Ind. (Milan), *51*, 1200, (1969).

(114) Pillai, C.N., and Pines, H.J., J. Am. Chem. Soc., *83*, 3274, (1961).

(115) Knozinger, H., Dantzenberg, D., J. of Catal., *33*, 142, (1974).

(116) Dohse, H., and Kalberer, W., Z. Physik. Chem. (Leipzig), B5, 131, (1929).

(117) Topchieva, K.V., and al., Vestn. Mosk. Univ., Ser. Khim., *14*, 217, (1959).

(118) Brey, W.S., and Krieger, K.A., J. Am. Chem. Soc., *71*, 3637, (1969).

(119) Antipina, T.V., and Frost, V.A., Dokl. Akad. Nauk. SSSR, *84*, 985, (1952).

(120) Kraus, M., Koechloefl, K., Collect. Czekoslov. Chem. Commun. *32*, 2320, (1967).

(121) Rosie, D.M, and Barry, E.F., J.Chromat.Sci.,*11*, 237, (1973).

(122) Carra, S., and al., Chim. Ind. (Milan), *48*, 229, (1966).

(123) Kiltrell, J.R., and Mezaki, R., Ind. Eng. Chem., *59*, 28, (1967).

(124) Bremer, H., and Werner, W., Chem. Techn., *21*, 353, (1969).

(125) Knozinger, H., Behl, H., Ber. Buns. Physik. Chem., *71*, 73, (1967).

(126) Jain, J.R., and Pillai, C.N., J. Catal., *9*, 322, (1967).

(127) Koechloefl, K., and al., Collect. Czekoslov. Chem. Commun., *27*, 1199, (1962).

(128) Stauffer, J.E., Kranich, W.L., Ind. Eng. Chem. Fund., *1*, 107, (1962).

(129) Gregg, S.J., and Singh, K.,"Adsorption, Surface Area and Porosity", Academic Press, Chap.3, 1967.

(130) Beranek, K., and al., J. Catal., *13*, 435, (1969).

(131) Koechloefl, K., Hajek, M., Duchet, J.C., Collect. Czchoslov. Chem. Commun., *35*, 2258, (1970).

(132) Knozinger, H., Koechloefl, K., Ber. Buns. Phys. Chem., *76*, 840, (1972).

(133) Breckstoff, J.K., and Van Dougen, P.J., in "Physical and Chemical Aspects of Adsorbents and Catalysts", Academic Press, New York, (1970).

(134) Dacey, J.R., Ind. Eng. Chem., *57*, (6), 27, (1965).

(135) De Boer, J.H., Adv. Catal., *8*, 18, (1959).

(136) Miller, D.N., Kirk, R.S., A.I. ChE. J., *8*, 183, (1962).

(137) Masanume, S., and Smith, J.M., A.I. ChE. J., *11*, 41, (1965).

(138) Bienert, R., and Gelbin, D., Chem. Techn. (Berlin), *19*, 207, (1967).

(139) Vanerberg, V.E., Makhlis, L., Izv. Otl. Khim. Nauk., Bulg. Akad. Nauk., *6*, 439, (1973).

(140) Vanerberg, V.E., Maklis, L.A., Izv. Akad. Nauk. SSSR, *3*, 476, (1976).

(141) Eischens, R.P., and Pliskin, W.A., Adv. Catal., *10*, 1-56, (1958).

(142) Little, L.H., "Infrared Spectra of Adsorbed Species", Academic Press, New York, 1966.

(143) Hair, M.L., "Infrared Spectroscopy in Surface Chemistry", Marcel Dekker, New York, 1967.

(144) Kiselev, A.V., Lygin, V.I., "Infrared Spectra of Surface Compounds", John Wiley and Sons, 1975.

(145) Parkyns, N.D., in "Laboratory Methods in Infrared Spectroscopy", (R.G.J. Miller and B.C. Stace, eds.), pp. 318-339, Heyden and Son, London, 1972.

(146) Bozon-Verduraz, F., J. Catal., *18*, 12, (1970).

(147) Baddour, R.F., Modell M., and Goldsmith, P.L., J. Phys. Chem., *72*, 3621, (1968).

(148) Dent, A.L., and Kokes, R.J., J. Phys. Chem., *74*, 3653, (1970).

(149) Tamane, K., and al., Trans. Faraday Soc., *63*, 2300, (1967).

(150) Thornton, R., Ph.D. Thesis, University of Delaware, 1973.

(151) Shih, S.S., Ph.D. Thesis, Purdue University, 1975.

(152) Lui, C.L., Ph.D. Thesis, University of Alberta, 1978.

(153) Voishvallo, N.A., and Mironova, L.R., Zh. Prikl. Specktrosk., *8*, 843, (1968).

(154) Eberly, P.E., J. Phys. Chem., *72*, 1042, (1968).

(155) Doraiswamy, L.K., Taybl, D.J., Catal. Rev.-Sci. Eng., *10*(2), 177, (1974).

(156) Carberry, J.J., Butt, J.B., Catal. Rev.-Sci. Eng., *11*, 513, 221, (1974).

(157) Kiperman, S.L., Int. Chem. Eng., *11*, 513, (1971).

(158) Salterfied, C.N., "Mass Transfer in Heterogeneous Catalysis", MIT Press, 1970.

(159) Carberry, J.J., Catal. Rev.-Sci. Eng., *3*, 62, (1970).

(160) Kranik, J.H., Smith, J.M., I. and EC Fund., *4*, 103, (1965).

(161) Levenspiel, O., "Chemical Reaction Engineering", John Wiley, N.Y., Chapter 14, 1962.

(162) Henry, J.P., Smith, J.M., A.I. ChE. J., *7*, 10, (1961).

(163) Hougen, O.A., Watson, K.M., "Chemical Process Principles", Vol. 3, Wiley, N.Y., 1967.

(164) Knozinger, H., Koechloefl, K., and Meye, W., J. Catal., *28*, 69, (1973).

(165) Weller, S., A.I. ChE. J., *2*, 59, (1964).

(166) Froment, G.M., A.I. ChE. J., *21*, No. 6, p. 1041, (1975).

(167) Mezaki, R., and Watson, C.C., Ind. Eng. Chem., Process Design and Development, *5*, 62, (1966).

(168) Kiltrell, J.R., Ph.D. Thesis, University of Wisconsin, Madison, Wisconsin, 1966.

(169) Cropley, J.B., Chemical Reaction Engineering, Houston, ACS Symposium Series 65, p. 92, 1978.

(170) Singh, H.M., M.Sci. Thesis, University of Alberta, Edmonton, Alberta, 1971.

(171) Knozinger, H., and Koechloefl , K., Ber.Buns.Geseilschaft, *75*, 840, (1971).

(172) Dumez, F.J., and Froment, G.F., Chem.Eng.Sci., *42*, 813, (1976).

(173) Kittrell, J.R., Adv.inChem. Eng.series, Vol.7, 314, 1972.

(174) Weller, S.W., Chemical Reaction Engineering Reviews, ACS 148, 26, 1974.

(175) Bard, Y., "Non Linear Parameter Estimation", Elsevier Publishing Co., p.201, 1974.

(176) Boudart, M., A.I.Ch.E.Journal, *18*, 465, (1972).

(177) Kittrell, J.R., Hunter, W.J., and Watson, C.C.,A.I.Ch.E.Journal, *12*, 5, (1966).

NOMENCLATURE

A	Specific external catalyst surface area(cm²)
A	G.C. peak area of component i
C	Concentration of reactant in reactor (g-mol/cc)
C	Concentration of reactant in feedstream (g-mol/cc)
C	Concentration of reactant near catalyst surface
D	Effective diffusivity
F	Molar flowrate entering the reactor (mol/h)
F	Molar flowrate of component i
k	Rate constant of surface reaction
K	Adsorption constant of alcohol
K	Adsorption constant of water
k	Gas diffusion coefficient
l ,l	Dual-dissimilar surface sites
L ,L	Total number of active sites
M	Molecular weight
P	Partial pressure of component i (atm)
r	Rate of reaction (g-mol/g-h)
R	G.C. response factor of component i
T	Temperature (K)
x	Molar fraction of component i
X	Fractional conversion of alcohol reactant
	Fractional coverage of catalyst surface
	Tortuosity factor

APPENDIX

SYRINGE PUMP CALIBRATIONS

Calibration points were determined for all pump and syringe combinations. Distilled water was used as the calibration fluid. Each calibration point was determined as follows. The water ejected through the syringe needle was collected in a 25 ml pycnometer submerged in an ice-water bath to prevent the loss of water due to evaporation. From the elapsed time and the weight of water injected a volumetric flow rate (given the density of water) was calculated. The duration of each calibration run was between one and three hours. Each piston speed was calibrated three or four times in such a way that the whole range of piston travel was covered. The discussion of the results was reported in section 5.5. The calibration points for various combinations of pumps and syringes are listed in Tables A.1 to A.3.

TABLE A-1

*SYRINGE PUMP CALIBRATION POINTS**

Setting	Run Duration (mn)	Flow Rate (ml/mn)	Average (ml/mn)
30/1000	60	0.0261	0.02612
	87	0.02614	
	75	0.02653	
	78	0.0257	
40/1000	63	0.03513	0.03451
	91	0.03488	
	92	0.0341	
	94	0.0339	
50/1000	62	0.04417	0.04377
	77	0.0436	
	108	0.04288	
	66	0.04443	
60/1000	143	0.05274	0.05256
	92	0.0529	
	84	0.05203	
70/1000	64	0.0615	0.06124
	61	0.06152	
	81	0.0607	
80/1000	62	0.07085	0.0707
	91	0.07049	
	63	0.07075	
90/1000	89	0.07956	0.07937
	67	0.07909	
	30	0.07945	

*Syringe Pump Number 1 and 50 cc syringe

TABLE A-2

SYRINGE PUMP CALIBRATION POINTS

Setting	Run Duration (mn)	Flow Rate (ml/mn)	Average (ml/mn)
30/1000	83	0.01244	0.01256
	89	0.01291	
	87	0.01233	
40/1000	112	0.01658	0.0167
	88	0.01701	
	89	0.0165	
50/1000	68	0.02096	0.02116
	55	0.0218	
	69	0.02072	
60/1000	92	0.02531	0.02526
	100	0.02508	
	63	0.02540	
70/1000	71	0.02936	0.02933
	59	0.02906	
	55	0.02958	
80/1000	81	0.03400	0.03384
	58	0.03338	
	70	0.03414	
90/1000	79	0.03823	0.03845
	51	0.03781	
	53	0.03930	
15/100	33	0.05918	0.05968
	63	0.05999	
	41	0.05987	
20/100	38	0.0817	0.0819
	41	0.0817	
	34	0.0823	
25/100	40	0.1042	0.1039
	44	0.1034	
	37	0.1043	

TABLE A-2 (CONTINUED)

Setting	Run Duration (mn)	Flow Rate (ml/mn)	Average (ml/mn)
30/100	34	0.1265	0.1261
	32	0.1257	
	38	0.1261	
35/100	27	0.1481	0.1486
	36	0.1491	

*Syringe Pump Number 1 and 20 cc syringe

TABLE A-3

SYRINGE PUMP CALIBRATION POINTS

Setting	Run Duration (mn)	Flow Rate (ml/mn)	Average (ml/mn)
30/1000	78	0.02484	0.02515
	103	0.02524	
	109	0.02536	
50/1000	116	0.04245	0.04237
	93	0.04247	
	97	0.04261	
	121	0.04229	
	92	0.04128	
	58	0.04227	
	64	0.04308	
	97	0.04204	
70/1000	71	0.0591	0.05893
	98	0.0590	
	77	0.05934	
	80	0.0583	
90/1000	62	0.07643	0.07635
	70	0.07648	
	78	0.07615	

*Syringe Pump Number 2 and 50 cc syringe

B. *PORE DIFFUSION LIMITATIONS*

The method reported by Satterfield ( ) estimating the effectiveness factor, y, for kinetic expressions such as Hougen-Watson type of rate equations was employed to determine whether the experimental results of section 6.2 could also be predicted independently by the method. The following parameter values are required:

$$D \quad = 9700.r\ .(T/M)^{1\ 2}.(\ /\ ) \qquad (C.1)$$

$$= \frac{L^2}{D}.(r\ /C\ ) \qquad (C.2)$$

The terms within the expressions for D , , are defined as follows:

D = effective diffusivity of reactant based on Knudsen diffusion within the pores, cm²/s

r = pore radius, cm

T = absolute temperature, K

M = molecular weight

= Dimensionless Thick diffusion modulus

r = observed reaction rate, g-mol/s. cc of catalyst

L = ratio of the catalyst volume to outside surface area through which reactant has access

C = concentration of reactant, g-mol/cc

Chuang and Liu (75,152) omitted the porosity and tortuosity factors in their calculations. In one study

(158) the values of porosity and tortuosity factors of an aluminia plug compressed from powder were 0.812 and 0.85. The pore radius of 9.6 nm was closed to that used in this work (84 nm). On the other hand, according to the list by Salterfield, the smallest porosity and largest tortuosity for catalysts with pore radius larger than 6 nm are 0.52 and 3.8 respectively. These considerations justify the value of 0.47 we used in these calculations.

$$D = 9700.84 * 10^{-8} * (547/60)^{1\ 2} * 0.47$$

$$= 1.16 \times 10^{-2}\ cm^2/s$$

The density of the pressed alumina was determined as approximately 2.3 g/cm³. We selected two runs of Figure 6-6 for our calculations. We noticed on the same figure that experimentally the pore diffusion limitations became important on the two thicker pellets (187.5 mg and 292 mg) at a given space velocity. It is interesting to take the experimental data closest to these values for our calculations since we will then be able to compare if the method of Salterfield also predicts the experimentally established onset of intraparticle diffusion in those conditions. The calculation results are shown below

$$r = \frac{3.435 \times 10^{-2}}{3600 \times .0815} = 1.17 \times 10^{-4}\ \text{GMOL/S X CM}^3$$

$$r = \frac{7.43 \times 10^{-2}}{} = 1.625 \times 10^{-4}\ \text{GMOL/S X C}$$

$$3600 \quad x \ .127$$

$$C = \frac{3.52 \quad x \ 10^{-2}}{82 \quad x \ 547} = 7.85 \ X \ 10^{-4} \ GMOL/CM^{3}$$

$$C = \frac{8.26 \quad x \ 10^{-2}}{82 \quad x \ 547} = 1.85 \ X \ 10^{-4} \ GMOL/CM^{3}$$

and therefore

$$\frac{r}{C} = 149 \ s^{-1} \qquad \frac{r}{C} = 87.8 \ s^{-1}$$

For equation (C.2), we get

$$= 1.045 \qquad\qquad = 1.48$$

Now from Figure 4.2 in Salterfield the pore diffusion is predicted to become important when is greater than 0.5 for a first order reaction and greater than 2 for a zero order reaction. We see that since the selected kinetic model M7 gives a fractional order dependence with reactant concentration in the conditions of the two runs selected here, the intermediate values of 1.045 and 1.48 are therefore expected to correspon to the onset of pore diffusion. This confirms the agreement between the experimental data and the behaviour predicted by the method of Satterfield.

To illustrate further the effectivenss factor method we selected the highest conversion kinetic rune T4D1 which had the highest possibility of pore diffusion rate controlled. The values of (r/C) is calculated as

$$\frac{R}{C} = 479$$

The corresponding value of the dimensionless thick modulus is

$$= .707$$

If we refer again to Figure 4.2 in Salterfield we see that the effectiveness factor approaches unity. Since the r / C ratios employed in other experimental runs were always lower than the value used in T4D1, pore diffusion can thus be neglected. These calculations tend to verify the experimental results obtained in section 6.2.

C. *SAMPLE DERIVATIONS OF RATE EQUATIONS*

E.1 *Reaction Mechanism M4*

This mechanism involves the dissociative adsorption of alcohol on two similar sites and the molecular adsorption of water on one identical site.

(1) $A + 1 + 1 \qquad A\,1 + A\,1$
(2) $W + 1 \qquad W1$
(3) $A\,1 + 1 \qquad P + R1 + 1$
(4) $A\,1 + R1 \qquad W1 + 1$

The following assumptions will be made:

(a) The adsorption steps of alcohol and water are assumed to be in equilibrium and thus

$$[A\,1] . [A\,1] = K .P .[1\,] \tag{E.1}$$

$$[W1] = K .P .[1\,] \tag{E.2}$$

(b) The surface rate reaction (3) is rate determining

$$r = k.[A\,1].[1\,] \tag{E.3}$$

and gives a free molecule of propylene and an unstable intermediate R1 .

(c) Step (4) is irreversible and fast compared to step (3)

$$[A\,1] = [A\,1] \tag{E.4}$$

and

$$[R1] \ll [1] + [A\ 1\ ] \qquad (E.5)$$

(d) The total number of active sites are assumed to remain constant

$$[1\ ] + [A\ 1] + [W1] = L$$

Rearranging these equations, we obtain an expression for the surface concentration of the dissociated species A 1

$$A\ 1 = \frac{L\ \ K\ P}{1 + K\ P + 2\ \ K\ P}, \qquad (E.6)$$

From equation (E.3) the final rate expression is written as

$$r = \frac{k\ L^2\ \ K\ P}{(1 + K\ P + 2\ \ K\ P\ )^2} \qquad (E.7)$$

which is the 3-parameter model M4 in Table 6.1

D.2 *Reaction Mechanism M5*

This mechanism involves the dissociative adsorption of alcohol on two dissimilar sites, 1 and 1 and the molecular adsorption of water on 1 .

$$(1)\quad A + l + l \qquad A\,l + A\,l$$

$$(2)\quad W + l \qquad Wl$$

$$(3)\quad A\,l + l \qquad P + l + R\,l$$

$$(4)\quad R\,l + A\,l \qquad W\,l + l$$

The following assumptions will be made:

(a) The adsorption steps of alcohol and water are assumed in equilibrium and thus

$$[A\,l\,] \times [A\,l\,] = K\,.P\,.[l\,][l\,] \tag{E.8}$$

$$[Wl\,] = K\,.P\,[l\,] \tag{E.9}$$

(b) The surface reaction (3) is assumed rate controlling

$$= k.[l\,].[A\,l\,] \tag{E.10}$$

and gives a free molecule of propylene and an unstable intermediate R l .

(c) Step (4) is irreversible and fast compared to step (3).

$$[A\,l\,] = [A\,l\,] \tag{E.11}$$

$$[Rl] << [A\,l\,] + [l\,] \tag{E.12}$$

(d) The total number of sites is assumed to remain constant

$$[A\,l\,] + [l\,] = L \tag{E.13}$$

$$[A\,l\,] + [Wl\,] + [l\,] = L \tag{E.14}$$

$$L = L \tag{E.15}$$

Rearranging these equations, we can obtain an expression for the surface concentration of the dissociated species A_1.

$$[A_1] = \frac{K P \ (1 + K P)}{1 + K P + K P \ (1 + K P)} \qquad (E.16)$$

From equation (E.10) the final rate expression is written as

$$r = \frac{k \ K P \ (1 + K P)}{1 + K P + K P \ (1 + K P)^2} \qquad (E.17)$$

which is analogous to the 3-parameter model M5 in Table 6-1.

TABLE E-1

CORRELATION RESULTS FOR MODEL M1 AGAINST VARIOUS ISOTHERMAL RATE DATA

Temperature (°C) Variance	Parameters	Correlation Matrix		
231.2	Model does not converge			
246.5	a = 0.00784±0.000670	1		
1.31×10^{-3}	b = 1551	-0.26	1	
	c = 194.8 ± 358.3	0.008	0.934	1
260.3	a = 0.0167 ± 0.001	1		
1.84×10^{-3}	b = 316.1 ± 118.5	-0.435	1	
	c = 41.37 ± 29.33	0.047	0.812	1
274.	a = 0.0299 ± 0.0023	1		
3.16×10^{-3}	b = 275.68 ± 241.48	-0.315	1	
	c = 56.45 ± 67.55	-0.015	0.930	1

TABLE E-2

CORRELATION RESULTS FOR MODEL M2 AGAINST VARIOUS ISOTHERMAL RATE DATA

Temperature (°C) Variance	Parameters	Correlation Matrix		
231.2	a = 0.0244 ± .00353	1		
5.72×10^{-4}	b = 109.17 ± 22.48	0.578	1	
	c = 51.97 ± 24.37	0.869	0.588	1
246.5	a = 0.0480 ± .004	1		
9.59×10^{-4}	b = 59.11 ± 6.72	0.352	1	
	c = 27.67 ± 8.17	0.871	0.487	1
260.3	a = 0.0807 ± .00336	1		
1.06×10^{-3}	b = 33.04 ± 2.	0.209	1	
	c = 10.98 ± 2.06	0.846	0.477	1
274.	a = 0.153 ± .0112	1		
2.17×10^{-3}	b = 18.80 ± 1.96	0.349	1	
	c = 8.44 ± 2.21	0.898	0.511	1

TABLE E-3

CORRELATION RESULTS FOR MODEL M3 AGAINST VARIOUS ISOTHERMAL RATE DATA

Temperature (°C) Variance	Parameters	Correlation Matrix		
231.2	a = .00474 ± .000665	1		
4.45×10^{-4}	b = 13172 ± 67988	-0.39	1	
	c = 58.26 ± 23.80	0.86	-0.08	1
246.5	a = .00999 ± .00104	1		
9.66×10^{-4}	b = 532.6 ± 176.7	-0.55	1	
	c = 20.85 ± 8.25	0.83	-0.20	1
260.3	a = .0217 ± .00819	1		
1.44×10^{-4}	b = 176.4 ± 30	-0.59	1	
	c = 13.7 ± 4.2	0.85	-0.21	1
274.	a = 0.044 ± .005	1		
2.1×10^{-3}	b = 91.2 ± 19.4	-0.58	1	
	c = 11.4 ± 3.4	0.9	-0.27	1

TABLE E-4

CORRELATION RESULTS FOR MODEL M4 AGAINST VARIOUS ISOTHERMAL RATE DATA

Temperature (°C) Variance	Parameters		Correlation Matrix		
231.2	a = .041	± .003	1		
8×10^{-8}	b = 45.4	± 13.6	0.62	1	
	c = 51.3	± 12.6	0.88	0.57	1
246.5	a = .073	± .0055	1		
9.5×10^{-7}	b = 8.52	± 2.75	-0.1	1	
	c = 15.3	± 5.4	0.76	0.31	1
260.3	a = 0.144	± 0.013	1		
3.6×10^{-6}	b = 2.14	± 0.83	-0.56	1	
	c = 6.72	± 2.6	0.58	0.22	1
274.	a = 0.28	± 0.03	1		
7.6×10^{-6}	b = 1.46	± 0.64	-0.49	1	
	c = 5.59	± 2.0	0.64	0.25	1

TABLE E-5

CORRELATION RESULTS FOR MODEL M5 AGAINST VARIOUS ISOTHERMAL RATE DATA

Temperature (°C) Variance	Parameters		Correlation Matrix		
231.2	a = 0.021	± .0015	1		
	b = 134.1	± 30.4	0.16	1	
	c = 56.2	± 26.0	0.89	0.03	1
246.5	a = 0.038	± .0033	1		
	b = 30.7	± 9.1	-0.32	1	
	c = 18.5	± 14.7	0.84	-0.04	1
260.3	a = 0.075	± .008	1		
	b = 8.8	± 2.9	-0.65	1	
	c = 8.7	± 8.5	0.75	-0.10	1
274.	a = 0.15	± 0.02	1		
	b = -5.	± 2.0	0.62	1	
	c = 7.2	± 6.5	0.80	0.13	1

TABLE E-7

CORRELATION RESULTS FOR MODEL M7 AGAINST VARIOUS ISOTHERMAL RATE DATA

Temperature (°C) Variance	Parameters	Correlation Matrix			
231.2	a = 0.018 ± .0017	1			
2.07×10^{-4}	b = 191.2 ± 39.	-0.66	1		
	c = 56.6 ± 10.	0.56	-0.06	1	
	d = 0.19 ± 0.035	-0.77	0.8	0	1
246.5	a = 0.037 ± 0.003	1			
4.22×10^{-4}	b = 78.6 ± 9.8	-0.82	1		
	c = 27.7 ± 4.5	0.68	-0.33	1	
	d = 0.17 ± 0.035	-0.85	0.86	-0.3	1
260.3	a = 0.07 ± 0.005	1			
7.3×10^{-4}	b = 38.2 ± 4.2	-0.86	1		
	c = 15.2 ± 2.2	0.53	-0.15	1	
	d = 0.156 ± 0.045	-0.87	0.9	0	1
274.	a = 0.125 ± 0.018	1			
1.42×10^{-3}	b = 22.9 ± 4.7	-0.88	1		
	c = 11.8 ± 2.35	0.48	-0.12	1	
	d = 0.225 ± 0.08	-0.88	0.92	0	1

TABLE E-8

CORRELATION RESULTS FOR MODEL M8 AGAINST VARIOUS ISOTHERMAL RATE DATA

Temperature (°C) Variance	Parameters		Correlation Matrix			
231.2	a = 0.025	± 37.	1			
5.84×10^{-4}	b = 109	± 165000	-1	1		
	c = 52	± 25	-0.18	0.18	1	
	d = 1.	± 3000	-1	1	0.18	1
246.5	a = 0.08	± 30	1			
9.7×10^{-4}	b = 33	± 12215	-1	1		
	c = 11	± 2.1	.175	-.175	1	
	d = 1.	± 739	-1	1	-.175	1
260.3	a = 0.05	± 17.	1			
1.07×10^{-3}	b = 59	± 21300	-1	1		
	c = 27.7	± 8.6	.29	-.29	1	
	d = 1.0	± 721	-1	1	-.29	1
274.	a = 0.15	± 110	1			
2.2×10^{-3}	b = 18.8	± 5000	-1	1		
	c = 8.4	± 2.27	0.17	-0.17	1	
	d = 1.00	± 1580	-1	1	-0.17	1

TABLE E-9

CORRELATION RESULTS FOR MODEL M9 AGAINST VARIOUS ISOTHERMAL RATE DATA

Temperature (°C) Variance	Parameters		Correlation Matrix			
231.2	a = .0096	± .004	1			
$7.5\text{x}10^{-4}$	b = 1190	± 7130	-0.47	1		
	c = 485	± 3164	-0.35	0.99	1	
	d = 0.29	± 0.20	-0.97	0.5	0.38	1
246.5	a = 0.019	± .006	1			
$1.3\text{x}10^{-3}$	b = 295	± 275	-0.63	1		
	c = 104	± 136	0.05	0.69	1	
	d = 0.37	± 0.20	-0.98	0.62	0	1
260.3	a = 0.05	± .007	1			
$1.5\text{x}10^{-3}$	b = 68.8	± 22.	-0.73	1		
	c = 34	± 17.	0.05	0.59	1	
	d = 0.197	± 0.10	-0.97	0.7	0	1
274.	a = 0.07	± 0.03	1			
$3.1\text{x}10^{-3}$	b = 70.7	± 60.	-0.72	1		
	c = 39.4	± 38.	-0.01	0.68	1	
	d = 0.34	± 0.26	-1	0.7	0	1

TABLE E-11

CORRELATION RESULTS FOR MODEL M11 AGAINST VARIOUS ISOTHERMAL RATE DATA

Temperature (°C) Variance	Parameters		Correlation Matrix			
231.2	a = .007	± .0009	1			
$2.6\text{x}10^{-4}$	b = 983	± 513	-0.78	1		
	c = 67.6	± 17.	0.71	-0.27	1	
	d = 10.9	± 4.7	0.86	-0.77	0.4	1
246.5	a = 0.016	± 0.002	1			
$6.0\text{x}10^{-4}$	b = 229	± 62.	-0.88	1		
	c = 34.	± 9.0	0.8	-0.52	1	
	d = 9.2	± 3.7	0.91	-0.84	0.6	1
260.3	a = 0.038	± .007	1			
$9.0\text{x}10^{-4}$	b = 77.7	± 18.	-0.95	1		
	c = 18.7	± 4.0	0.7	-0.50	1	
	d = 10.2	± 3.8	-0.96	-0.91	0.57	1
274.	a = 0.06	± 0.015	1			
$1.6\text{x}10^{-4}$	b = 51.7	± 15.8	-0.92	1		
	c = 13.7	± 3.6	0.75	-0.5	1	
	d = 3.75	± 2.3	0.94	-0.9	0.54	1

TABLE E-12

CORRELATION RESULTS FOR MODEL M12 AGAINST VARIOUS ISOTHERMAL RATE DATA

Temperature (°C) Variance	Parameters		Correlation Matrix			
231.2	a = .035	± .005	1			
2.07×10^{-4}	b = 94.3	± 23.2	-0.82	1		
	c = 56.7	± 10.6	0.37	-0.05	1	
	d = 0.102	± 0.02	-0.91	0.88	0	1
246.5	a = 0.72	± .009	1			
4.08×10^{-4}	b = 39.	± 6.5	-0.92	1		
	c = 27.4	± 4.3	0.53	-0.31	1	
	d = 0.09	± 0.02	-0.94	0.93	-0.25	1
260.3	a = 0.137	± 0.017	1			
6.9×10^{-4}	b = 19.	± 3.1	-0.95	1		
	c = 15.2	± 2.1	0.36	-0.14	1	
	d = 0.088	± 0.02	-0.86	0.96	-0.1	1
274.	a = 0.221	± 0.05	1			
1.4×10^{-3}	b = 12.7	± 3.9	-0.95	1		
	c = 11.9	± 2.3	0.30	-0.09	1	
	d = 0.133	± 0.06	-0.35	0.96	-0.03	1

TABLE E-13

CORRELATION RESULTS FOR MODEL M13 AGAINST VARIOUS ISOTHERMAL RATE DATA

Temperature (°C) Variance	Parameters		Correlation Matrix			
231.2	a = 0.016	± 0.0014	1			
2.07×10^{-4}	b = 219	± 43.4	-0.63	1		
	c = 56.6	± 10.6	0.59	-0.06	1	
	d = 1.78	± 0.04	0.75	0.80	-0.004	1
246.5	a = 0.032	± .0025	1			
4.2×10^{-4}	b = 90.3	± 11.0	-0.80	1		
	c = 27.7	± 4.5	0.70	-0.33	1	
	d = 1.80	± 0.04	0.84	-0.85	0.26	1
260.3	a = 0.06	± .0044	1			
7.3×10^{-4}	b = 44.	± 4.6	-0.84	1		
	c = 15.2	± 2.2	0.57	-0.15	1	
	d = 1.82	± 0.05	0.84	-0.90	0.1	1
274.	a = 0.11	± 0.015	1			
1.4×10^{-3}	b = 26.0	± 5.0	-0.85	1		
	c = 11.8	± 2.35	0.52	-0.12	1	
	d = 1.74	± 0.09	0.85	-0.90	0.03	1

TABLE E-14

CORRELATION RESULTS FOR MODEL M14 AGAINST VARIOUS ISOTHERMAL RATE DATA

Temperature (°C) Variance	Parameters	Correlation Matrix			
231.2	a = 0.012 ± 0.001	1			
2.06×10^{-4}	b = 259. ± 50.	-0.61	1		
	c = 56.6 ± 10.6	0.61	0.06	1	
	d = 0.284 ± 0.05	-0.73	0.79	0	1
246.5	a = 0.025 ± .0018	1			
4.05×10^{-4}	b = 110 ± 12.1	-0.79	1		
	c = 27.7 ± 4.3	0.72	-0.33	1	
	d = 0.26 ± 0.045	-0.81	0.84	-0.25	1
260.3	a = 0.047 ± 0.003	1			
6.9×10^{-4}	b = 54.3 ± 5.1	-0.82	1		
	c = 15.4 ± 2.1	0.61	-0.16	1	
	d = 0.25 ± 0.06	-0.81	0.88	-0.1	1
274.	a = 0.085 ± 0.01	1			
1.4×10^{-4}	b = 32.1 ± 5.8	-0.83	1		
	c = 11.9 ± 2.3	0.56	-0.13	1	
	d = 0.35 ± 0.11	-0.82	0.9	-0.03	1

TABLE E-15

CORRELATION RESULTS FOR MODEL M15 AGAINST VARIOUS ISOTHERMAL RATE DATA

Temperature (°C) Variance	Parameters	Correlation Matrix			
231.2	a = 0.032 ± .002	1			
2.17x10^{-4}	b = 90.5 ± 7.2	0.36	1		
	c = 57.0 ± 11.1	0.66	-0.06	1	
	d = 0.136 ± .012	-0.41	0.15	0.07	1
246.5	a = 0.062 ± .0027	1			
3.9x10^{-4}	b = 43.5 ± 2.1	-0.15	1		
	c = 27.3 ± 4.1	0.78	-0.33	1	
	d = 0.143 ± .011	-0.47	0.55	-0.15	1
260.3	a = 0.112 ± .004	1			
6.5x10^{-4}	b = 23.0 ± 0.98	-0.27	1		
	c = 15.5 ± 2.00	0.82	-0.15	1	
	d = 0.155 ± .015	-0.43	0.77	-0.05	1
274.	a = 0.205 ± 0.014	1			
1.36x10^{-4}	b = 13.3 ± 1.05	-0.22	1		
	c = 12.0 ± 2.26	0.81	-0.11	1	
	d = 0.194 ± 0.03	-0.38	0.74	0.05	1

E. *DATA REDUCTION*

The ideal gas law is inherent in the data reduction calculation procedure. The kinetic run No. T2D1 (see following tables) was chosen to demonstrate how the rate data was obtained by the data reduction procedure. The measured data of this kinetic run is summarized as follows.

GC Area Ratios

$AP/AA = 0.0443$
$AN/AP = 126.9$
$AW/AN = 0.0234$

Reactor Temperature = 246.5°C

Reactor Pressure = 0.93 atm

Nitrogen Flow rate = 1.07 gmol/h

Catalyst Weight = 86mg

By applying the GC calibration results in Chapter 5 and equation 5.9, the fractional conversion of alcohol is obtained

$$X = 4.65\%$$

We can now obtain from equation 5.12 the molar feed rate ratio of nitrogen relative to isopropanol.

$$a = 9.21$$

Similarly, the molar feed rate ratio of water relative to isopropanol is calculated

$$a = .289$$

Subsequently it was necessary to calculate the two independent variables of the kinetic models (e.g. the partial pressure of alcohol P and the partial pressure of water P). To do that, the molar fractions of the various compounds at steady state were first estimated according to the simple stoichiometry of the reaction.

$$x = \frac{a}{1 + a + a \quad + X}$$

$$x = \frac{1-X}{1 + a + a \quad + X}$$

$$x = \frac{X}{1 + a + a \quad + X}$$

$$X = \frac{a + X}{1 + a + a \quad + X}$$

PA and PW are then calculated applying Dalton's law

$$PA = x .P = 0.084 \text{ atm}$$

$$PW = x .P = 0.0296 \text{ atm}$$

The molar feed rate of isopropanol given by equation 5.13 is

$$F = \frac{1.07}{9.21} = 0.116 \text{ gmol/h}$$

Reaction rate of isopropanol dehydration

$$= \frac{.116 \times .0465}{.086}$$

$$= 6.27 \times 10^{-2} \text{ gmol/gcatalyst} \times \text{h}$$

Other kinetic data obtained by same method of calculation are summarized in Tables F-1 to F-3.

The discussion in Chapter 5 explained why this method of calculation was adopted in our study. Basically it relies upon the exactness of the material balance across the reactor instead of relying on the exactnes of the calibrated feed flow rates entering the reactor. This reverse procedure is more suitable for obtaining accurate data when instabilities are present in the feed lines as was shown in Chapter 5. The consistency of our calculation method was checked rather stringently by comparing the values of the calibrated valud of a and its average value on a series of runs at the same dial setting of the syringe feeder. The good agreement between these two values ensured use of the judiciousness of the calculation method.

TABLE F-1

GLOBAL RUNS CONDITIONS

Run Number	Reaction		Nitrogen Flow Rate (gmol/h)	Dial Setting of Alcohol Feeder	Dial Setting of Water Feeder
	Temp (OC)	Press (atm)			
T1A1	231.2	.932	1.065	40/100 (20)	Nil
T1A2	--	--	--	30/100 (20)	--
T1A3	--	--	--	20/100 (20)	--
T1A4	--	--	--	15/100 (20)	--
T1A5	--	--	--	90/1000 (20)	--
T1A6	--	--	--	70/1000 (20)	--
T1A7	--	--	--	50/1000 (20)	--
T1A8	--	--	--	40/1000 (20)	--
T1A9	--	--	--	30/1000 (20)	--
T1A10	--	--	--	25/1000 (20)	--
T1A11	--	--	--	20/1000 (20)	--
T1B1	231.2	.932	1.065	40/100 (20)	50/1000 (5)
T1B2	--	--	--	30/100 (20)	--
T1B3	--	--	--	20/100 (20)	--
T1B4	--	--	--	15/100 (20)	--
T1B5	--	--	--	90/1000 (20)	--
T1B6	--	--	--	70/1000 (20)	--
T1B7	--	--	--	50/1000 (20)	--
T1B8	--	--	--	40/1000 (20)	--
T1B9	--	--	--	30/1000 (20)	--
T1B10	--	--	--	25/1000 (20)	--
T1B11	--	--	--	20/1000 (20)	--
T1B12	--	--	--	15/1000 (20)	--
T1C1	231.2	.932	.425	15/100 (20)	Nil
T1C2	--	--	--	90/1000 (20)	--
T1C3	--	--	--	70/1000 (20)	--
T1C4	--	--	--	50/1000 (20)	--
T2A1	246.5	.954	.390	60/1000 (20)	Nil
T2A2	--	--	--	40/1000 (20)	--
T2A3	--	--	--	30/1000 (20)	--
T2A4	--	--	--	25/1000 (20)	--
T2A5	--	--	--	20/1000 (20)	--
T2A6	--	--	--	15/1000 (20)	--
T2A7	--	--	--	25/100 (20)	--
T2A8	--	--	--	15/100 (20)	--
T2A9	--	--	--	12/100 (20)	--

TABLE F-1 (Continued)

T2B1	246.5	.954	.390	75/1000 (20)	60/1000 (5)
T2B2	--	--	--	--	40/1000 (5)
T2B3	--	--	--	--	20/1000 (5)
T2B4	--	--	--	--	Nil
T2C1	246.5	.930	1.07	35/100 (20)	Nil
T2C2	--	--	--	25/100 (20)	--
T2C3	--	--	--	20/100 (20)	--
T2C4	--	--	--	15/100 (20)	--
T2C5	--	--	--	12/100 (20)	--
T2C6	--	--	--	90/1000 (20)	--
T2C7	--	--	--	75/1000 (20)	--
T2C8	--	--	--	60/1000 (20)	--
T2C9	--	--	--	50/1000 (20)	--
T2C10	--	--	--	40/1000 (20)	--
T2C11	--	--	--	30/1000 (20)	--
T2C12	--	--	--	25/1000 (20)	--
T2C13	--	--	--	20/1000 (20)	--
T2D1	246.5	.930	1.07	35/100 (20)	80/1000 (5)
T2D2	--	--	--	25/100 (20)	--
T2D3	--	--	--	15/100 (20)	--
T2D4	--	--	--	12/100 (20)	--
T2D5	--	--	--	90/1000 (20)	--
T2D6	--	--	--	75/1000 (20)	--
T2D7	--	--	--	60/1000 (20)	--
T2D8	--	--	--	50/1000 (20)	--
T2D9	--	--	--	40/1000 (20)	--
T2D10	--	--	--	30/1000 (20)	--
T2D11	--	--	--	25/1000 (20)	--
T2D12	--	--	--	20/1000 (20)	--
T3A1	260.2	.940	1.07	20/100 (20)	Nil
T3A2	--	--	--	30/100 (20)	--
T3A3	--	--	--	40/100 (20)	--
T3A4	--	--	--	20/100 (20)	--
T3A5	--	--	--	15/100 (20)	--
T3A6	--	--	--	12/100 (20)	--
T3A7	--	--	--	90/1000 (20)	--
T3A8	--	--	--	75/1000 (20)	--
T3A9	--	--	--	60/1000 (20)	--
T3A10	--	--	--	50/1000 (20)	--
T3A11	--	--	--	40/1000 (20)	--
T3A12	--	--	--	30/1000 (20)	--

TABLE F-1 (Continued)

T3B1	260.2	.940	1.07	30/100 (20)	40/1000 (5)
T3B2	--	--	--	20/100 (20)	--
T3B3	--	--	--	15/100 (20)	--
T3B4	--	--	--	12/100 (20)	--
T3B5	--	--	--	90/1000 (20)	--
T3B6	--	--	--	75/1000 (20)	--
T3B7	--	--	--	60/1000 (20)	--
T3B8	--	--	--	50/1000 (20)	--
T3B9	--	--	--	40/1000 (20)	--
T3B10	--	--	--	30/1000 (20)	--
T3C1	260.2	.940	.396	40/100 (20)	Nil
T3C2	--	--	--	30/100 (20)	--
T3C3	--	--	--	18/100 (20)	--
T3C4	--	--	--	12/100 (20)	--
T3C5	--	--	--	90/1000 (20)	--
T3C6	--	--	--	75/1000 (20)	--
T3C7	--	--	--	60/1000 (20)	--
T3C8	--	--	--	50/1000 (20)	--
T3C9	--	--	--	40/1000 (20)	--
T3C10	--	--	--	30/1000 (20)	--
T3C11	--	--	--	20/1000 (20)	--
T3D1	260.2	.930	1.08	30/100 (20)	20/100 (5)
T3D2	--	--	--	20/100 (20)	--
T3D3	--	--	--	15/100 (20)	--
T3D4	--	--	--	90/1000 (20)	--
T3D5	--	--	--	75/1000 (20)	--
T3D6	--	--	--	60/1000 (20)	--
T3D7	--	--	--	50/1000 (20)	--
T3D8	--	--	--	40/1000 (20)	--
T3D9	--	--	--	35/1000 (20)	--
T3D10	--	--	--	30/1000 (20)	--
T3D11	--	--	--	40/100 (20)	--
T3E1	260.2	.930	1.08	40/100 (20)	Nil
T3E2	--	--	--	30/100 (20)	--
T3E3	--	--	--	20/100 (20)	--
T3E4	--	--	--	15/100 (20)	--
T3E5	--	--	--	12/100 (20)	--
T3E6	--	--	--	90/1000 (20)	--
T3E7	--	--	--	75/1000 (20)	--
T3E8	--	--	--	50/1000 (20)	--
T3E9	--	--	--	30/1000 (20)	--

TABLE F-1 (Continued)

T3F1	260.2	.930	1.034	40/100	(20)	Nil
T3F2	--	--	--	--		80/1000 (5)
T3F3	--	--	--	30/100	(20)	--
T3F4	--	--	--	20/100	(20)	--
T3F5	--	--	--	15/100	(20)	--
T3F6	--	--	--	12/100	(20)	--
T3F7	--	--	--	90/1000	(20)	--
T3F8	--	--	--	75/1000	(20)	--
T3F9	--	--	--	60/1000	(20)	--
T3F10	--	--	--	50/1000	(20)	--
T3F11	--	--	--	40/1000	(20)	--
T3F12	--	--	--	30/1000	(20)	--
T3F13	--	--	--	25/1000	(20)	--
T3F14	--	--	--	20/1000	(20)	--
T3F15	--	--	--	20/1000	(20)	Nil
T3G1	260.2	.940	1.065	40/100	(20)	Nil
T3G2	--	--	--	30/100	(20)	--
T3G3	--	--	--	20/100	(20)	--
T3G4	--	--	--	15/100	(20)	--
T3G5	--	--	--	12/100	(20)	--
T3G6	--	--	--	90/1000	(20)	--
T3G7	--	--	--	75/1000	(20)	--
T3G8	--	--	--	60/1000	(20)	--
T3G9	--	--	--	50/1000	(20)	--
T3G10	--	--	--	40/1000	(20)	--
T3G11	--	--	--	30/1000	(20)	--
T3G12	--	--	--	25/1000	(20)	--
T3G13	--	--	--	20/1000	(20)	--
T4A1	274.0	.925	1.065	25/100	(50)	Nil
T4A2	--	--	--	20/100	(50)	--
T4A3	--	--	--	15/100	(50)	--
T4A4	--	--	--	12/100	(50)	--
T4A5	--	--	--	90/1000	(50)	--
T4A6	--	--	--	75/1000	(50)	--
T4A7	--	--	--	65/1000	(50)	--
T4A8	--	--	--	55/1000	(50)	--
T4A9	--	--	--	45/1000	(50)	--
T4A10	--	--	--	35/1000	(50)	--
T4A11	--	--	--	30/1000	(50)	--
T4A12	--	--	--	25/1000	(50)	--
T4A13	--	--	--	25/1000	(50)	90/1000 (10)

TABLE F-1 (Continued)

T4B1	274.0	.925	1.065	25/100 (50)	15/100 (10)
T4B2	--	--	--	15/100 (50)	--
T4B3	--	--	--	90/1000 (50)	--
T4B4	--	--	--	75/1000 (50)	--
T4B5	--	--	--	65/1000 (50)	--
T4B6	--	--	--	55/1000 (50)	--
T4B7	--	--	--	45/1000 (50)	--
T4B8	--	--	--	35/1000 (50)	--
T4B9	--	--	--	25/1000 (50)	--
T4B10	--	--	--	25/1000 (50)	--
T4B11	--	--	--	--	--
T4B12	--	--	--	--	10/100 (10)
T4B13	--	--	--	--	80/1000 (10)
					Nil
T4C1	274.0	.950	1.075	25/100 (50)	Nil
T4C2	--	--	--	30/100 (50)	--
T4C3	--	--	--	25/100 (50)	--
T4C4	--	--	--	20/100 (50)	--
T4C5	--	--	--	15/100 (50)	--
T4C6	--	--	--	12/100 (50)	--
T4C7	--	--	--	90/1000 (50)	--
T4C8	--	--	--	75/1000 (50)	--
T4C9	--	--	--	65/1000 (50)	--
T4C10	--	--	--	55/1000 (50)	--
T4C11	--	--	--	45/1000 (50)	--
T4C12	--	--	--	35/1000 (50)	--
T4C13	--	--	--	30/1000 (50)	--
T4C14	--	--	--	25/1000 (50)	--

TABLE F-2

SUMMARY OF KINETIC DATA

Run Number	AP/AA	Alcohol Conversion (%)	AN/AP	a	AW/AN	a
T1A1	.0216	2.32	222.2	8.04	--	Nil
T1A2	.0326	3.46	198.4	10.70	--	--
T1A3	.0525	5.46	198.1	16.87	--	--
T1A4	.0866	8.70	176	23.89	--	--
T1A5	.1413	13.5	198.1	16.87	--	--
T1A6	.205	18.4	159.4	45.75	--	--
T1A7	.359	28.3	158.3	69.86	--	--
T1A8	.533	37.0	152.9	88.3	--	--
T1A9	.822	47.5	157.0	116.3	--	--
T1A10	1.129	55.5	169.0	146.3	--	--
T1A11	1.15	56.0	202.4	176.8	--	--
T1B1	.0149	1.61	320	8.04	--	.159
T1B2	.0203	2.18	320	10.88	--	.209
T1B3	.0353	3.74	287.4	16.77	--	.325
T1B4	.0492	5.13	281.6	22.54	--	.415
T1B5	.0763	7.74	272.8	32.34	--	.608
T1B6	.112	11.0	266.4	45.71	--	.869
T1B7	.175	16.1	246.8	62.0	--	1.16
T1B8	.234	20.5	252.2	80.7	--	1.5
T1B9	.360	28.4	257.9	114.3	--	2.19
T1B10	.405	30.9	300.1	144.7	--	2.62
T1B11	.468	34.0	369.7	196.1	--	3.67
T1B12	.830	47.7	403.0	299.9	--	5.29
T1C1	.0578	5.98	97.34	9.08	--	Nil
T1C2	.0975	9.7	94.9	14.36	--	--
T1C3	.134	12.8	88.35	17.64	--	--
T1C4	.214	19.1	84.5	25.17	--	--
T2A1	.612	40.2	34.5	21.64	--	Nil
T2A2	1.475	61.9	34.98	35.78	--	--
T2A3	2.318	71.8	40.16	44.98	--	--
T2A4	2.69	74.7	43.56	50.76	--	--
T2A5	3.01	76.8	57.56	68.96	--	--
T2A6	3.15	77.6	78.35	95.5	--	--
T2A7	0.0894	8.95	42.28	5.9	--	--
T2A8	0.0166	15.45	38.53	9.29	--	--
T2A9	0.0245	21.21	36.53	12.08	--	--

TABLE F-2 (Continued)

T2B1	.174	16.0	68.49	17.09	.447	1.03
T2B2	.209	18.7	59.29	17.30	.317	.67
T2B3	.300	24.8	46.38	17.94	.216	.355
T2B4	.414	31.3	34.98	17.08	--	Nil
T2C1	.0641	6.56	92.53	9.47	--	Nil
T2C2	.106	10.5	82.66	13.54	--	--
T2C3	.1369	13.1	81.63	16.68	--	--
T2C4	.230	20.2	76.20	24.0	--	--
T2C5	.304	25.1	74.85	29.3	--	--
T2C6	.389	30.0	76.10	35.6	--	--
T2C7	.534	37.0	75.9	43.8	--	--
T2C8	.839	48.0	76.8	57.5	--	--
T2C9	.915	50.3	81.8	64.2	--	--
T2C10	1.037	53.3	103.2	85.8	--	--
T2C11	1.26	58.1	121.5	110.	--	--
T2C12	1.32	59.2	153.8	142.	--	--
T2C13	1.64	64.4	191.4	192.3	--	--
T2D1	.0443	4.65	126.9	9.21	.0234	.289
T2D2	.0697	7.12	118.3	13.14	.0222	.385
T2D3	.1307	12.6	121.4	23.86	.0224	.708
T2D4	.187	17.1	119.8	31.95	.0214	.893
T2D5	.206	18.5	118.9	34.3	.0236	1.078
T2D6	.253	21.75	118.9	40.3	.0234	1.256
T2D7	.364	28.6	116.1	51.8	.0214	1.44
T2D8	.456	33.4	122.4	63.7	.0219	1.84
T2D9	.536	37.0	134.0	77.4	.0215	2.23
T2D10	.743	45.0	160	112.3	.0217	3.36
T2D11	.956	51.3	175.5	140.5	.022	4.31
T2D12	1.03	53.1	208.0	172.3	.0204	4.97
T3A1	.3278	26.5	42.26	17.47	--	Nil
T3A2	.1702	15.8	43.66	10.76	--	--
T3A3	.1170	11.4	46.48	8.26	--	--
T3A4	.3127	25.6	43.33	17.30	--	--
T3A5	.5337	27.0	40.39	23.31	--	--
T3A6	.7807	46.2	42.07	30.32	--	--
T3A7	.8679	48.8	48.35	36.81	--	--
T3A8	.9474	51.0	53.33	42.43	--	--
T3A9	1.06	53.9	64.0	53.81	--	--
T3A10	1.21	57.0	71.87	63.91	--	--
T3A11	1.24	57.7	93.6	84.2	--	--
T3A12	1.345	59.7	119.35	111.1	--	--

TABLE F-2 (Continued)

T3B1	.140	13.4	50.53	10.56	58.93	.179
T3B2	.2658	22.6	48.76	17.19	63.3	.272
T3B3	.422	31.7	45.66	22.58	67.8	.333
T3B4	.558	38.1	48.0	28.53	65.1	.4384
T3B5	.743	45.0	50.81	35.67	65.4	.545
T3B6	.846	48.2	58.38	43.90	60.7	.723
T3B7	.958	51.3	68.06	54.47	66.85	.815
T3B8	1.092	54.6	74.85	63.75	67.8	.840
T3B9	1.102	54.8	98.98	84.6	61.5	1.375
T3B10	1.284	58.6	127.0	116.2	72.9	1.594
T3C1	.0945		20.23	2.97	--	Nil
T3C2	.1414		19.35	4.07	--	--
T3C3	.315	25.75	19.23	7.73	--	--
T3C4	.666	42.3	18.2	12.0	--	--
T3C5	.834	47.9	18.2	13.6	--	--
T3C6	1.08	54.3	18.7	15.8	--	--
T3C7	1.741	65.7	20.84	21.4	--	--
T3C8	2.01	68.9	21.68	23.3	--	--
T3C9	2.637	74.4	27.48	31.9	--	--
T3C10	3.09	77.3	34.42	41.5	--	--
T3C11	3.13	77.4	51.3	61.9	--	--
T3D1	.1144	11.2	62.90	10.99	14.33	.767
T3D2	.1763	16.2	68.65	17.35	14.78	1.17
T3D3	.2557	22.0	69.71	23.93	15.45	1.54
T3D4	.381	29.5	75.7	34.83	15.61	2.23
T3D5	.482	34.6	85.1	45.94	15.3	3.00
T3D6	.595	39.6	95.4	58.9	15.78	3.73
T3D7	.557	38.0	113.4	67.2	15.36	4.38
T3D8	.669	42.4	122	80.7	14.73	5.48
T3D9	.680	42.8	139.4	93.1	14.46	6.44
T3D10	.755	45.4	175.2	124.	14.71	8.43
T3D11	.0688	7.04	76.26	8.38	15.15	0.553
T3E1	.122	11.8	44.86	8.25	--	Nil
T3E2	.1878	17.1	42.66	11.38	--	--
T3E3	.3333	26.8	40.	16.72	--	--
T3E4	.5514	37.8	39.2	23.12	--	--
T3E5	.788	46.4	42.4	30.72	--	--
T3E6	.841	48.0	46.2	34.61	--	--
T3E7	.965	51.5	55.5	44.6	--	--
T3E8	1.18	56.5	76.2	67.15	--	--
T3E9	1.55	63.1	119.9	118.	--	--

TABLE F-2 (Continued)

T3F1	.118	11.5	44.30	7.95	--	Nil
T3F2	.089	8.93	54.93	7.65	30.65	.25
T3F3	.134.	12.8	51.83	10.35	33.78	.306
T3F4	.222	19.6	51.2	15.65	31.16	.502
T3F5	.3515	27.9	50.7	22.06	32.72	.674
T3F6	.468	34.0	56.05	29.73	33.74	.881
T3F7	.539	37.2	57.69	33.48	35.08	.954
T3F8	.684	42.9	63.5	42.5	35.35	1.20
T3F9	.775	46.0	73.14	52.5	35.97	1.46
T3F10	.916	50.2	80.31	62.9	34.71	1.81
T3F11	.917	50.2	96	75.2	33.03	2.28
T3F12	1.19	56.7	122.6	108.5	32.70	3.30
T3F13	1.195	56.8	145.8	129.2	34.75	3.72
T3F14	1.335	59.5	182.5	169.4	34.00	4.98
T3F15	1.7	65.2	178.0	181.0	--	Nil
T3G1	.1154	11.3	44.19	7.79	--	Nil
T3G2	.178	16.4	43.85	11.22	--	--
T3G3	.337	27.1	40.20	17.0	--	--
T3G4	.512	36.0	40.55	22.77	--	--
T3G5	.768	45.8	41.47	29.62	--	--
T3G6	.879	49.2	46.84	35.95	--	--
T3G7	.946	51.0	53.47	42.54	--	--
T3G8	1.07	54.0	61.64	51.93	--	--
T3G9	1.132	55.5	71.47	61.88	--	--
T3G10	1.246	57.8	88.66	79.9	--	--
T3G11	1.377	60.2	117.4	110.3	--	--
T3G12	1.452	61.5	140.6	134.8	--	--
T3G13	1.574	63.4	176	174.0	--	--
T4A1	.2212	19.6	21.96	6.72	--	Nil
T4A2	.309	25.4	20.92	8.29	--	--
T4A3	.466	33.9	21.35	11.29	--	--
T4A4	.668	42.4	23.44	15.50	--	--
T4A5	.746	45.1	23.24	16.35	--	--
T4A6	.892	49.5	25.87	19.97	--	--
T4A7	1.01	52.8	29.96	24.67	--	--
T4A8	1.08	54.3	35.52	30.1	--	--
T4A9	1.17	56.4	42.62	37.5	--	--
T4A10	1.32	59.4	53.12	49.2	--	--
T4A11	1.40	60.6	59.55	56.3	--	--
T4A12	.207	18.5	22.26	6.42	--	--
T4A13	.152	14.3	28.24	6.30	--	--

TABLE F-2 (Continued)

T4B1	.134	12.87	28.79	6.55	.0723	.598
T4B2	.239	20.8	34.41	11.17	.0746	1.091
T4B3	.374	29.2	39.18	17.85	.0724	1.72
T4B4	.423	31.7	40.66	20.1	.0706	1.90
T4B5	.504	35.7	46.14	25.7	.0696	2.43
T4B6	.559	38.1	48.	28.53	.0729	2.86
T4B7	.649	41.7	57.4	37.35	.0702	3.67
T4B8	.710	43.9	66.13	45.3	.0675	4.34
T4B9	.851	48.4	80.64	60.3	.0665	5.83
T4B10	.129	12.4	34.56	6.69	.0706	.613
T4B12	.160	15.0	28.52	6.68	.0432	.300
T4B13	.213	19.0	22.66	6.75	--	Nil
T4C1	.189	17.2	23.75	6.37	--	Nil
T4C2	.130	12.6	10.36	2.04	--	--
T4C3	.163	15.2	10.07	2.39	--	--
T4C4	.216	19.2	10.30	3.09	--	--
T4C5	.332	26.8	10.54	4.41	--	--
T4C6	.522	36.5	10.27	5.85	--	--
T4C7	.565	38.3	10.88	6.50	--	--
T4C8	.882	49.1	11.27	7.97	--	--
T4C9	1.03	53.2	10.99	9.12	--	--
T4C10	1.31	59.0	11.69	10.76	--	--
T4C11	1.6	63.8	12.29	12.23	--	--
T4C12	2.27	71.3	14.54	16.18	--	--
T4C13	2.58	74.0	17.04	19.67	--	--
T4C14	2.98	76.6	20.23	24.20	--	--

TABLE F-3

SUMMARY OF MODELING DATA

Run Number	Partial Pressures (atmx100) Alcohol	Water	Reaction Rates (g.molx100/gxh) Observed	Predicted
T1A1	10.0	.494	3.62	3.62
T1A2	7.65	.475	4.02	3.78
T1A3	4.91	.410	4.05	4.15
T1A4	3.40	.419	4.56	4.41
T1A5	2.25	.419	4.87	4.75
T1A6	1.62	.419	5.03	5.
T1A7	.932	.40	5.07	5.3
T1A8	.655	.41	5.25	5.25
T1A9	.415	.396	5.12	4.90
T1A10	.280	.363	4.75	4.38
T1A11	.230	.308	3.96	4.13
T1B1	9.95	1.77	2.50	2.32
T1B2	7.53	1.77	2.50	2.39
T1B3	4.95	1.86	2.8	2.49
T1B4	3.68	1.81	2.85	2.66
T1B5	2.48	1.85	2.94	2.84
T1B6	1.74	1.91	3.01	2.94
T1B7	1.21	1.91	3.26	3.07
T1B8	.888	1.90	3.19	3.13
T1B9	.566	1.96	3.12	3.01
T1B10	.433	1.84	2.67	2.96
T1B11	.306	1.87	2.18	2.60
T1B12	.158	1.75	1.99	2.0
T1C1	8.62	.777	3.29	3.27
T1C2	5.43	.734	3.39	3.55
T1C3	4.32	.758	3.62	3.66
T1C4	2.86	.764	3.8	3.93
T2A1	2.48	1.66	8.53	8.86
T2A2	1.03	1.67	8.39	8.33
T2A3	.576	1.47	7.34	7.10
T2A4	.46	1.35	6.74	6.52
T2A5	.313	1.04	5.09	5.55
T2A6	.219	7.6	3.72	4.6
T2A7	12.4	1.22	6.98	7.27
T2A8	7.72	1.41	7.61	7.69
T2A9	5.66	1.52	8.02	8.02

TABLE F-3 (Continued)

T2B1	4.16	5.89	4.29	4.6
T2B2	4.04	4.26	4.95	5.57
T2B3	3.67	2.95	6.35	6.8
T2B4	3.57	1.62	8.41	8.55
T2C1	8.24	.85	8.71	8.54
T2C2	5.67	.83	9.76	9.27
T2C3	4.53	.815	9.9	9.71
T2C4	2.95	.837	10.6	10.3
T2C5	2.28	.837	10.8	10.5
T2C6	1.77	.82	10.6	10.6
T2C7	1.29	.81	10.6	10.4
T2C8	.807	.80	10.5	9.3
T2C9	.707	.745	9.9	9.0
T2C10	.498	.595	7.8	8.0
T2C11	.350	.50	6.65	6.72
T2C12	.264	.40	5.25	5.74
T2C13	.171	.316	4.21	4.25
T2D1	8.4	2.96	6.35	5.8
T2D2	6.08	2.99	6.5	6.15
T2D3	3.16	3.02	6.64	6.87
T2D4	2.27	2.91	6.74	7.2
T2D5	2.07	3.21	6.79	6.9
T2D6	1.7	3.20	6.79	6.89
T2D7	1.22	2.95	6.94	6.92
T2D8	.93	3.02	6.6	6.5
T2D9	.723	2.99	6.0	6.0
T2D10	.437	3.02	5.0	4.75
T2D11	.309	3.07	4.6	3.9
T2D12	.284	2.86	3.9	3.4
T3A1	3.68	1.33	19.0	20.2
T3A2	6.63	1.25	18.5	19.5
T3A3	8.88	1.15	17.4	18.8
T3A4	3.76	1.30	18.6	20.3
T3A5	2.40	1.41	20	19.3
T3A6	1.59	1.36	19.2	17.5
T3A7	1.26	1.19	16.7	16.4
T3A8	1.05	1.09	15.2	15.3
T3A9	.783	.915	12.6	13.4
T3A10	.617	.818	11.2	11.7
T3A11	.463	.632	8.7	9.8
T3A12	.336	.498	6.8	7.7

TABLE F-3 (Continued)

T3B1	6.85	2.48	16	15.6
T3B2	3.89	2.50	16.6	17.0
T3B3	2.65	2.52	17.6	16.9
T3B4	1.92	2.54	16.8	15.9
T3B5	1.37	2.48	15.9	14.4
T3B6	1.05	2.45	13.9	12.8
T3B7	.805	2.20	11.8	11.5
T3B8	.643	2.11	10.8	10.1
T3B9	.485	2.07	8.15	8.34
T3B10	.326	1.72	6.35	6.4
T3C1	20.8	2.7	14.1	12.9
T3C2	15.5	2.88	15.4	13.6
T3C3	7.75	2.97	15.5	15.6
T3C4	4.04	2.96	16.5	16.8
T3C5	3.25	2.99	16.5	16.7
T3C6	2.48	2.94	16.	16.2
T3C7	1.40	2.68	14.4	14.4
T3C8	1.17	2.58	13.8	13.4
T3C9	.715	2.08	10.9	10.97
T3C10	.692	1.68	8.7	8.96
T3C11	.334	1.15	5.9	7.15
T3D1	6.42	6.35	12.9	12.4
T3D2	3.96	6.30	11.9	12.4
T3D3	2.72	6.13	11.7	12.4
T3D4	1.71	6.12	10.8	11.2
T3D5	1.21	6.19	9.6	9.8
T3D6	.877	5.99	8.54	8.5
T3D7	.791	6.06	7.2	7.9
T3D8	.612	6.27	6.67	6.69
T3D9	.526	6.32	5.84	6.01
T3D10	.380	6.18	4.65	4.8
T3D11	8.64	5.79	10.7	11.7
T3E1	8.72	1.47	18.1	18.1
T3E2	6.13	1.52	19.1	19.1
T3E3	3.77	1.63	20.4	19.5
T3E4	2.35	1.66	20.7	18.6
T3E5	1.54	1.54	19.2	17.0
T3E6	1.34	1.45	17.6	16.2
T3E7	.976	1.04	14.7	14.8
T3E8	.589	.764	10.7	11.4
T3E9	.286	.490	6.8	6.9

TABLE F-3 (Continued)

T3F1	9.05	1.47	17.6	18.
T3F2	9.42	3.51	14.1	14.2
T3F3	6.88	3.42	15.1	15.2
T3F4	4.32	3.74	15.3	15.4
T3F5	2.79	3.69	15.4	15.3
T3F6	1.93	3.55	13.9	14.6
T3F7	1.63	3.44	13.5	14.
T3F8	1.18	3.36	12.2	12.5
T3F9	.906	3.22	10.7	11.0
T3F10	.699	3.25	9.7	9.5
T3F11	.586	3.27	8.1	8.5
T3F12	.355	3.19	6.35	5.9
T3F13	.298	2.37	5.35	5.3
T3F14	.214	2.95	4.27	4.0
T3F15	.177	.332	4.38	4.7
T3G1	9.33	1.49	18.1	17.9
T3G2	6.33	1.53	18.4	19.0
T3G3	3.74	1.58	20	19.6
T3G4	2.49	1.51	19.8	19.2
T3G5	1.64	1.50	19.4	17.4
T3G6	1.28	1.34	17.4	16.2
T3G7	41.04	1.18	15.1	15.1
T3G8	.807	1.08	13.06	13.3
T3G9	.659	.822	11.2	12.2
T3G10	.487	.666	9.05	10.1
T3G11	.355	.506	6.8	7.8
T3G12	.265	.424	5.7	6.4
T3G13	.196	.339	4.56	5.0
T4A1	9.36	2.57	36.6	36.2
T4A2	7.21	2.69	38.4	35.9
T4A3	4.83	2.66	37.6	34.8
T4A4	3.15	2.45	34.2	32.2
T4A5	2.85	2.47	34.6	31.2
T4A6	2.17	2.24	31.0	28.7
T4A7	1.67	1.95	26.8	26.
T4A8	1.33	1.67	22.6	23.5
T4A9	1.04	1.40	18.8	20.6
T4A10	0.74	1.13	15.2	16.7
T4A11	0.63	1.01	13.5	14.9
T4A12	9.92	2.55	36.2	36.2
T4A13	10.11	6.36	28.5	26.9